INTEGRATION OF PHOTOVOLTAIC CELLS INTO COMPOSITE WING SKINS

By

JAMES LEONARD

Bachelor of Science in Aerospace and Mechanical Engineering

Oklahoma State University

Stillwater, Oklahoma

2010

Submitted to the Faculty of the
Graduate College of the
Oklahoma State University
in partial fulfillment of
the requirements for
the Degree of
MASTER OF SCIENCE
December, 2014

INTEGRATION OF PHOTOVOLTAIC CELLS INTO

COMPOSITE WING SKINS

Thesis Approved:

Dr. Jamey Jacob
Thesis Adviser

Dr. Andy Arena

Dr. Joe Conner

Name: JAMES LEONARD

Date of Degree: DECEMBER, 2014

Title of Study: INTEGRATION OF PHOTOVOLTAIC CELLS INTO COMPOSITE WING SKINS

Major Field: MECHANICAL AND AEROSPACE ENGINEERING

ABSTRACT:

The integration of thin film solar cells into composite wing skins is explored by first testing and evaluating the integration of single solar cells into small composite samples with no encapsulating material, fiberglass encapsulating material and polyurethane film encapsulating material for the impacts that these processes and materials have on solar cell performance, aircraft performance and solar cell durability. Moving on from single cell samples, three encapsulation methods were chosen to be used in the construction of two wings utilizing arrays of multiple solar cells with each encapsulation method being utilized on 3 of the four wing skins comprising the 2 complete wings. The fourth wing skin was integrated with a functioning removable solar panel manufactured to the contours of the wing. Performance and weight data gathered from the development and fabrication of single cell and wing-skin specimens was used to develop a basic model of endurance for each encapsulation material evaluated in order to compare the effects of encapsulation materials and processes on the primary parameter that the integration of the photovoltaic cells into the wing skins is intended to improve.

TABLE OF CONTENTS

LIST OF TABLES

Table Page

LIST OF FIGURES

Figure Page

CHAPTER I

INTRODUCTION

Propulsion systems for Small Unmanned Aerial Systems (SUAS) often involve the implementation of electric motors for their ease of use and reduced acoustic signature; however, the endurance offered by these electric propulsion systems is normally far less than that of their combustion engine counterparts due to the essential fact that the energy density of fossil fuels is still much higher than that of batteries. Batteries are heavy for the potential energy they have to offer when compared to fossil fuels, and additional power consuming systems on a SUAV such as IR cameras and avionics can become power sinks that further sap endurance from SUAV platforms.

A potential method of extending electric propulsion endurance for aircraft lies in energy harvesting; that is, to collect energy from the environment during operation of the Unmanned Aerial Vehicle (UAV) in order to extend mission time. Energy harvesting can come in the form of soaring on thermals, landing on power-lines to collect energy or harnessing solar power via photovoltaic cells. Thin film photovoltaic cells, in particular, can easily be attached to the surfaces of wings to harvest energy in flight for daytime operation. This thesis will cover processes of integration of solar cells into composite wing skins and the impacts that those processes have on photovoltaic cell performance and aircraft performance.

Photovoltaic (PV) cells can be integrated into wing skins using a number of methods that can have impacts on not only the effectiveness of the PV cells themselves, but also on the performance of the aircraft they are being integrated into. The introduction of PV cells into the wings of an aircraft introduces a weight penalty and, depending on the process of integration, can also impact the aerodynamic performance of the airframe. Therefore, not only the cells themselves but also the process of their integration into the aircraft is expected to be at least efficient enough to overcome the weight and possible aerodynamic penalties in order to produce an increase in endurance. If the PV cells are too inefficient or if the process of integrating them into the wing skin too heavy, then the introduction of the PV cells themselves can have a negative net impact on the performance of the UAV. Consideration must also be taken into the potential for potential damage to attached PV cells during normal operation of the UAV. The operation of SUAS platforms can result in damage of a varying degree to the airframe, including the surfaces of the wings. The integration of PV cells into the wings warrants investigation into different protective laminates that can potentially offer a higher degree of protection to the solar cells while also providing a minimal negative impact on the performance of the PV modules. In the case of molded composites, flexible laminates can be embedded into the manufacturing process along with the photovoltaic cell modules themselves in order to ensure that the contours of the aerodynamic surface of the composite skin they are being integrated into are not compromised.

Desirable qualities of PV cell integration into composite skins include the following

- Flush, seamless integration into the composite skin surface
- Minimal impacts on PV module performance
- Minimal increases in overall weight

Weight increases from PV cell integration into wing skins not only come from the solar cells themselves, but also any additional wiring or circuitry that is required to integrate the power produced by the solar cells into the propulsion system of the aircraft. The scope of this thesis will focus more on the structural integration processes of the solar cells into composite skins and the impacts that those processes have on aircraft and PV cell performance with less emphasis on the integration of solar power into the propulsion system of the aircraft.

Goals and Objectives

The goal of this research is to investigate methods of solar cell integration into structural composite skins using different processes and laminates and evaluate the impact that the integration process has on photovoltaic cell performance and overall system performance

Objectives

1. Develop a model for solar SUAS for evaluation of integration of solar cells into UAVS
2. Develop different processes of PV cell integration into composite skins for various laminates and evaluate the impact those processes have on PV cell performance; select best processes for each laminate based on desirable qualities
3. Based on results from (1), test the performance impacts that various weights or thicknesses of previously chosen laminates have on both PV cells and potential aircraft performance

4. Evaluate the strength of different lamination materials in order to determine any possible relationships between laminate materials and the level of protection they might provide for encapsulated PV cells
5. Design and fabricate a wing with a multi-cell array of solar cells for each laminate type using similar construction methods
6. Investigate and develop a potential method for replacing damaged or mal-functioning cell arrays in a structural composite wing skin.

Outline of Thesis

The structure of the thesis will follow background describing solar cells, solar flight and the development of a basic aircraft endurance model before transitioning into a design of experiments section containing information on the experiments developed to satisfy this research's objectives and the methodology of testing. Results will then be covered as well as any conclusions that can be drawn from those results.

CHAPTER II

BACKGROUND

The marriage of solar cells and electric motors for solar flight was met with its first success in the form of Project Sunrise in 1974, where Robert J. Boucher and Atro Flight designed, built and eventually flew the solar powered Sunrise I in November that year. Its cleaner, more powerful successor, Sunrise II, was to follow in September of 1975 with greater success. Sunrise II was expected to reach an altitude of 75,000 feet if not for the unfortunate failure of its command and control system at 17,200 ft. With the flights of Sunrise I and II, Boucher ushered in the era of not only solar flight, but also unmanned solar flight. [1]

As photovoltaic (PV) cells have grown cheaper to produce at higher efficiencies effort put into adapting photovoltaic technology into aerospace applications has risen since the 1970s, with the existence of solar powered aircraft such as the solar power assisted Silent Falcon SUAV, which has been developed for commercial observation uses, as well as the manned Solar Impulse, which recently completed a flight of over 24 hours on solar power alone while its successor is planned to fly around the world in 2015. Titan Aerospace is also conducting research on the development of atmospheric satellites, aircraft designed to fly at the edge of the atmosphere on solar power.

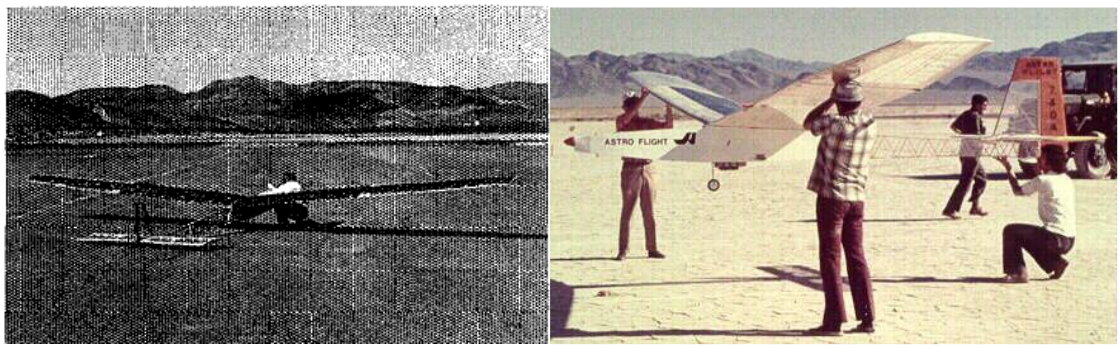

Figure 1: Sunrise I (left) in 1974 and Sunrise II (right) in 1975 from [1]and [2] respectively

Solar Flight

The birth of solar powered flight came with the development and maiden flight of Sunrise I, developed by Robert J. Boucher and Astro Flight in November of 1974 (Figure 1). Sunrise I, powered by 4,096 solar cells on its wings made a number of three to four hour flights during the winter before it was severely damaged in a sand storm. There were some notable difficulties with Sunrise I, such as unexpected weight increases and a lower than desired amount of solar power available from its solar cell banks. The solar cells themselves, which had been claimed to be 14% efficient, totaled 6.5lb, a full 2 lb heavier than what was expected and a power output of 450W as opposed to the desired output of 600W. The extra weight of the solar cells and the need for lead ballast in the nose to counter the weight added to the wings brought Sunrise I up to a total weight of 27.5lb instead of its desired weight of approximately 24lb. [1]

These issues were resolved with the development of Sunrise II, which was expected to be capable of flights exceeding 24 hours at altitudes near 75,000 ft if not for damage sustained in a command and control system failure during initial flight tests. While Sunrise II was an improvement over Sunrise I, both aircraft suffered increases in profile

drag due to the combination of selection of an Eppler 387 airfoil and the addition of solar cells to the upper surface of the wing. [1]

Figure 2: Solar Challenger developed by Paul MacReady and AeroVironment, Inc.

At this point in time, commercially available solar cells were only available as rigid, flat units, so the designers of solar aircraft were forced to take that into account when designing and fabricating their wings to accommodate solar cells. Solar Challenger (Figure 2) by Paul MacCready's Aerovironment, which flew across in the English Channel in 1981, found a solution to this problem by utilizing an airfoil with a top surface that was flat for 85% of its chord (Figure 3). Another solar aircraft designed at around the same time to cross the channel, Solair I by Gunter Rochett (Figure 4), got around this problem by mounting solar cells in segments along the top surface of the wing and then matching the desired profile of the top surface using clear pieces of silicon, which were sanded into shape and polished to a high clarity. [1]

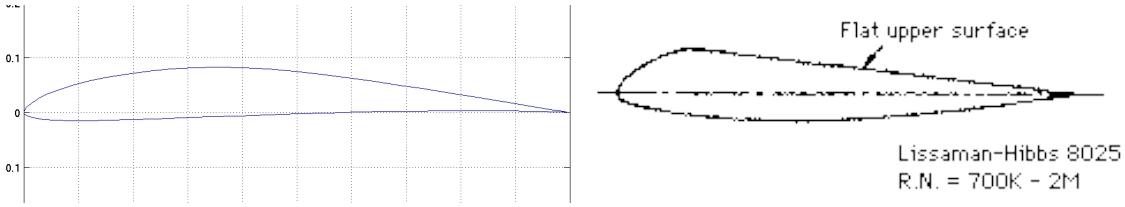

Figure 3: Eppler 387 airfoil used in Sunrise I and II (left) and Lissaman airfoil used in Solar Challenger (right)

Figure 4: Solair I by Gunter Rochett

High altitude long endurance (HALE) UAVs became a topic of interest for NASA's Environmental Research Aircraft and Sensor Technology (ERAST) program in the 1990s, beginning with AeroVironment's Pathfinder and Pathfinder Plus aircraft, which eventually evolved into Centurion and HELIOS around the turn of the millennium (Figure 5).

Figure 5: Pathfinder Plus (left) and HELIOS (right)

These UAVs were designed to chase the goal to develop aircraft that could stay aloft at high altitudes for long periods of time between landings, with the idea being that energy collected by solar cells would be both stored during the day and utilized to climb to a

high altitude. At night, the aircraft would use its stored battery power for its sensor suite while slowly expending the stored potential energy of its high altitude and also taking advantage of thermals and night to remain aloft. This strategy was also aided by the fact that photovoltaic cell performance is greater at higher altitudes where less energy from sunlight being absorbed or reflected by the Earth's atmosphere. Despite the structural failure of HELIOS during test flights, the aircraft set a world record altitude of 96,863ft. The objective of 24 hour solar flight was eventually fulfilled by Alan Cocconi's Solong aircraft in 2005 with a 24hr, 11 minute flight using only solar power. Later that year, Solong performed another even longer flight of 48 hours to confirm its performance. [2] Titan Aerospace possesses a similar vision of HALE UAVs and as a cheaper alternative to satellites. These aircraft are expected to become capable of years of uninterrupted flight in the upper-most edges of the Earth's atmosphere.

Figure 6: Concept Image of the solar aircraft envisioned by Titan Aerospace aloft high in the earth's atmosphere

Oklahoma State Univeristy also developed two competing designs of a solar powered aircraft in 1997 dubbed Helios and Sol-Air. These aircraft possessed arrays or rigid photovoltaic cells built into the structure of their wings beneath a clear upper wing surface covering.

Figure 7: OSU Helios (1997)

The lower costs of higher quality photovoltaics as well as the use of flexible film PV cells has created additional interest in the retrofitting of existing military UAVs with photovoltaic cell arrays for the purposes of increasing aircraft endurance. The addition of solar cells to the wings of an existing UAV, if implemented properly, not only provides the benefit of longer endurance, but allows soldiers in the field to charge the batteries of the aircraft on the ground between flights using solar power, cutting down on the need for extra batteries to be brought along in the field. The Raven UAS, developed in 2002 under the US Army's "Pathfinder" Advanced Concept Technology Demonstration (ACTD) program by AeroVironment, Inc. is a popular platform in use by the US Army. Its small size, portability, impressive sensor suite and small ground station make the Raven a well desired SUAV for mobile ground forces, but it still suffers from the short-falls of battery powered aircraft. With a maximum endurance of 60 to 90 minutes, depending on flight conditions, and the need to spend long period of time recharging batteries between flights with the need for a suitable power source, the Raven's capabilities are limited to shorter periods of reconnaissance. [3]

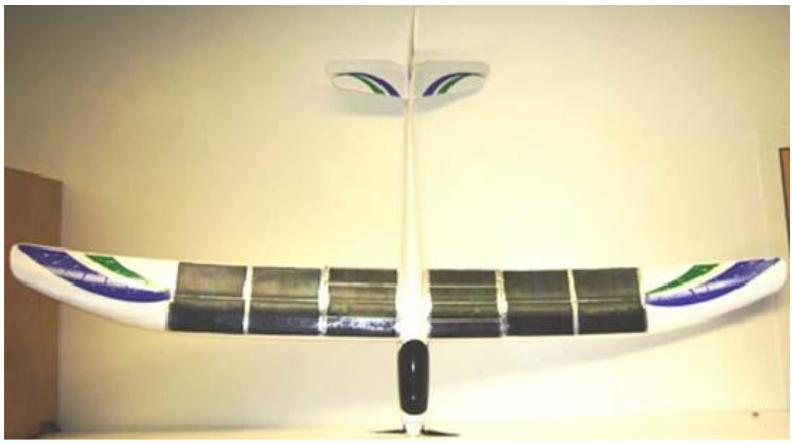

Figure 8: Hurd's *Thin Film Flyer* fully assembled from [3]

Hurd, 2009, and Coba, 2010, both perform investigations into the adaptation of solar cells to the wing surfaces of both a small commercial, off-the-shelf, (COTS) UAV as well as a functioning Raven to investigate potential increases in endurance compared to a default battery-motor configuration. The wing surface of an aircraft makes an ideal surface for the adaptation of thin film photovoltaic (TFPV) cell arrays because of the usually plentiful amount of useable space that normally lacks many of the awkward angles or bulges that would be present on the fuselage of an SUAV that might make the attachment of cell arrays difficult or impossible. The efficient use of space in PV cell arrays depends on the shape of the cells themselves, but most cells are available as rectangles, and the surfaces of wings are a good place for arrays of rectangular shaped cells.[3]

Figure 9: Raven RQ-11B from [4]

Through the use of flexible film solar cells and other necessary electronics such as a maximum power point tracker (MPPT), both parties were able to produce significant increases in baseline performance of both the tested COTS platform as well as the Raven using 8% and 13% efficient solar cells respectively. Hurd, who used a Parkzone Radian RPV for its similar size and profile compared to the Raven, was able to achieve level flight periods of 93 minutes compared to the Radian's approximated 37 minute normal flight endurance without the assistance of solar cells. [3] Coba, who was able to procure a Raven for his tests, experienced increased from a normal 1hour 53 minute flight time for optimal conditions testing without solar panels to up to 3 hours and12 minutes with solar power. For simulation of higher winds, the Raven's normal endurance fell to 1 hour 26 minutes without solar cells and 1 hour 58 minutes endurance with solar cells. That is, Hurd experienced a 151% projected increase in endurance with the Parkzone Radian on 8% efficient photovoltaic cells, while Coba achieved a 37-70% increase in endurance on the Raven UAV with 13% efficient photovoltaic cells. [4]

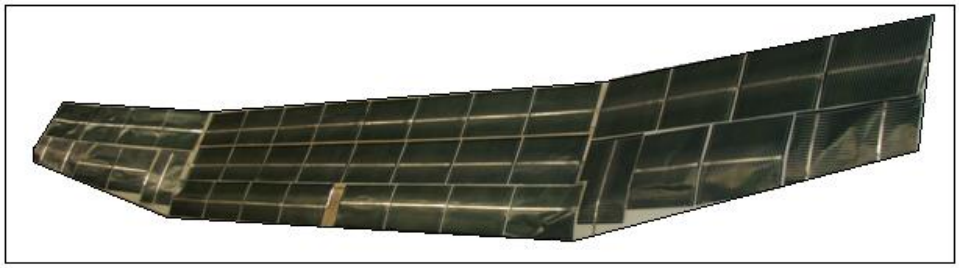

Figure 10: Coba's modified Raven wing with full solar panel from [4]

While refitting existing UAV platforms with PV cells remains an option, future SUAVs like the Silent Falcon are likely to be designed specifically for the integration of photovoltaic cells or other energy harvesting technology. Silent Falcon is an 11-11.5kg (24.2-25.4lb) solar/electric SUAS with a 2.7-5.1m (8.9-16.7ft) wing span developed by

Silent Falcon UAS Technologies in Albuquerque, New Mexico. The aircraft will be available in a small range of sizes with advertised endurances of 5 to 12 hours, designed from the ground up to utilize solar and electric power with a Li-Ion battery and thin film photovoltaic (TFPV) cells.

Figure 11: *Silent Falcon* SUAV

Solar Cells

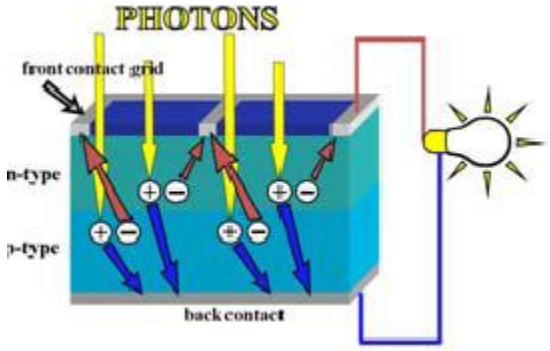

Figure 12: Basic p-n solar cell diagram from [3]

Solar cells are comprised of p-n junctions. At a very basic level, they are essentially a wafer of multiple materials, two of which comprise the p-n junction layers with one serving as the p-type semiconductor, the donator of electrons, and the other material serving as the n-type semiconductor which accepts electrons. In silicon solar cells, each

junction is doped by different elements that give it a tendency toward easily giving up electrons or easily receiving electrons. In semiconductors, a certain amount of energy is required for electrons to jump from the conduction band to the valence band of a single atom of semiconductor. This energy difference is referred to as an energy gap or bandgap. In conductors, the energy gap between the valance and the conduction band is very small or even inconsequential, which allows electrons to move much more easily out of the valence shell without much energy. Insulators have a much larger bandgap, and it is difficult to free electrons from their valence shell into the conduction band. Semiconductors possess an energy gap that lies between that of conductors and insulators.

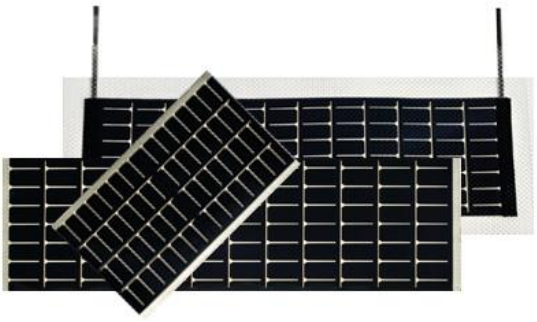

Figure 13: Examples of OEM amorphous silicon TFPV cells made by PowerFilm

The bandgap of the p-n junction and its materials is a key parameter in determining the effectiveness of a solar cell because the band gap determines the amount of energy required to be imparted on the semiconductor to make it susceptible to the transfer of electrons between, in this case, the p-n junction of the solar cell. In the case of solar cells, this energy comes from photons in light. If a load is applied to the solar cell, usually in the form of a voltage in the appropriate orientation or the existence of a resistance in-circuit with the photovoltaic cell, then the solar cell produces current. Changing the

bandgap of the solar cell is a matter of changing the materials out of which it is made, which can be used to tune a solar cell to respond to certain wavelengths of light. Single junction cells, for instance, are tuned to obtain the most energy from a specific region in the spectrum of light, and triple junction solar cells are tuned for three different regions of the light spectrum. Multi-junction solar cells consist of multiple layers of differently doped semiconductors that are intended to absorb different bands of light for photogeneration. Triple-junction solar cells are more expensive to manufacture than single-junction solar cells and are more efficient for use in sunlight.

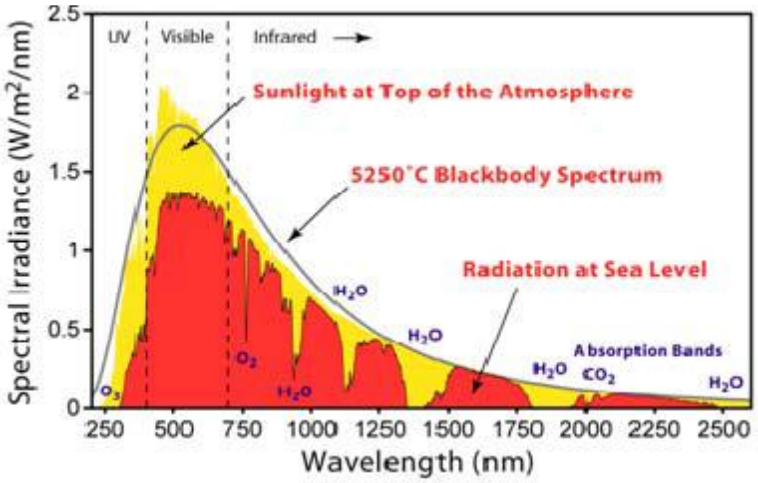

Figure 14: Solar Radiation Spectrum from [3]

Thin film photovoltaic (TFPV) cells are advantageous to uses in curved surfaces, such as wings, due to their flexibility, but are typically more expensive than their rigid counterparts, especially at higher efficiencies. While there are other emerging types of TFPV cells, the three main commercially available TFPV cells are amorphous silicon, cadmium telluride and copper indium gallium diselenide, where their names describe the semiconductor materials used in their manufacture. Gallium arsenide (GeAs) solar cells are also becoming more popular and produce the highest of efficiencies available from

thin film solar cells, but are primarily only used in space applications and are quite expensive in comparison to other alternatives. Information on the performance for GeAs cells is available in Table 1 for comparison purposes.

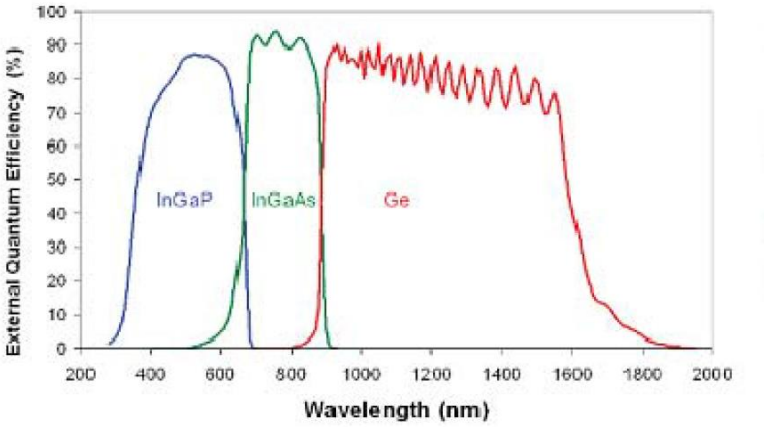

Figure 15: Quantum efficiency of triple-junction solar cells from [3]

Table 1: Confirmed terrestrial cell performance as measured at AM1.5 at 25°C from [5]

Classification	Efficiency (%)	Fill Factor (%)
a-Si	10.1± 0.3	67.8
CdTe	19.6± 0.4	80.0
CIGS	20.5± 0.5	77.2
GeAs	28.8± 0.9	82.7

Amorphous silicon (a-Si) cells are the most mature technology out of the three alternatives and are relatively cheap to obtain, but they operate at a lower efficiency (5-13%) than both cadmium telluride (CdTe) cells and copper indium gallium diselenide (CIGS) cells. Another issue that specifically only affects a-Si cells is the Staebler-Wronski Effect (SWE). While there are a number of different theories as to how this effect occurs, it is commonly believed to be related to the breaking of bonds between silicon atoms in the cells as they are exposed to light, which can result in losses of up to

25% conversion efficiency over time as a-Si cells are exposed to sunlight over a period of months. [3]

Cadmium telluride cells and CIGS cells are, in general more efficient than a-Si cells, with CdTe cells being cheaper to produce out of the two and CIGS cells being more efficient. However, CdTe cells contain more cadmium than CIGS cells, which is a toxic substance believed to be carcinogenic, and research into CdTe cells has plateaued while CIGS cells continue to show improvement.[3]

The efficiency of photovoltaic cells is traditionally determined by comparing a tested cell's performance to that of a reference cell, which a cell of the same model as the tested cell with a known measured efficiency. Comparing performance data between the reference cell and the tested cell allows the experimenter to extrapolate the efficiency of the tested cell. Photovoltaic cell performance is quantified in output via voltage and current. When the PV cell is activated by a light source under open circuit conditions, the voltage produced by that PV cells is referred to its open circuit voltage (VOC). Consequently, there is no current produced by the solar cell under this condition.. Similarly, the maximum current that the activated cell will produce is its closed circuit current (I_{SC}) when the terminals of the solar cell are connected without a load between them. Under this condition, the voltage across the terminals of the PV cell is effectively zero. [6]

Between the conditions of V_{OC} and I_{SC} there exists a point where the solar cell produces it's maximum power, which occurs at V_M and I_M. This point is visualized as a knee in the I-V curve of a characterized photovoltaic cell. This peak power point is the point at which

it is most desirable to have a solar cell operating; however, V_M and I_M will change according to lighting conditions or lighting intensity. The fill factor (FF) of a cell, another important measure of performance alongside efficiency, is the ratio of the maximum power point to the maximum theoretical power formed by the product of V_{OC} and I_{SC}. A higher fill factor implies that the 'knee' in the I-V curve of a solar cell is more defined and, therefore, has a more clearly defined maximum point that is closer to the theoretical maximum power formed by the open and closed circuit conditions of the solar cell.

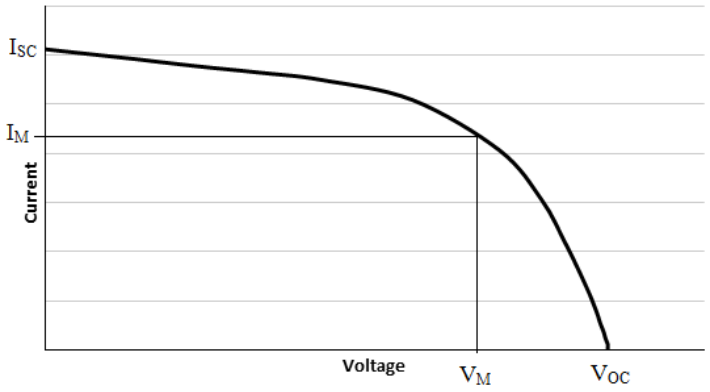

Figure 16: Example I-V curve of a solar cell showing short circuit and open circuit conditions as well as the point of maximum power marked at the 'knee' of the curve

An activated cell can be characterized by placing it into a simple circuit containing a resistance load and adjusting the voltage of the circuit or the resistance of the circuit. The cell's output will adjust depending on the parameter that is being changed. In industry, the voltage of the circuit is usually controlled and the operating current of the solar cell is observed between the conditions of V_{OC} and 0V while the cell is activated by a light source, but care must be taken to avoid exceeding this voltage conditions or possibly reversing the polarity of the voltage and risking damaging the PV cell. Placing a reverse voltage load on a PV cell, referred to as forward bias, is an undesirable but potential condition when PV cells are connected to batteries. Blocking diodes are typically added

to circuits involving PV cells and external voltage loads, to prevent the external load from attempting to charge the PV cells instead of powering a given system. Bypass diodes are also used in multi-cell arrays in order to bypass current around damaged or non-functioning solar cells, which behave like resistors when they are non-functioning and negatively impact performance of the circuit.

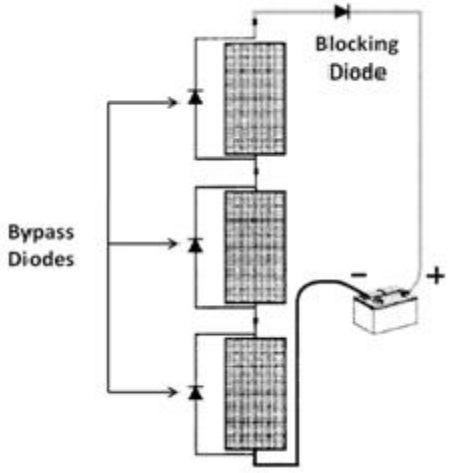

Figure 17: Solar array incorporating blocking and bypass diodes, connected to a battery [3]

Maximum power point trackers (MPPTs) are necessary in order to account for changes in lighting conditions of solar cells because the maximum power produced by a solar cell can vary depending on light intensity and spectrum. A MPPT tracks cell performance and constantly adjusts the load on a solar cell in order to keep the PV cell operating at the knee, or maximum power point, of the I-V curve. However, this means that the voltage and current produced by the solar cell array can still vary. In the case of charging batteries, the power produced by solar cells must be additionally conditioned before being applied to charging using voltage regulation. Both Hurd and Coba utilized MPPTs and DC voltage regulators in their solar power system in order to condition the maximum amount of power out of their PV cell arrays.

While thin film photovoltaic (TFPV) cells are made for flexible applications, they are still susceptible to damage from mild elongation and compression. Specifically, in amorphous silicon TFPV cells, tensile strain greater than 0.7% and compressive strains greater than 1.7% can lead to gradual mechanical failure and, consequently, degradation in performance. At a 2.0% tensile strain, it has been found that a triple-junction amorphous silicon solar cell will suffer an approximate 50% loss in solar cell efficiency. [7]

This mechanical failure of the solar cell in tension is the result of the formation of cracks in the outer layers of the TFPV cell, which restricts electron flow and degrades performance. After the application of higher tensile strains (>0.7%) and the unloading of specimens, it is also possible for cracks formed perpendicular to the direction of the load to relax back into place and reestablish some of the performance lost when the load had been applied.

Thin film photovoltaic cells were adhered to a carbon fiber backing in experiments performed by Maung, K. and the resulting carbon fiber backed TFPVs were tested under both quasistatic loading conditions as well as cyclic loading conditions at multiple strain levels to characterize the susceptibility of solar cells to damage induced by cyclical tensile loading compared to their behavior in static tensile load testing. [8]

Under their quasistatic loading tests, the TFPV cells were bonded to carbon fiber and loaded in tension. Similar to previous studies, no significant degradation was observed in the tested samples until strains exceeded 1.5%. However, degradation appeared to occur at significantly lower strains once the loading was cycled. While cyclical loading of specimens at a strain of 0.3% produced no significant losses in performance, cycled strain

of 1% produced apparent degradation in performance in as few as 5 cycles, and suggested a tendency for further degradation after 100 cycles. In tested samples, the open circuit voltage remained largely unaffected, while short circuit current, maximum power and fill factor showed gradual degradation with an increasing number of cycles. [8]

Preliminary Evaluation

Prior to actual testing a number of preliminary samples were produced using both non-functioning solar cells as well as aluminum foil used to serve as an analogue to solar cells because of its flexibility and similar bonding qualities to composites. A thicker copper foil was also sometimes used in place of aluminum foil, but was not quite as readily available as aluminum foil. These samples were created to experiment with the general processes and procedures of embedding solar cells into composite skins in order to eliminate some of the potentially larger manufacturing defects that might crop up before using real functioning TFPV cells.

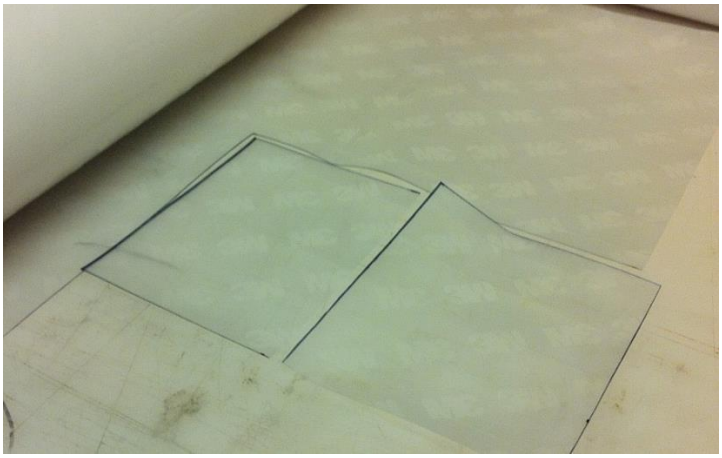

Figure 18: 3M frosted style film, cut from its roll

In addition to some samples being manufactured without a laminate covering, other samples were manufactured with two different types of laminates:

- 3M Polyurethane Film: A flexible, abrasive resistant covering normally used for the leading edges of aircraft, this film possesses an adhesive backing. Samples acquired were a thicker, frosted-finish film and a thinner clear-finish film
- Fiberglass: This composite material is silvery and opaque (depending on weave tightness) until it is wetted with epoxy, at which point it becomes relatively clear. Once cured, this material offers some resistance to abrasion and a significant amount of resistance to in-plane stresses depending on fiber orientation and the type of in-plane loading

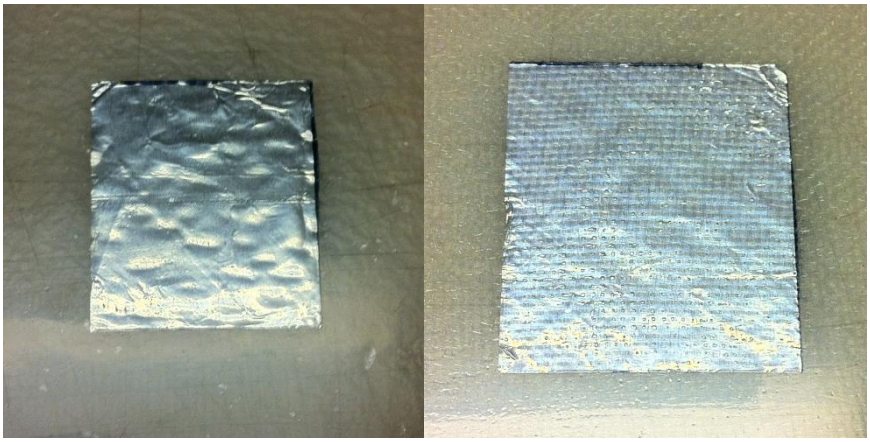

Figure 19: Aluminum sample laminated in 1.4 oz./ sq. yd fiberglass (left) and 9.0 oz. / sq. yd fiberglass (right)

Defects experienced with the 3M Polyurethane Film stem primarily from the method of attaching the adhesive backing of the film to the solar cells. Attaching the dummy cells to the film proved to be unforgiving and difficult. Improper adhesion often results in the production of voids, or air pockets, between the surface of the dummy cell and the film. Attempting to work these voids out of the samples would sometimes result in either damage to the dummy cells themselves or worse surface defects in the film from stretching and wrinkling. The use of water, or even a small amount of dish detergent in solution with water, sprayed onto the adhesive backing of the film before attachment of the dummy cells made the process of adhesion much more forgiving, as the dummy cell could be properly placed and worked free of defects before it became set permanently in

place. Provided the water or water-detergent solution is appropriately cleaned up before integration into a composite wing skin, this method of adhering dummy cells to the 3M Polyurethane film proved to be effective at eliminating defects in samples.

However, concerns still remained as to the potential for water-related damage to the solar cells and composite skin the 3M film covered cells would be attached to, should the water used to attach the cells to the film not be properly cleaned. Water, when introduced to fiberglass, tends to be absorbed by the material. In studies performed by Okeson, impact test samples that were introduced to water post-impact showed a significant degree of increased delamination when compared to test samples that were left dry. If water moistened samples were then introduced to cold extremes of temperature, delamination was even further increased due to the expansion of water molecules in their state transition between liquid and solid. [9]

The adhesion between dummy cells and composites themselves showed a tendency to delaminate easily due to the nature of the smooth, “solid,” surface of the dummy cells themselves. When samples were bent, it was common that the backing layer of the composite skin would delaminate from the cells themselves. It is suggested that, for real uses, an adhesive layer be added between solar cells and the composite skin they are to be embedded into in order to avoid potential issues due to delamination between the solar cells and the composites. Additionally, if water is present between the solar cells and their composite backing, this can result in problems with delamination between solar cells and their composite backings under much smaller normal stresses.

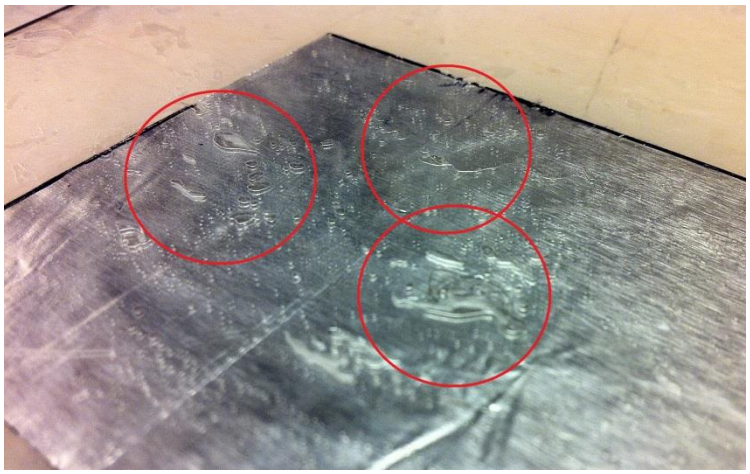

Figure 20: Air bubbles and voids between clear film and an aluminum dummy cell

While the potential for delamination between composite layers and the surfaces of TFPVs remains an issue, it is not expected to produce any structure problems if delamination does not encompass the entire solar cell or solar cell array. Furthermore, delamination between solar cells and composite layers seems to occur only in situations where there are high normal stresses, that is, opposing stresses applied normal to the surfaces of the composite and solar cell, suggesting that the shear strength of the bond between the cells and the composite skin to be stronger, which is the type of loading configuration that would be experienced for the composite skin of an aircraft. Situations of high normal stresses in the skin of a wing, which is the most suitable surface for attaching PV cell arrays to an aircraft, would normally occur during crash landings or unexpected failures, resulting in impact damage to localized points of the wing.

Solar Aircraft Performance

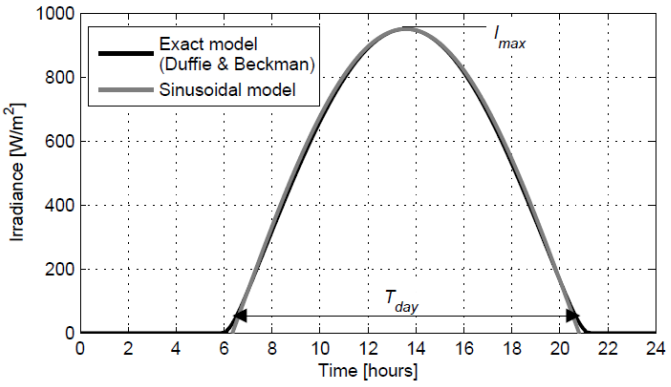

Figure 21: Solar irradiance during daytime conditions as compared with a sinusoidal curve from [10]

While designing, fabricating and testing an aircraft with embedded solar cells lies outside the scope of this research, it is still possible to obtain some basic estimates of performance if a few assumptions are made for flight conditions in order to simplify the estimates. These estimates are important for providing a quantifying value for the impact that the addition of a bank of solar cells and other necessary components might have on the performance of an aircraft. Essentially, the addition of solar cells to an electric aircraft both has the benefit of providing additional power to the aircraft but also the drawback of increasing the overall weight of the aircraft, which can negatively affect its performance.

$$P_{req} = \frac{1}{\eta_P} T_R V_\infty$$

$$\text{where, in steady flight, } T_R = \frac{W}{L/D}$$

The following estimates will focus on the impact that the addition of solar cells to an electric aircraft will have on its endurance for the reasons that 1) the intention of adding solar cells to an electric aircraft is to increase its endurance and 2) the additional weight

of the solar cells and accessories competes with the additional power provided by those solar cells to have either a positive or negative net effect on aircraft endurance. The power required for flight is the product of thrust and velocity. In this case, the required power is additionally a product of the inverse of its combined propulsion system efficiency. The combined propulsion system efficiency is the equivalent efficiency of the normal propulsion components of the aircraft such as the batteries, motor, speed controller and propeller. From the transfer of stored energy from the batteries themselves to the application of that power to rotate the propeller produces a series of small losses that multiply to produce an equivalent efficiency for the propulsion system.

$$\eta_P = (\eta_{battery})(\eta_{motor})(\eta_{esc})(\eta_{propeller})$$

If steady flight conditions are assumed, then the thrust produced by the aircraft is equivalent to the drag that it experiences. The weight of the aircraft, in this case, is the combined weight of the aircraft and its normal components as well as the additional weight increase of the solar cells and their respective additional components (wiring, MPPT, voltage regulator).

$$T = D = \frac{1}{2}\rho V^2 S\left(C_{D_i} - C_{D_o}\right)$$

$$T = \frac{1}{2}\rho V^2 S\left(KC_L^2 - C_{D_o}\right)$$

where $C_L = \frac{W}{\frac{1}{2}\rho V^2 S}$

and $K = \frac{1}{\pi AR}$

A second assumption has to be made for the velocity the aircraft is traveling at. In this case, it is appropriate to assume that the aircraft is traveling at the velocity that will provide it with the maximum possible endurance.

$$V = V_{\max \text{ end.}} = \left(\frac{2W}{\rho S} \sqrt{\frac{K}{C_{D_o}}} \right)^{1/2}$$

The calculation of endurance for an electric aircraft involves the ratio of the product of battery voltage and battery capacity (which is usually in amp-hours or milliamp hours) over the power required for flight minus the power provided by the solar cells. Calculation of the power of the solar cells, in this simplified case, is based on the combined products of the power provided by sunlight, which at AM2.0 conditions is approximately 750 W/m2, the efficiency of the solar cells themselves, the efficiency of the equipment used to apply the solar power to the aircraft (MPPT, voltage regulator), and the area of solar cell coverage on the wing. This estimate for solar power production neglects potential differences in power produced by operation at higher elevations, cloud coverage or incident angles between the sun and the photovoltaic cells themselves.

$$\text{Endurance} = \frac{V_{\text{battery}} \text{Cap}_{\text{battery}}}{(P_{\text{req}} - P_{\text{solar}})}$$

$$P_{\text{solar}} = P_{\text{light}} (\eta_{\text{solar}}) (\eta_{\text{elec}}) (A_{\text{cells}})$$

For the case of a 50 inch wing span, 5.0 lb SUAV, the impact on endurance between increases in weight and increases in cell efficiency can be visualized in Figure 22. It is important to keep in mind that these values are based on a model that does not include

any real mission profile other than loitering, neglecting takeoff, climb and landing sequences and the power that they might consume.

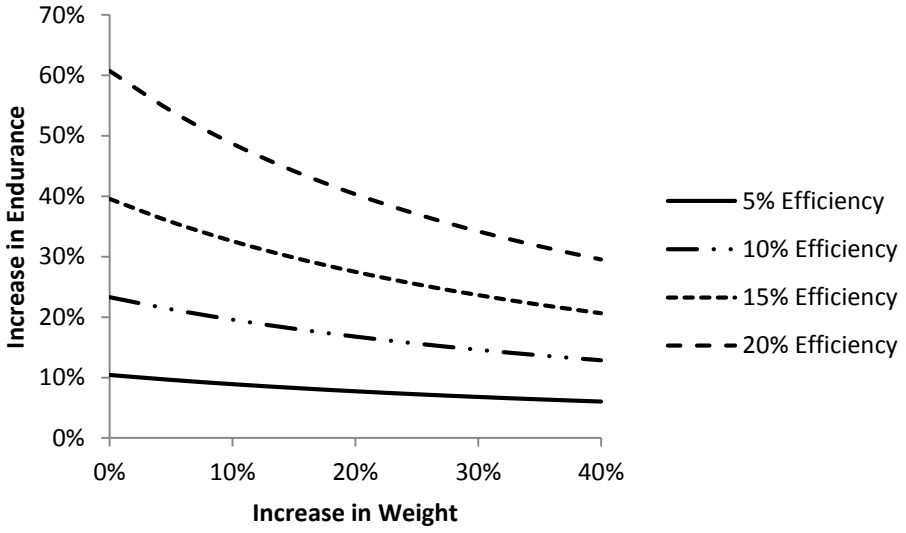

Figure 22: Simplified Estimates for weight and cell efficiency impacts on endurance

The impact that increases in cell efficiency have on aircraft endurance outweigh proportional increases in weigh. Taking a closer look, if an aircraft is 20% overweight after the addition of a bank of photovoltaic cells, a 5% increase in cell endurance is worth a larger increase in endurance than a 5% decrease in weight. However, considering the cost of increasing endurance of solar cells, decreasing weight would be expected to be the economical and therefore favored route toward increasing the endurance of a solar power assisted aircraft.

Table 2: Relative impacts on endurance for increases in cell efficiency versus decreases in weight at 20% overweight conditions

At 120% Weight:

Increasing Cell Eff. by 5% intervals		Decreasing Weight by 5% intervals	
From 0% Eff. to 5%	+7.8% Endurance	From 120% Wt to 115%	+6.6% Endurance
From 5% Eff. to 10%	+9.0% Endurance	From 115% Wt to 110%	+7.1% Endurance
From 10% Eff. to 15%	+10.7% Endurance	From 110% Wt to 105%	+7.8% Endurance
From 15% Eff. to 20%	+12.8% Endurance	From 105% Wt to 100%	+8.6% Ednruance

Some aircraft, such as the Solar Impulse and HELIOS of the ERAST program produce more power from their solar arrays than is required to operate the aircraft. These aircraft are capable of flying as long as sunlight is available at a high enough level of irradiance, and potentially longer if on-board batteries are used to supplement power needs during night time conditions as well as stored potential energy. Maintaining the operating conditions needed for Case 1 to be possible, however, is difficult at lower altitudes due to the potential for poor climate conditions, and operating efficiently under the conditions for Case 1 is more achievable at high altitudes where more power from sunlight is available to the aircraft and climate conditions become much less likely to affect solar performance of the aircraft.

Figure 23, Case 2, describes a condition where the solar power of the aircraft does not meet the minimum power requirements of the aircraft's operation, requiring that additional power be supplemented by batteries in order for the aircraft to remain aloft. Case 2 might apply to a solar powered aircraft that is operating in low-light conditions, or it could apply to aircraft with propulsion systems that are being supplemented or assisted by solar power in order to extend their endurance. This research will focus primarily on

Case 2, using an aircraft that is not designed to fly solely on solar power, but with the assistance of solar power with the goal of extending baseline endurance.

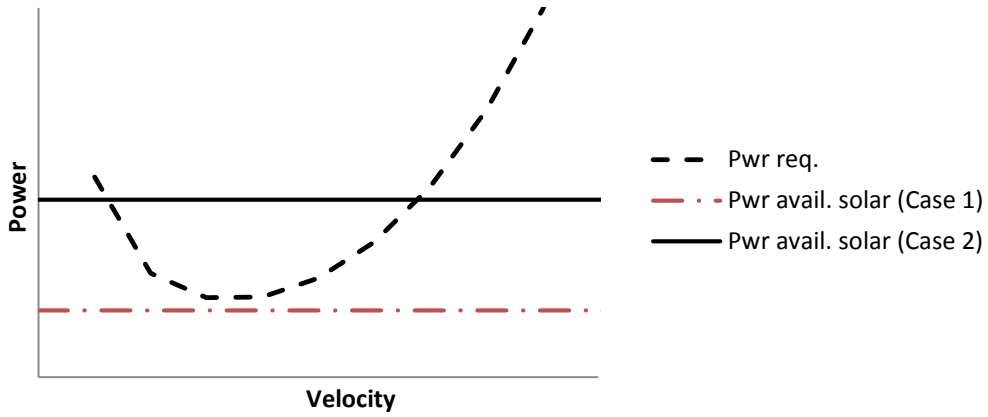

Figure 23: Simplified power required and power available for two conditions of available solar power for aircraft

CHAPTER III

EXPERIMENTAL DESIGN

Composite Layup Processes

Composite materials for industrial applications often come in a form where they are pre-impregnated with epoxy, and are referred to as pre-preg composites. These composites are often cured at higher temperatures and pressures. The composites used for this research, however, come as dry rolls of fabric that are then cut to the rough dimensions of the pieces being created. Epoxies are manually infused into the fabrics during the layup process. These epoxies are made to cure at room temperature, and a vacuum is applied to parts to ensure parts both conform to the contours of their molding surface and that all composite layers are bonded together.

Parting Surface

The molding or parting surface used can vary just as much as the composite materials themselves. For flat, featureless pieces, a flat plate of glass makes a very suitable parting surface, while contoured or more complex pieces usually require the production of a mold. Glass is the primary parting surface used for parts that are cut out from stock

such as composite-laminated plywood or balsa, and molds are used for skin pieces because they can be fabricated to contain complex curves and are durable and strong enough to last for a number of repeated uses.

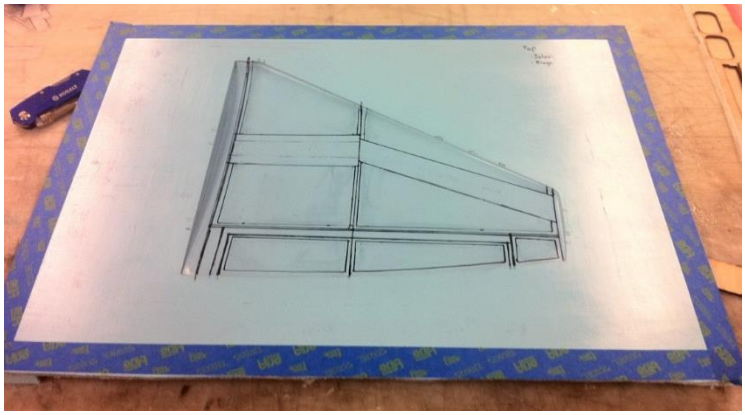

Figure 24: Example of a mold prepped for a composite layup

Composite Fabric and Epoxy

Fiberglass fabric is the primary composite fabric used in both the single cell samples and wings produced in this research. Fiberglass, like other composite fabrics, comes in multiple weights, strengths and weave types. Variants of fiberglass weight, usually measured in ounces per square yard, have different strengths, fiber count and fiber thicknesses associated with them. Multiple weave types can exist for different fiberglass fabric weights, but fiberglass used in this research is primarily traditional weave fabric. Different weaves can produce different behaviors under differing types of stress. Some weaves are more suited for shear, for instance, while others are better adapted for tensile loads.

Figure 25: Various fiberglass fabrics denoted by their fabric weight in oz. / sq. yd

Fiberglass, when compared to aramid fabric or carbon fiber, was chosen as an ideal composite for this research because it is relatively clear when infused with epoxy, and is also an insulator. Aramid fabric, which is traditionally more durable and resistant to rupture than fiberglass, can be somewhat translucent, but not to the same degree that fiberglass can very easily achieve. Aramid was considered for use as a backing for solar cell samples and for wing skins, but is more difficult to work with and expensive compared to fiberglass. Carbon fiber, while traditionally stronger that fiberglass, is also opaque and conductive, making it unsuitable for work in this research because of exposed low voltage wiring.

The epoxy, or matrix, in composites serves as the mechanism by which loads are transferred between fibers in the fabric. In manufacturing of composites in this research, the epoxies used cure at room temperature, so there is no need for high heat devices such as ovens or autoclaves, leaving samples embedded with photovoltaic cells safe from any damage that might come from overheating during the layup process. The epoxies used in this research are also resistant to being conductive. That is, they are only potentially conductive at high voltages. These epoxies come in two different parts, the hardener and

the resin, which, when mixed to the appropriate proportions, produce a chemical reaction that is the curing process. Once mixed, the epoxy is workable only for a limited amount of time before it begins to set up and become sticky and difficult to manipulate. After several hours, depending on the epoxy itself, the epoxy is sufficiently cured that he can be considered dry. However, cure times can vary depending on errors in the mixing proportions of the hardener and resin, relative humidity and temperature. Cure times can be reduced by placing samples in a warm, dry area.

Surface Preparation

Surface preparation for parting surfaces used in this research first involves a thorough cleaning of the parting surface itself. Collected dust and other shop debris can easily foul the finish of the final part after it cured, and care was taken to clean parting surfaces before their use in fabricating new parts. Once the parting surface is clean, agents are added to the surface itself to make the parting process after curing easier and to prevent the part itself from bonding to the parting surface. A few coats of wax are applied to the parting surface followed by a few coats of liquid release, which was dried between layers. The wax layer helps to smooth out small imperfections in the parting surface as well as provide a very thin, protective layer between the part and the parting surface makes it difficult for outside agents to bond to the waxed part. The liquid release is made to peel easily from the parting surface is water soluble so that it may be cleaned or peeled from the cured part itself after it has been removed. The combination of wax and release produces a surface that can free be coated in epoxy-impregnated composites without fear

of bonding between the parting surface and the composites themselves, and allows for composite parts to be removed from their parting surfaces with only minor effort.

Figure 26: A sample of fiberglass as it is infused with epoxy on its parting surface from left to right

Fabric placement and epoxy infusion

Once the parting surface of the layup is prepared, the layup process can be started. In general, this involves the layering of composite fabrics over one another in a predetermined orientation or position in combination with other materials such as wood, foam core or honeycomb. Wood and core materials are normally sandwiched between layers of composites, which increases the specimen's bending resistance in the area where core is applied. This increase in stiffness can also be achieved by adding more layers to the composite layup itself, but core materials can be a more weight-conservative method of doing so, especially when utilized with lighter fabrics that are more flexible after curing.

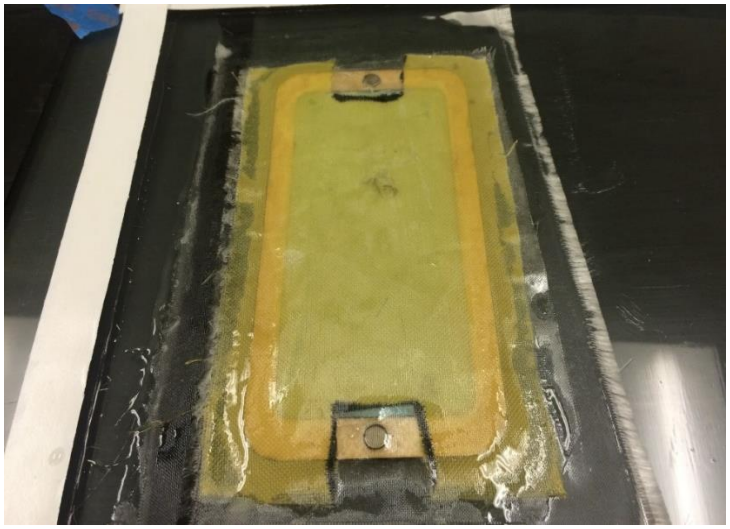

Figure 27: A multi-layer layup specimen before it is bagged and vacuumed to the parting surface

Bagging of layup specimen

After a layup specimen has been properly arranged and prepared on its parting surface, the specimen must often be vacuum bagged in order to ensure that all pieces are bonded together in order to form a contiguous unit. Voids between layers of composites can act as areas of stress concentrations and result in undesirable behaviors when the part is placed under stress.

The bagging process of a specimen involves multiple materials. The material in contact with the curing layup specimen itself will usually consist of a porous plastic referred to as bleeder material. That is, the pores in the plastic are intended to allow excess epoxy and air pockets in the layup to bleed into the next layer of the bagging process, which is referred to as breather. Breather typically consists of a spongy polyester fabric and serves both the purpose of absorbing excess epoxy through the bleeder and distributing the vacuum over the surface of the specimen. In Figure 28, the bleeder in this layup is a sheet

of black trash bag material that has been made porous with a few passes of a spiked roller. The breather is the white fabric that covers the bleeder. To the side of the layup specimen is the medallion where the vacuum hose and pump interface with the parting surface.

Figure 28: Bagging materials; Bleeder is black and porous with white Breather placed on top.

The parting surface itself is bordered by a zinc chromate tape, which is a rubber based adhesive tape that helps to form an air-tight seal around the parting surface and bagging materials and maintain a vacuum on the part. The bag itself consists of a stretchy film that is placed over the rest of bagging materials and sealed around the chromate tape. Once a vacuum is applied to the piece, this bagging film will stretch over the contours of the part and ensure that the piece is held under pressure and bonded together properly. In some cases, the bagging film may not be able to stretch enough to conform to the contours of more complex parting surfaces such as molds for complex parts, and additional slack has to be built into the bagging materials to allow the bagging film to stretch securely into the crevices of the specimen. It is important to establish a satisfactory bagging process for a specimen. The inner surface of the part itself, which is

the surface that is visible when the part is vacuumed to the parting surface, will cure to the contours of the bagging material.

Figure 29: Bagging material is sealed around layup specimen (left) and vacuum is applied (right)

Once the part is cured, which can take hours to days depending on the epoxy used, the vacuum is removed and the part is debagged and pried from its parting surface. Excess material on the outer edges of parts is removed as necessary, and any release film still clinging to the part is later cleaned off with either alcohol or water.

Figure 30: Layup specimen partially debagged after being fully cured.

Small Scale Photovoltaic Cell and Composites Sample Preparation and Testing

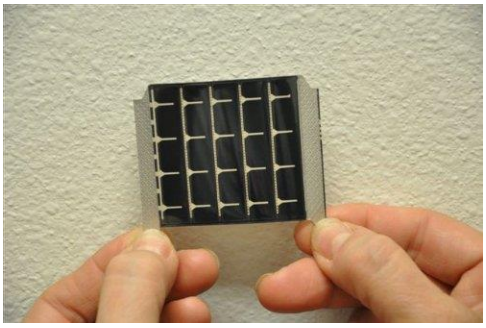

Figure 31: PowerFilm MP3-50 Photovoltaic Cell

The solar cells tested in this research are amorphous silicon cells available from PowerFilm, model number MP3-50. These cells are intended to produce 28mA of current at 3V, tested at air mass 1.5 and 25°C with a claimed efficiency of around 5%. Temperature sensitivity of these cells affects output by -0.2% per degree Celsius above 25°C. The normalized spectral response of these solar cells suggests that PowerFilm cells respond favorably to blue and green light, but not quite as strongly to orange and red wavelengths of light. This is typical of amorphous silicon solar cells, which normally have a good blue response to light but typically fall in red-response performance. Sunlight intensity is claimed to have a much stronger effect on the current output of the solar cell rather than the voltage output of the solar cell. That is, the current produced by the cell will drop substantially from its peak value at lower sunlight intensities while the voltage produced by the cell will remain relatively unchanged until sunlight intensity reaches a critically low point at which voltage produced by the cell will decline rapidly as sunlight intensity decreases further. This suggests that the differences in observable voltage outputs between outdoor tests in sunlight and indoor tests in artificial light may be might smaller than differences in current production under the same conditions.

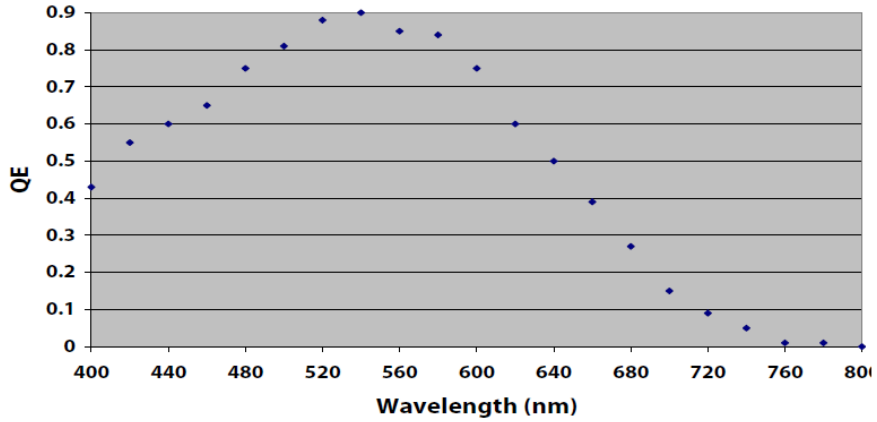

Figure 32: Normalized spectral response of PowerFilm cells from powerfilmsolar.com

These amorphous silicon cells were favored over other alternatives because the nature of the testing conducted in this research is focused more on the affects that embedding processes might have on the performance of solar cells and their durability, and does not necessarily demand a need for higher efficiency and more expensive photovoltaic cells such as CdTe or CIGS cells.The square 2x2" cell area of these cells make them an suitable choice for small scale solar cell testing when compared to alternatives available from PowerFilm that were more rectangular in shape, which may not be as evenly activated by a single source of artificial light in indoor testing. The silver colored tabs at either side of the solar cell are the leads upon which tabs are soldered. Referring to Figure 31, the left terminal is positive and the right terminal is negative.

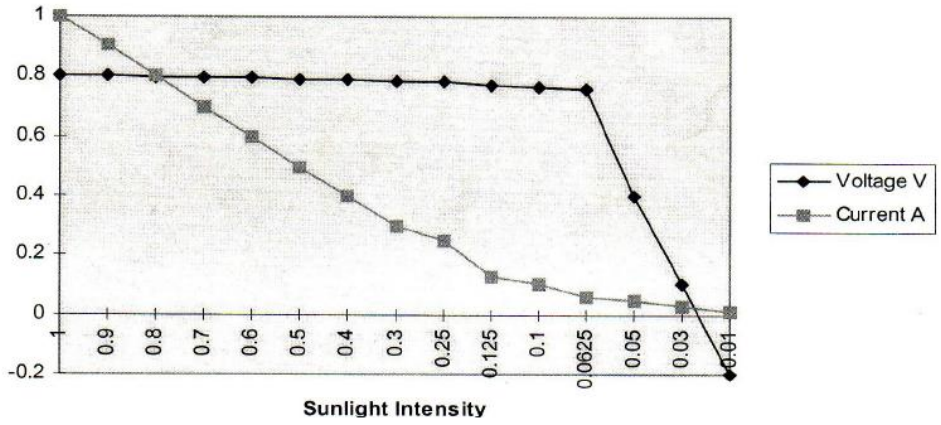

Figure 33: Sunlight Intensity vs Current and Voltage output for PowerFilm cells from powerfilmsolar.com

Single Cell Specimens and Evaluation Strategy

In order to evaluate the impact on solar performance and durability that embedding an array of solar cells into the composite skin of a wing might have on the solar cells themselves, small scale samples containing only single cells were fabricated using different lamination processes and evaluated at different stages of testing. This allowed for solar cell testing to remain on a small scale to be later extrapolated to a larger scale for the consideration of arrays of solar cells that would be embedded into an actual wing.

Three different laminate conditions were tested for the embedding of photovoltaic cells into composites:

1. No laminate – Cells would be left exposed on the top surface of a wing
2. Fiberglass – Cells would be embedded into the surface of the wing under a layer of fiberglass
3. Polyurethane Film –Cells would be embedded into the surface of a wing under an abrasion resistant polyurethane film

Because multiple types of fiberglass and two types of polyurethane film were available to be tested, and different processes of embedding solar cells into composite wings skins could exist for each laminate type, this produced three separate variables for testing:

1. Laminate types
2. The processes used to embed solar cells for each laminate type
3. The different laminate options available for each laminate type

In order to reduce the number of samples required to evaluate each dimension of these three variables, testing for single solar cell samples was divided into two stages:

1. Keeping the materials constant for each laminate type, develop different processes of embedding solar cells into composite wing skins and evaluate them based on complexity, weight and their impacts on the solar performance of single cell specimens
2. Utilizing the favored process from 1 for each laminate type, evaluate the impacts that variations in different laminate options for each laminate type have on weight, solar performance and durability of single cell specimens

The materials used for the first stage of testing would remain constant for each laminate type while the actual process of embedding a solar cell into the representative composite skin would be varied. That is, for solar cell samples that were intended to be laminated in fiberglass, the same weight of fiberglass would be used for all samples while different processes of embedding those cells beneath that fiberglass would be tested and evaluated. The second stage of single cell testing would, in this example, involve varying the different weights of fiberglass while applying the same method of integrating the solar cell beneath that fiberglass layer for each sample.

This strategy would allow for the individual conceptualized processes of embedding solar cells into wings, within the scope of the manufacturing methods discussed in the previous section, to be evaluated separately from the variations in the laminate options themselves by constraining those two variables between stages. The laminate types themselves require fundamentally different processes for embedding solar cells into composite skins, so they cannot be condensed into any single process. Because there are no real variations for the first laminate type, which is no laminate at all, the second stage of testing would focus only on evaluating the use of different materials within each laminate type. For this research, seven different types of fiberglass fabric were tested and two types of polyurethane film.

Table 3: Different types of fiberglass and polyurethane tested

Laminate Type	Weight/Model#	Weight (oz. / yd^2)
Fiberglass	0.7 oz. / yd^2	0.78
Fiberglass	1.4 oz. / yd^2	1.43
Fiberglass	2.0 oz. / yd^2	2.12
Fiberglass	3.0 oz. / yd^2	3.19
Fiberglass	5.4 oz. / yd^2	5.49
Fiberglass	8.6 oz. / yd^2	8.30
Fiberglass	9.0 oz. / yd^2	9.56
Film	3M 8681HS	12.96
Film	3M 8674 (Thin Film)	6.78

For both stages of testing, all samples would be adhered to a 3oz. / sq. yd fiberglass backing that would represent the outer structural layer of fiberglass skin of a wing in which they would be embedded. All potential layers in a wing layup that might lie beneath that outermost layer of structural fiberglass such as core, carbon tow or the inner layer of structural fiberglass would normally vary depending on where the cells

themselves would be placed on the wing skin so they were not included in the backing layer of the single cell samples in order to avoid adding more variables of complexity to the evaluation of encapsulated samples.

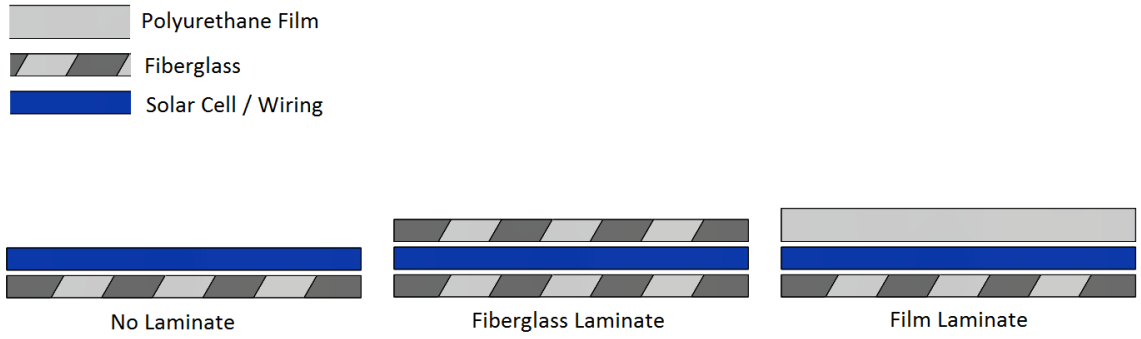

Figure 34: Cutaway examples of the layers for single cell encapsulated samples

Single cell samples without any laminate represent cells that would be embedded directly into the outer surface of a wing. Because the process of adhering the cells and wiring to the skin of the wing is to remain constant throughout all laminate types, this method of embedding a cell or an array of cells has the obvious benefit of producing the lowest weight penalty due to the fact that there are no extra materials or epoxy added for this embedding process other than the solar cells and wiring themselves. Samples with a fiberglass laminate would be cells embedded into a wing beneath a layer of fiberglass. The fiberglass fabric itself is normally opaque in appearance when it is dry, but becomes, for the most part, transparent once it is infused with clear epoxy. It is the hope of this research that embedding solar cells beneath a layer of fiberglass in the skin of a wing will not only provide a seamless integration of the thin film cells into the surface of the wing but also an addition level of protection against impact or abrasion. However, once the fiberglass is scuffed or scraped, it loses some of its transparency. The polyurethane film is an alternative encapsulation laminate to the fiberglass because of its greater resistance

to abrasion and potentially greater level of transparency, but comes as a greater weight and significantly greater cost penalty than the fiberglass itself.

Table 4: Comparing costs of 3 oz. fiberglass to 3M Polyurethane film

		Cost		
Product	Size	Per Roll	Per yd^2	Per / sq^2
3 oz./yd^2 Fiberglass	38in x 36yd	$185	$5.88	$0.54
3M 8674 (Thin Film)	12in x 36yd	$2,112	$176	$19.56
3M 8681HS	12in x 36yd	$2,213	$184	$20.49

While these laminate types have apparent advantages and disadvantages over each other, results from testing will be conducted with the assumption that the choice between the actual use of one of these three laminate types in a situation where solar cells are being embedded into the composite skin of a wing would ultimately be up to the designer based on the application of the aircraft itself. Therefore, no laminate types will ultimately be eliminated, and different laminate material options that are tested for each laminate type (i.e. heavy fiberglass versus light fiberglass) will also not be eliminated from consideration. Instead, these laminate types, their respective material options and their impacts on solar performance, durability and aircraft performance will only be compared.

The First Stage of Individual Cell Testing

The goal of the first stage of single cell specimen testing was to investigate a number of different methods for encapsulating solar cells for each type of laminate. Different methods of encapsulating cells beneath a layer of fiberglass, for example, might yield a greater reduction in the number of voids present between the fiberglass layer and solar cells and hopefully a greater level of solar performance and structural reliability when

scaled up to arrays of solar cells. Each of the methods developed for encapsulation would be evaluated based on weight increase and impacts on solar performance with the idea being that these negative effects would be multiplied when scaled up to arrays of multiple cells embedded into wing skins using similar processes. Increases in weight for different encapsulation processes will, when applied to an aircraft system, have a negative impact on the performance of the aircraft itself. More specifically, increasing the weight of an aircraft negatively affects its endurance, which is both a consequence of embedding solar cells into an aircraft and the primary parameter that is intended to be increased with the addition of solar cells into an aircraft. Negative impacts in the light transmission between a laminate type and the surface of the solar cells can likewise result in reduced additional aircraft endurance due to a reduced output of power from the solar cells themselves.

For all fiberglass samples in the first stage of individual cell testing, the fiberglass weight used was chosen to be 3 oz. per square yard because previous experience with that particular weight of fiberglass had proven that it was reliable and easy to work with because of its high fiber count and tight weave. Handling the fiberglass prior to layup would usually not warp or distort the fiber, which is a potential issue in other lighter fiberglass fabrics, and layups could be performed with more focus applied to the process of encapsulating the solar cell samples instead of being delicate when handling the fabric itself. For all polyurethane samples created in the first stage of individual cell testing, the thicker, frosted finish polyurethane film was used for the various tested processes for the reasons that 1) this particular film was easier to work with than the thinner and less forgiving clear film and 2) the frosted polyurethane film was available in higher quantity

than the clear film, which was available in much more limited supply due to being used in other projects.

For each process tested under every laminate type, three test samples were produced using that encapsulation process. For some fiberglass samples, multiple simple encapsulation methods were combined into more complex processes for testing in later samples.

Table 5: Stage one sample and process list

Laminate Type	Sample Range	Process Used
None	001 - 003	Standard
None	004 - 006	Epoxy Edges
None	007 - 009	Epoxy Clearcoat
Fiberglass	010 - 012	Standard
Fiberglass	013 - 015	Painted Epoxy
Fiberglass	016 - 018	Epoxy Edges
Fiberglass	019 - 021	Sanded, Painted Epoxy
Fiberglass	022 - 024	Epoxy Clearcoat, Painted Epoxy
Film	025 - 027	Standard
Film	028 - 030	Water
Film	031 - 033	Epoxy

A detailed overview of each of the embedding and encapsulation processes tested is provided. Processes described as ‘normal’ are the baseline processes for embedding and encapsulating cells using each laminate type, while all methods that follow are simply variations on that baseline process.

No Laminate:

- Standard – cells are placed onto the prepared parting surface without any additional processing added before the backing layer of fiberglass is applied

- Epoxy Edges – cells are placed onto layup surface and epoxy is brushed along the edges of the cell to create a smooth transition between skin and the edges of the solar cell after curing
- Epoxy Clearcoat – A thin layer of epoxy is painted on the layup surface and allowed to partially cure. The solar cell is placed over the partially cured layer of epoxy.

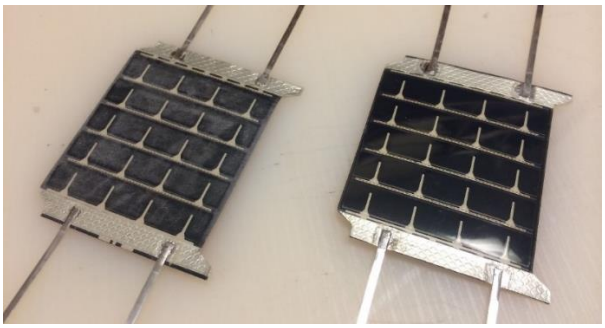

Figure 35: Comparing a lightly abraded cell and unmodified cell

Fiberglass:

- Standard – cells are placed onto a layer of fiberglass impregnated with epoxy, and then a backing layer is added
- Epoxy Edges – epoxy is brushed along the edges of the solar cells to remove any gabs between the edges of cells and the encapsulating layers of fiberglass
- Painted Epoxy – a thin layer of epoxy is painted onto the surface of the solar cell before it is placed over the encapsulating layer f fiberglass in order to reduce the number of surface flaws, which primarily consist of small pockets of air trapped between the solar cell and fiberglass laminate
- Sanded, Painted Epoxy – In addition to the Painted Epoxy process, the laminate that the solar cell is manufactured with is lightly sanded with the intention of increasing the adhesion between the surface of the solar cell and the fiberglass laminate and reduce the likelihood of delamination between the two surfaces when the laminate is placed under load. The

PowerFilm cells used in this research have a protective film coating, and care was taken not to sand through this coating into the solar cell material itself

- Epoxy Clearcoat, Painted Epoxy – A thin layer of epoxy is brushed on the layup surface and allowed to partially cure prior to layup taking place. This step is intended to ensure that a clear surface finish is applied to the fiberglass laminate layer

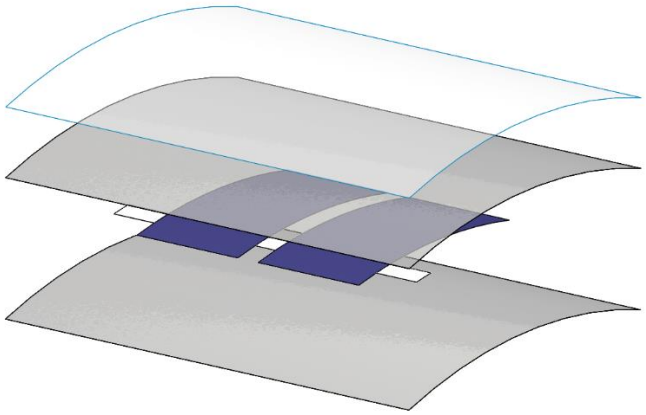

Figure 36: An exploded view of the 'Epoxy Cleacoat, Painted Epoxy' process showing the layers of the process. Layers from top to bottom: Epoxy clearcoat, Fiberglass Laminate, Solar Cell, Fiberglass backing

3M Film:

- Standard – Before layup, the cell is placed on the 3M film and all possible air pockets are carefully worked out via a plastic squeegee
- Water – Water is sprayed over the adhesive backing of the film before the solar cell is worked into the film in order to reduce visual defects and reduce the difficulty of placing the cells onto the film.
- Epoxy – Epoxy is painted over the surface of the solar cell before it is adhered to the film backing. This is done during the layup and any excess epoxy squeegeed out from the edges of the cell is worked into the fiberglass backing.

Second Stage of Individual Cell Testing

This stage of cell testing was performed after a suitable process of encapsulation was settled upon for each laminate type. This time, keeping that desired encapsulation process constant, the material varieties of each laminate were varied to characterize their performance impacts on photovoltaic cell output, additional weight and durability. In this case, since there were only two polyurethane films tested and one of them had already been tested in stage one, there was only one set of extra samples to encapsulate using the other film. Similar to the first stage of cell testing, three samples per laminate material were tested and fabricated. The 3oz. yd^2 fiberglass backing was repeated for these samples.

Table 6: Specimen list stage two of single cell testing using various fiberglass materials

Laminate Type	Sample Range	Laminate Material
Fiberglass	101 - 103	0.7 oz / yd^2
Fiberglass	104 -106	1.4 oz / yd^2
Fiberglass	107 - 109	2.0 oz / yd^2
Fiberglass	110 - 112	3.0 oz / yd^2
Fiberglass	113 - 115	5.4 oz / yd^2
Fiberglass	116 - 118	8.0 oz / yd^2
Fiberglass	119 - 121	9.0 oz / yd^2
Film	122 - 124	3M 8674 (Thin Film)

Processing of Individual Cell Samples

Photovoltaic cell specimens for small scale, individual cell testing were produced by first soldering tabs to individual cells. These tabs consisted of 2mm wide flat tin plated copper wires, obtained as part of a DIY solar cell tabbing kit along with w wider 5mm bus wire that is used when multiple cells are connected in parallel to form an array. These tabbed

cells were then characterized for their performance under an artificial light source, three times per cell, to establish the baseline performance of each cell prior to any modification.

These single cell test samples, once initially characterized, were then weighed and encapsulated in their pre-designated layup process with prepared materials. Flashing and excess material from the layup process was trimmed once specimens were cured and all samples were weighed again and characterized once for I-V response under artificial light in order to gain comparative data of performance before and after encapsulation. All samples were trimmed to the same size, thus allowing for the possibility of detailed weight breakdown of both the materials and epoxy used for each sample.

Solar Cell Testing

Solar cell testing in this research involved evaluating the I-V curve of a solar cell by changing the resistance of a simple circuit connected to the solar cell as it was activated under a light source. Choosing a light source was based around the goal of achieving conditions that were 1) repeatable and 2) produced a low or consistent amount of heat over the test period. While sunlight remains as the optimal choice for testing the output of a solar cell, it is difficult to reproduce sunlight conditions over a period of weeks of testing, and testing sessions would be entirely dependent on favorable weather. Because cells would need to be tested before and after layup periods, which could happen days or weeks apart, it was necessary to produce an experimental setup that would have the ability to reproduce the same light consistently, even if that light source may not have the same output as the sun. It was for this reason that it was necessary to develop an indoor

test setup and procedure with an artificial light source that could meet those qualifications.

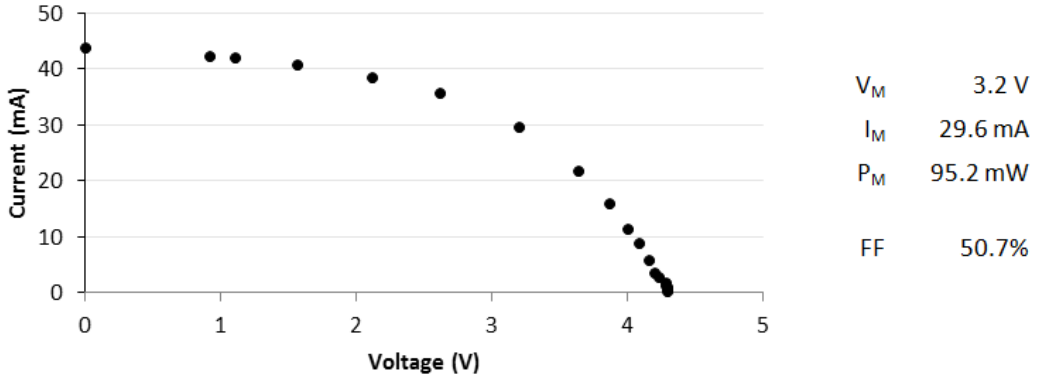

Figure 37: MP3-50 single cell output tested during clear, sunny conditions

The acquisition of a solar simulator lay outside of the available budget for this research, so a custom light source confinement would need to be fabricated around a chosen light source. While filtered xenon lamps are ideal for their more accurate representation of the solar spectrum at AM1.5 conditions, xenon lamps are both expensive and require routine maintenance. As an alternative to xenon arc lamps, quartz tungsten halogen lamps have been evaluated to provide similar performance with <2% error in other solar cell tests [11].

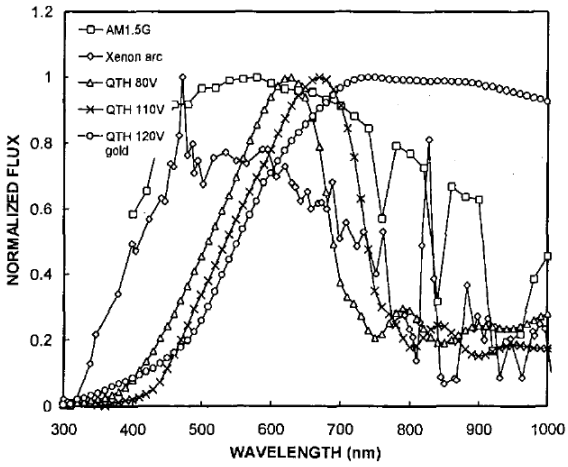

Figure 38: Normalized flux comparing sunlight, xenon arc lamp and QTH light sources

In addition to halogen light sources, LED light sources are an attractive alternative for their high brightness and low heat production. However, there was significant concern that an LED lamp may not produce equivalent or better activation results from a solar cell when compared to a halogen lamp because its spectrum is limited to the types of LEDs it contains. Commercial, off the shelf light sources remained preferable as opposed to custom operated light sources because of the ease of replacement should light sources be damaged. It was possible to custom-fabricate an LED lamp to tailor it to the desired spectrum, but the ease of purchasing an off-the-shelf unit was more appealing due to the fact that reproducibility of the response of tested solar cells was more important than matching the output with that of the sun.

The goal of testing the cells used this research was to achieve a high level of reproducibility in results. That is, that, under similar temperature conditions, the I-V curve produced by a cell would need to have minimal variations in results of tests performed days or weeks apart. Based on this goal, the desired qualities of tested light sources are:

1. Reproducibility in light output over short periods of time
2. Minimal increases in temperature over a test period
3. High power output from test cells

Increases in temperature can result in an overall loss in efficiency for the PowerFilm cells being tested in this research, reported to be -0.2% per degree Celsius above 25°C. For this reason. It was unknown at this point how small variations in cell performance might be when compared before and after encapsulation, so consistency in test results was necessary. While the actual decreases in performance are small for each degree Celsius, it

was entirely possible that differences of over 10°C could be seen over one period of testing for light sources that run particularly hot which could potentially result in a loss of 2% efficiency.

Equipment and Basic Setup

As stated previously, cells will be tested by varying resistance in a simple circuit connected to the solar cell. This will be achieved using a decade resistance box rated to 1W of power. Due to the low power produced by the PowerFilm cells tested, it was not necessary to utilize any higher power circuitry or resistors. For this reason, low current multimeters instead of clamp-meters were utilized for measuring both current and voltage passing through the circuit.

Outside of the solar cell circuit, light was measured using a vernier light sensor measuring luminous flux, or lux, which is based on the visual brightness of a light source rather than the energy produced by that light source. A K-type temperature probe, also attached to the vernier measurement hub, was also implemented for measuring the temperature of cells before and after test completion.

Choosing a Light Source

Two types of light sources received the majority of focus during the process of choosing a light source for single cell testing: halogen lamps and LED lamps. Halogen lamps seemed to be an ideal light source for simulating sunlight in place of the more expensive Xenon lamps, and were available off-the-shelf in the form of high power flood or stage lights. An LED light source was also an attractive alternative because of their relatively

low operating temperature and expected steady-state operation. The chief concern of halogen light sources was their high heat production while the mismatching spectral distribution of off-the-shelf LED light sources compared to sunlight remained a concern for those light sources.

Three different lamps were purchased for testing as potential light sources for single cell testing:

1. 24W LED Lamp
2. 500W Halogen Flood Lamp
3. 1000W Halogen Studio Lamp

The 24W LED light source was commercially available from Lumiram as part of their Chromalux full-spectrum series of LED light sources. With a beam angle of 25 degrees and a color temperature of 6000k, producing a cool light compared to the more yellow hued light of lower color temperature sources such as fluorescents and floodlights, and mimics the color temperature of sunlight. This lamp fits into traditional Edison Screw base fixtures, and was chosen for the ease with which it could be built into an experimental apparatus. The narrow beam angle was ideal for single cell testing, and was intended to focus the intensity of light onto a small area for single cell testing as it was unnecessary for that light to be spread over a wider area.

Figure 39: The 24W LED Lamp

The group of LEDs within this light source is spread evenly over a diameter of approximately 3.25in and the distribution of light intensity was, as expected, narrow due to the low beam angle. At 5.75 in from the face of the lamp, the area of high intensity illumination has a diameteter of approximately 5.80 in. In the case of an array of cells, this light source would be unsuitable for testing, but in the interest of single cell testing this small area of high intensity light for cells measuring approximately 2 by 2 inches is suitable. Claimed brightness of this lamp was rated at 1650 lumens. By integrating the measured light intensity of this lamp, the measured brightness of this lamp was closer to 852 lumens at a resolution of 0.5 inches between measurements measured over a radius of 6 inches from the center of the light source at 5.75 inches away from the light source. Further distances from the center of the light source lay outside of the beam of the lamp and had only negligible light intensity.

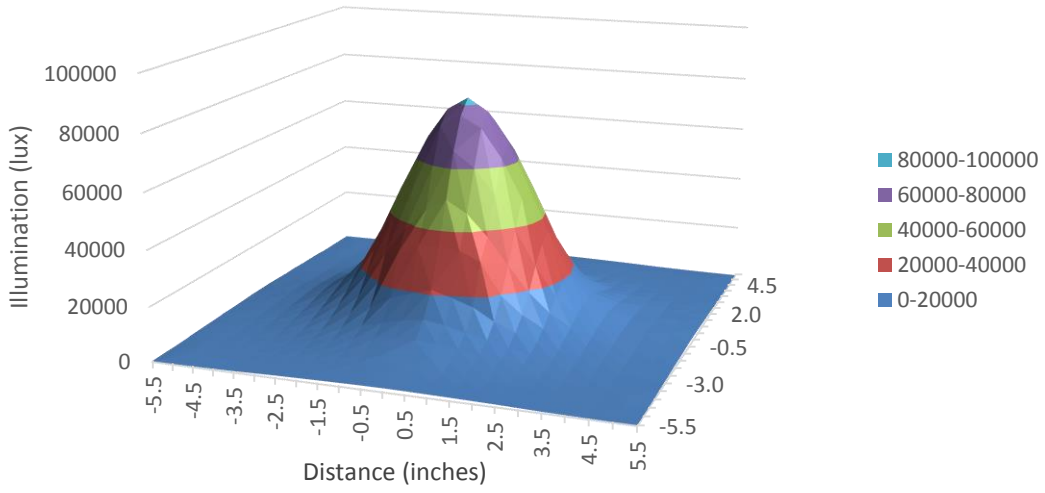

Figure 40: The distribution of light intensity of the 24W LED Lamp

Temperature produced by by the light emitted from this lamp was relatively low but still noticeable. The temperature of the bulb itself, when enclosed within a can fixture, would

become hot to the touch over an extended period of operation, but not as quickly as fluorescent or halogen light sources.

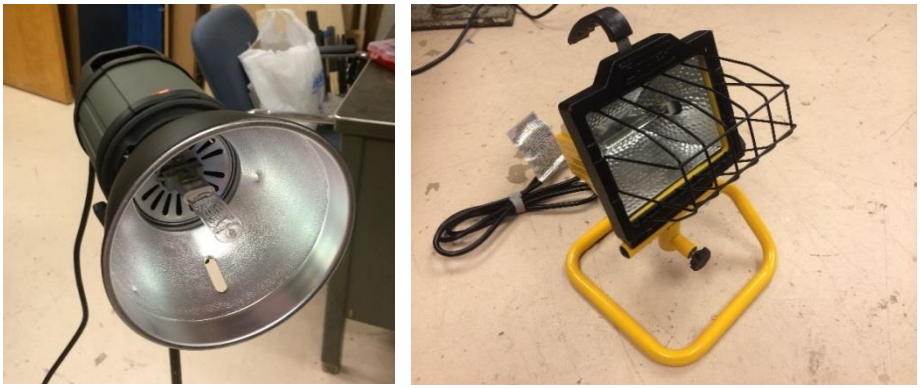

Figure 41: 1000W halogen studio light (left) and 500W halogen flood light (right)

The halogen light sources considered in this research were of two different styles. The 500W flight lamp was purchased along with a quartz tungsten bulb and a generic bulb was used for the 1000W halogen studio light. The color temperature of halogen lamps is usually closer to around 3000k, producing a warmer hued light. Light intensity distribution for these light sources was much broader, with higher levels of brightness further away from the center axis of their respective bulbs. This results in an overall greater brightness from the halogen lamps over the entirety of their usable area, but perhaps not as much brightness as the LED lamp when integrated over the area of the MP3-50 PowerFilm cells due to the lower level of light intensity produced at their respective points of focus. The total brightness of the 500W QTH lamp was 6076 lumens over an area of 28x22” measured 12 inches away from the light source.

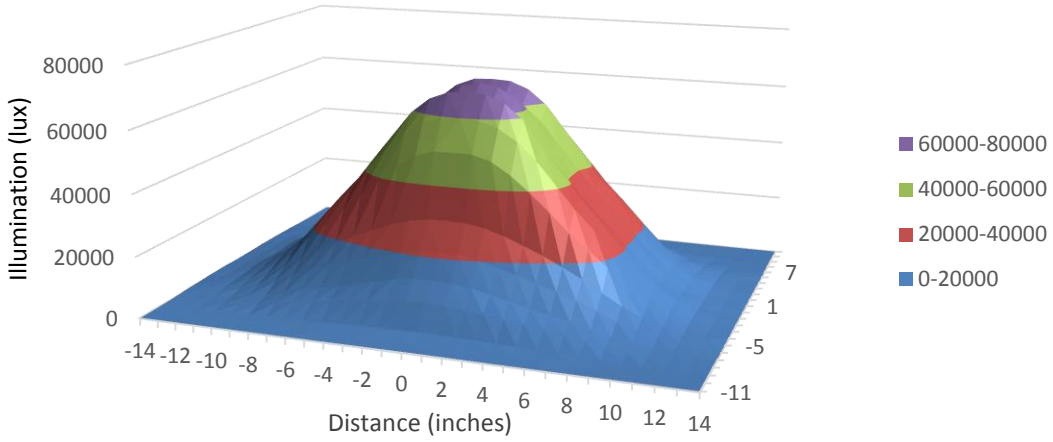

Figure 42: Distribution of light intensity produced by the 500W halogen flood lamp

Similar results of lower intensity were produced by the 1000W stage light. Surprisingly, the maximum brightness at the center of the studio light was lower than both the 500W halogen flood lamp and 24W LED lamp. However, the drop-off of light intensity produced by the studio light was much more shallow than either of the two other sources with a comparatively high 5447 lumens of brightness at 12 inches within a 23 inch radius of the central axis of the light source. While the flood light and studio light would both be suitable choices for testing large arrays of solar cells, the focus of this apparatus was to test single cells. If each light source is evaluated only over the area of a test specimen, which is approximately 4 in^2, then the visible brightness seen by a photovoltaic cell for each light source follows.

Light intensity over cell sample area:

- 24W LED Lamp - 563 lumens
- 500W Halogen Flood Light –874 lumens
- 1000W Halogen Studio Light – 185 lumens

The 500W halogen flood lamp appears to make an ideal choice for single cell testing based on brightness alone, but it was still noted that the brightness of the 500W halogen

lamp came at a cost of significant temperature increases over the area illuminated by the lamp.

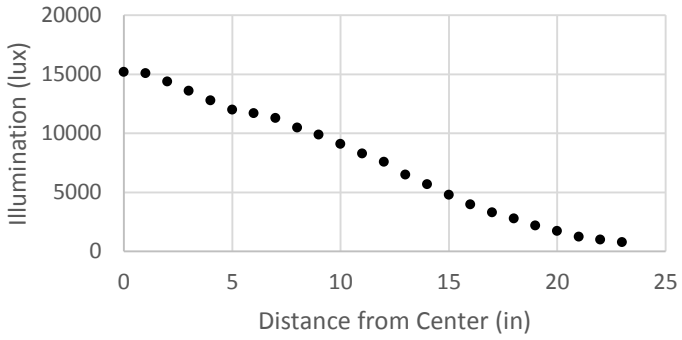

Figure 43: Light intensity versus distance aray from the center axis of the 1000W halogen lamp

The brightness of each light source also could not be presumed to directly correlate to a greater response from the tested cells. Light intensity measured from the halogen light sources overtime seemed to have a habit of increasing over the first minute or so of illumination, then slowly decrease again beyond that point. Over a testing period for a photovoltaic cell, which could last 2 to 3.5 minutes, this increase and decrease in brightness as well as the relatively high amount of heat produced by the halogen light sources might make them less attractive for single cell testing than the LED lamp, which produces very little heat and seems to only decrease in light output gradually as temperature of the lamp itself increases.

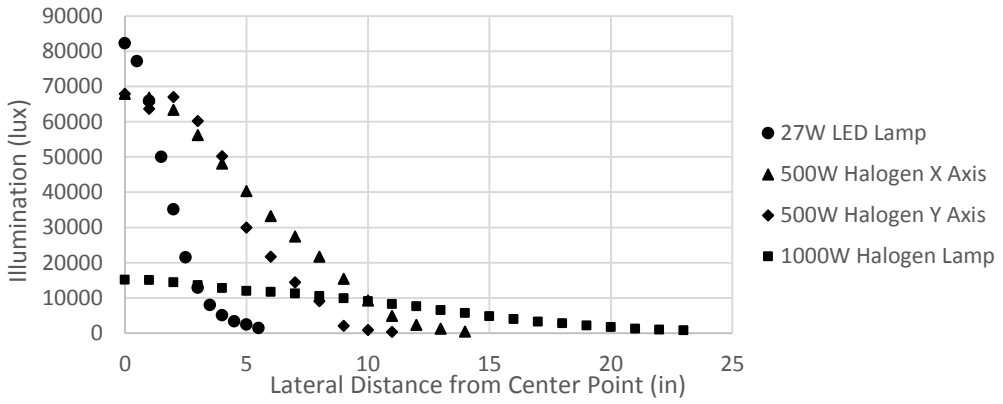

Figure 44: Comparison of the light intensity of each light source as distance from the central axis is increased

Evaluation of each light source will be based around their performance paired with solar cell performance over a period of a number of photovoltaic cell tests. For each light source, three separate cell-tests were performed, measuring the I-V response curve between short circuit and open circuit conditions as well as the temperature of the cell and light output of the light source both at the beginning and end of each test. Tests were timed on a stop watch, allowing for a comparison to be drawn for temperature increases and any decreases in light output from each light source. Each test was performed with the cell starting at room temperature.

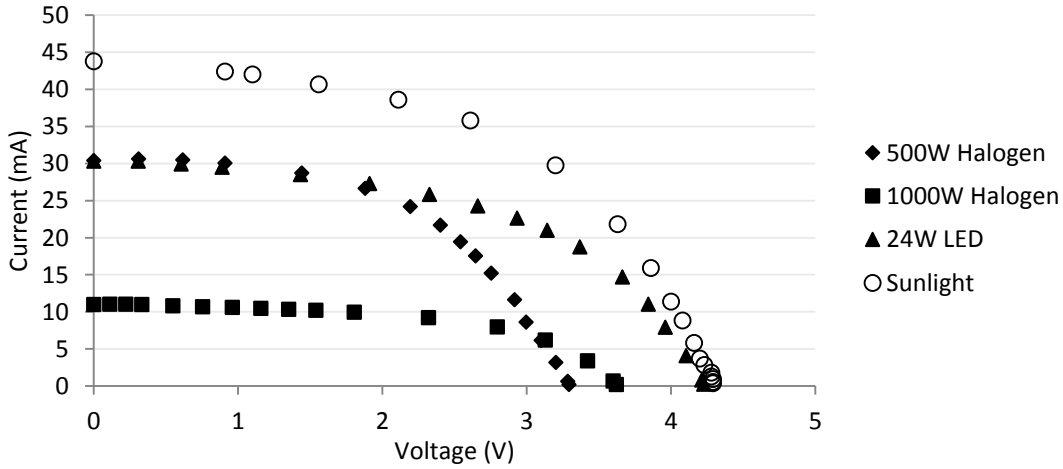

Figure 45: I-V response curves for all three tested light sources

Based on the I-V response curves of each light source when tested with a MP3-50 cell, the 24W LED seems to show the more favorable response despite some slightly higher currents produced by the 500W halogen lamp at lower voltages. Tests progress from low voltage to high voltage, so temperature of the cell will increase as voltage increases due to time of the test progressing. Based on Figure 33, the voltage output of the cell would be expected to match the voltage produced under the 24W LED lamp based on the I-V curve behavior at lower voltages. It was suspected that the I-V curve's distinct low voltage output beyond the 2V point for the 500W Halogen bulb are due in part to the large temperature increase seen by the test solar cell over the course of each test. For example, the temperature of the test cell was at 143°F at the end of one test when it had started at 76.5°F, which is a significant enough increase in cell temperature that a decrease in performance is expected. Such a temperature actually lies at the borderline of the tested operating temperature of the MP3-50 PowerFilm cells, and may cause wearing effects in the amorphous silicon cells themselves to potentially be accelerated.

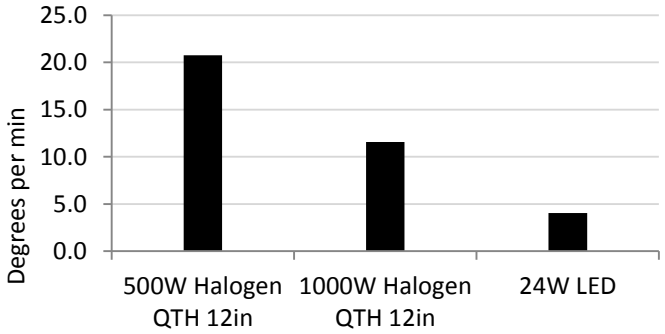

Figure 46: Temperature increase per minute of test cells when illuminated by each light source

The 24W LED, by comparison, produced a higher level of output from the MP3-50 PowerFilm cells than both the 500W or 1000W halogen bulbs with a lowest increases in temperature over testing period. However, the 24W LED lamp does possess a decrease in

brightness over time to that of the 500W halogen lamp, but some modification of the fixture it is contained in could yield some greater cooling potential as well as more consistent light production. The 24W LED remained as the most ideal light source for single cell testing. The consistency between results for I-V output of cells is greater for the LED light source, possibly due to lower heat and light output variations.

Table 7: Table of other measured parameters, including standard deviation in measured voltage and current fore different tests in each light source

	P_{MAX} (mW)	FF	$V_{Std.\ Dev.}$	$I_{Std.\ Dev.}$	Ill.(lux)
500W Halogen	53.10	0.53	2.89%	1.78%	62960
1000W Halogen	22.29	0.56	1.90%	1.54%	21518
24W LED	66.42	0.52	0.40%	0.74%	55618

Based on the 24W LED's favorable results in cell response, low temperature increase and result consistency between tests, the 24W LED lamp was chosen as the ideal light source for indoor testing with some modifications to further reduce increases in temperature, which was expected to both increase consistency with test results and decrease the gradual decay of light output over time.

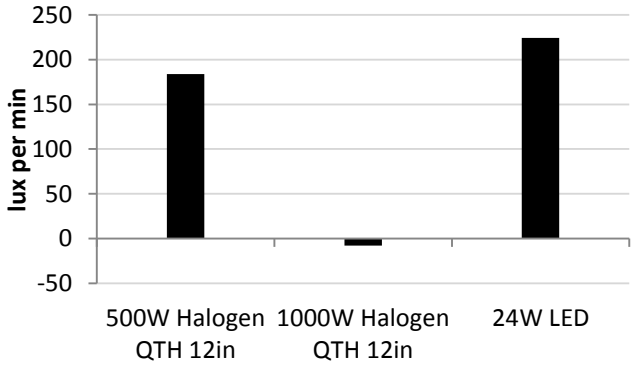

Figure 47: Decrease in lux per minute for each tested ligth source based on light intensity measured at the beginnig and end of a cell testing period

Single Cell Testing Apparatus

Figure 48: LED Lamp within its fixture, the initial iteration of the light box

The 24 LED fixture was built into a box made of MDF boards with its inner surface painted white to provide as much light saturation as possible inside the box. This initial iteration of the light box possessed a couple of known issues: 1) The lamp itself shift within its fixture unpredictably, which sometimes produced undesired variations in cell tests, and 2) the work surface and the lamp itself could become warm over a series of tests, resulting in unwanted variations in test results.

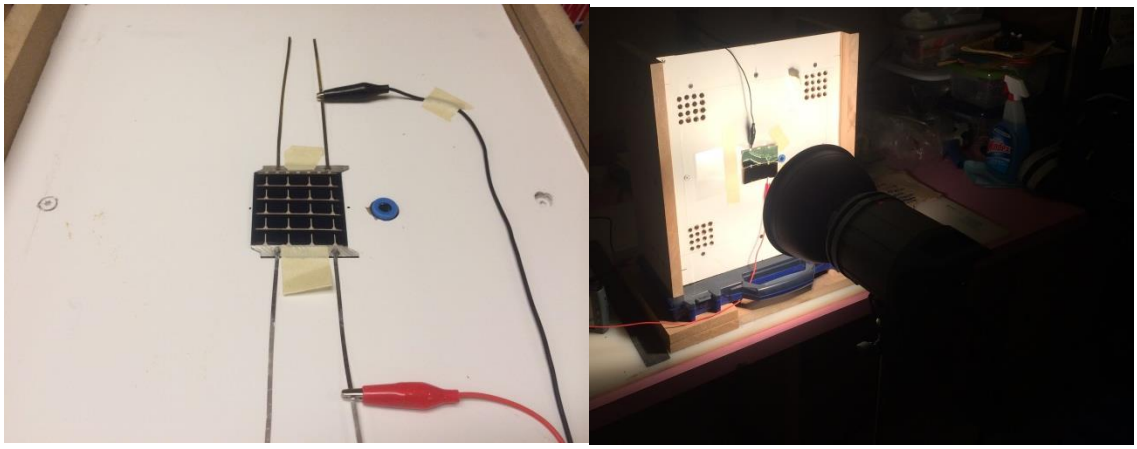

Figure 49: Left: The test surface with light sensore mounted displaced to one side. The bead-tip thermocouple touches the back surface of the cell. Right: The test platform with a mounted cell under activation by the 1000W Halogen Studio Light

The second iteration of the light box contained a separator at the face of the lamp that would restrain its movement, as well as a DIY cabinet cooling kit with mounted USB powered fans that would pull cool intake air through holes in the test platform through the heatsink fins in the lamp with the help of the wooden separator. This was expected to help keep the lamp cool and cycle the hot air contained within the lit chamber of the light box out and replace it with new cool air during operation. The fans were powered separately from the LED lamp itself, and could be kept running between tests in order to cool the lamp when it is turned off.

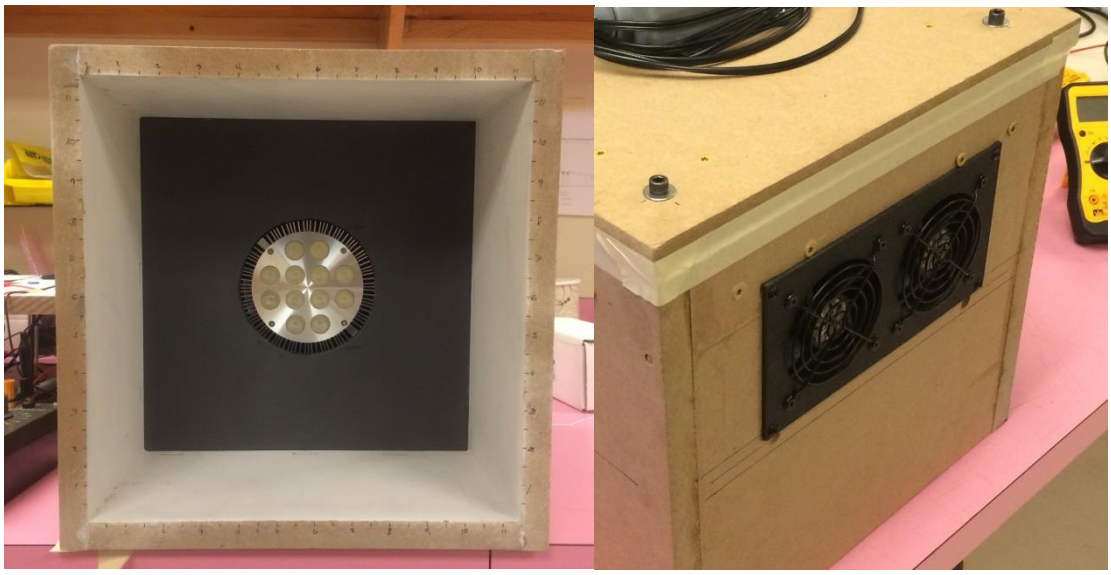

Figure 50: The inside of the corrected light box, showing separating plate (right) and the air-cooling system (left)

Test results after modifications to the light box seemed to confirm that the lamp would experience a decreased amount of heat increase, which had the benefit of slowing the decay of light output over time and producing more consistent results from cell testing.

Figure 51: Cell testing apparatus with light box, test platform, multimeters, decade resistance box and vernier datalogger connected to thermocouple and light intensity sensor

Structural Testing

The goal of the structural testing of this research was to examine and compare the structural integrity of the single cell samples once they had been characterized and evaluated for solar performance. Static out of plane testing was decided upon as a good representative of the type of loadings that might cause embedded solar cells or arrays to fail as opposed to tensile testing. Impacts with objects, drops, or damage from mishandling are common sources of damage for the wings of an SUAV when it's being assembled, disassembled or landing. Out of plane stress testing, primarily intended to simulate those types of impact failures under static conditions. Composite wings for SUAVs are often overbuilt when they are fabricated; meaning that, unless the SUAV is expected to experience particularly high loadings during normal flight, the skin and structure of a wing is usually considerably stronger than the flight loadings would normally require. This is because the handling of the wings is usually considered to be more stressful and a more likely source of damage to the skin and structure of the wing

than aerodynamic loading, and has a high potential for accidents. Taking this into consideration, the tensile or shear loadings experienced by an aircraft's wing skin during normal operation will normally be quite small compared to the limitations the wing itself was built for. Tensile testing simulates static loadings which are most similar to distributed aerodynamic loadings in this case, and tensile failure is a less likely condition of failure compared to impact which is more likely to result in damage to the solar cells.

The variation of laminate materials, particularly for fiberglass, was believed to provide different levels of protection against impact or puncture. A light 0.7 oz. / yd2 fiberglass laminate should be much weaker in impact testing compared to a heavier 9.0 oz. / yd2 fiberglass laminate. While it is expected that there will be a greater impact to solar cell and aircraft performance when an array of cells is encapsulated beneath a layer of heavy fiberglass, it's still possible that the additional structural protection of that fiberglass might justify its use as a laminating material if the aircraft is being operated in conditions where crashes or crash landings might be more likely.

These out of plane static loading tests will be conducted using the samples fabricated from the single cell testing phase of research. Samples will be placed into a holder that restrains them from moving to simulate the rigid surface of the skin. While there are other layers of composite materials normally placed beneath the outer layer of the skin surface, those materials can vary and it is simpler to neglect the use of other structural materials in order to evaluate the strength of each sample on the merits of its outer laminate material and its backing material.

Samples will be restrained in and a point load will be applied in their center using a rounded tipped tool. As the material is deflected, the resulting resistance force will be measured and plotted with the deflection. Due to the complexity of the composites, the adhesion between layers and the way in which a point load can affect a composite layup when applied out-of-plane, multiple different types of failures are anticipated as a result of these deflection tests. However, absolute failure of the tested encapsulated solar cells is not intended. The goal of these static loading tests is focused more on showing the relationship between laminate types and durability. That is, the intention of these tests is to compare the additional strength that different laminate types provide over one another.

A number of samples using different laminate materials will be tested and compared for their strength in out of plane load resistance. Each static loading test will run from unloaded conditions to a set deflection point, at which the specimen will be unloaded, inspected post-test and have its cell performance evaluated in the photovoltaic cell testing apparatus. Any visible damage to the sample will be recorded, including:

- Rupture of fibers
- Delamination
- Visible disturbances in different sample layers
- Crack formations in photovoltaic cell surface

Cells will be reevaluated for their response under light, and results will be compared with response data gathered before the cells were placed under load. It was important to keep in mind that damage made to the cells during the test may mend themselves to a certain degree when the samples are unloaded, similar to the partial return of performance in cells that have been elongated to strains greater than 1.6% and then relaxed again in static

tensile testing. Because samples will be relaxed before being evaluated after testing, it's possible that performance results may indicate less damage to the performance of the photovoltaic cell than there actually is.

Static Loading Apparatus

Samples from single cell testing will be restrained by a pair of aluminum plates and a rubber gasket material that is intended to hold the parts rigid. The plates will hold each specimen by its fiberglass border, with a "window" in the middle of the restraining device where the sample can deflect freely. The tool used to apply pressure to the samples will be a 5/16 inch rod with a slightly rounded tip, the size of which seemed appropriate for the size of objects that might be involved in a collision such as tree branches, the corners of rocks or from mishandling.

The actual testing will be performed using an Instron 5966 equipped with a 10kN load cell, so that deflection of the tool and the responding force against the tool can be accurately measured. The other load cell that was available for testing was a 100N load cell, but preliminary tests using a dummy specimen indicated that the 100N load cell would become overloaded before the desired amount of deflection would be achieved, even for the weakest of samples.

Wing Construction

The wings built utilizing the methods evaluated in single cell testing are built in 3 major parts:

1. Top skin

2. Internal Structure
3. Bottom skin

For wings with cambered airfoils, the top and bottom skins will be different in shape, where the top skin represents the upper surface of the airfoil conforming to the wing planform and the bottom skin represents the lower surface of the airfoil conforming to the wing planform. For this research, the wings constructed used symmetrical airfoils for the purpose of simplifying construction. That is, the top and bottom skins are mirrors of one another, and there would be no real distinction between top or bottom skins.

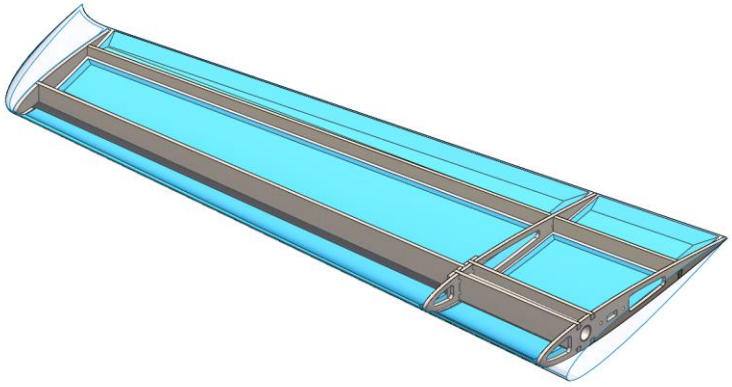

Figure 52: Wing model cutaway, showing structure inside skin

The skin in a composite wing of this construction performs several structural tasks

1. Maintains airfoil shape of the wing
2. Resists torsional forces along the spanwise axis
3. Resists and transfers bending forces along the spanwise axis to the internal structure

The internal structure also maintains the airfoil shape, but only in such a way as to act as a supporting member to the skin. Otherwise, the internal structure serves to work in tandem with the skin to resist bending forces. There are different methods for

constructing the internal structure of a wing, such as using composite c-channels for structural members, but composite laminated plywood and balsa wood serve as appropriate inexpensive and less process intensive structural parts for this research.

Another purpose of the structure is to transfer overall loading from the wing into the structure of the rest of the airframe. This is usually done through some sort of tie-in structural member that acts as a connecting extension of the wing. In this case, there is a socket built into the wing at the same point as the into which a rod of aluminum or carbon fiber would be inserted. The position of the rod itself matches the other members in the wing that resist bending loads in order to efficiently transfer bending loads, the primary loads experienced by the wing, into the structure of the aircraft.

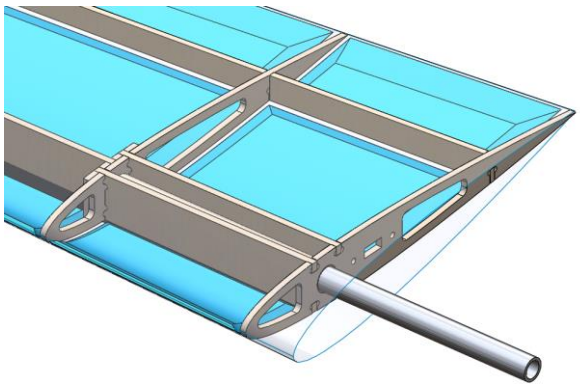

Figure 53: Wing root, showing joining rod within socket

Components of the Wing Skin

The wing skin is constructed primarily of four components, each of which serve different structural purposes.

1. Outer Skin Fabric – The outer skin of the wing is the surface that can be touched. Compared to the inner skin, the outer skin is usually composed of a significantly stronger fabric because it has to withstand handling and aerodynamic loads in addition to any outside damage from drops and knocks that the wing might suffer in operation. In this research, the outer skin is composed of 3 oz. /yd2 fiberglass fabric with an epoxy clearcoat covering. The clearcoat serves as a layer that can be sanded in preparation for painting without actually having to sand directly into the outer skin.
2. Inner Skin Fabric – The inner skin serves to laminate the other components of the wing skin together. Because of this, the inner skin fabric is usually levels of magnitude lighter than the outer skin fabric. In this case, the inner fabric layer is 0.7 oz. / yd2 fiberglass.
3. Core – Core is used to produce rigidity in the skin. In these wings, it is divided into panels between areas where the structure makes contact with the skin. Core allows for the internal structure of the aircraft to be fairly minimalistic instead of demanding numerous ribs that is typical of other wing construction types because they replace ribs as structural members intended to hole the airfoil shape of the wing. The core used in this research is a closed cell rigid vinyl foam. This foam can be heated for added levels of flexibility, and becomes rigid again once cooled. Termination points in the core must be chamfered carefully in order to avoid the formation of voids in the skin.

Figure 54: A piece of vinyl core with one edge partially chamfered

4. Carbon Tow – The carbon tow is a unidirectional carbon fiber strip, an inch wide in this case, that runs along the quarter chord from root to tip of the wing. The carbon tow serves the purpose of providing resistance to bending loads in the wing. This tow is present in both bottom and top surfaces of the wing with a balsa wood shear web in between that forms an I-beam structure which provides the wing with bending strength. Carbon tow, like the fiberglass inner and outer skins, is infused with epoxy during the layup process.

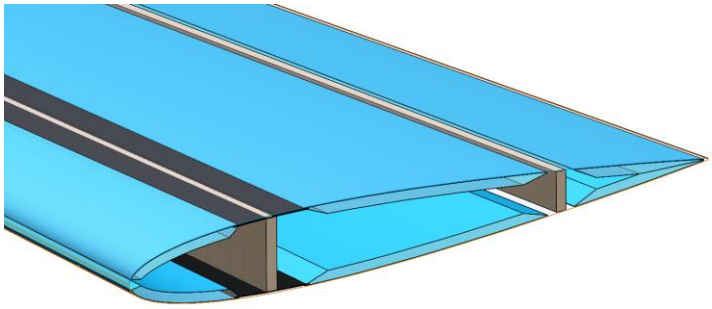

Figure 55: Cross section, showing core in blue, carbon tow in black and internal structure in brown

The skin of a wing is fabricated using the layup process by carefully layering the necessary materials and then applying vacuum using a molded parting surface. Female molds are used to make the outer surface of the wing smooth. Lines representing the placement of internal structure are often drawn into the mold using permanent marker prior to the layup process in order to make the arrangement of layup pieces during the layup easier due to the transparency of the fiberglass.

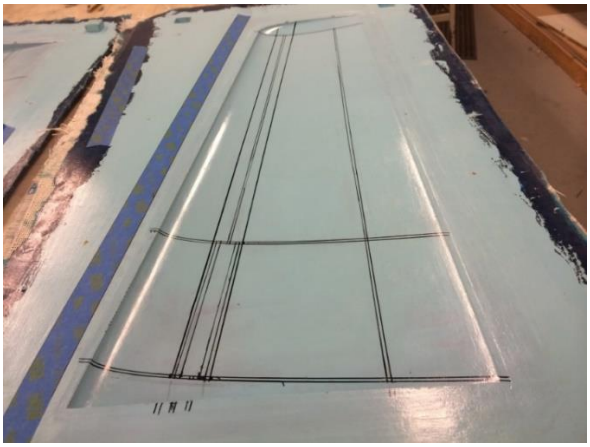

Figure 56: A female mold with guiding lines drawn on the surface

Components of the Internal Structure

The internal structure is fitted into the wing skin prior to bonding, and requires that the skin be produced first. The internal structure is made of multiple parts that are bonded together either before being bonded to the skin or at the same time as they are bonded to the skin. The major components for the wings used in this research are ribs and shear webs. The ribs serve the primary purpose of maintaining the airfoil shape of the wing by resisting compressive forces, but they also serve as points were the shear stresses between the skin halves can be transferred into the internal structure and thus into the rest of the airframe. Ribs run chord-wise and resemble cross-sections of the wing's airfoil. The ribs used in the construction of the wings in this research are mad e of 1/8 inch thick birch plywood laminated in 3 oz. /yd2 fiberglass.

Figure 57: Wing structure, showing ribs, shear webs and joinin rod structure

The shear webs of the wing run span-wise along the wing and are made of balsa with the grain of the wood oriented perpendicular to the top plane of the wing. They serve as the shear web in the I-beam wing spar formed by the web itself and the top and bottom aircraft skins. In this case, there is a primary shear web located at the quarter chord that is capped in carbon tow existing in the skin and a secondary shear web at the ¾-chord. The secondary shear web exists to help the wing resist torsional loads and provide rigidity to the skin, but the loads experienced by the secondary shear web are usually smaller than those experienced by the primary shear web and do not require carbon tow caps.

The components of the structure are usually bonded together with a quick-curing glue or a slower curing epoxy. In this case, CA glue was used to bond structural components to each other.

Building the Wing

The wing components were bonded together using a thickened epoxy. First, one skin half is bonded to the assembled structure, allowed to cure and then the other skin half is bonded to the structure and skin and allowed to cure. This otherwise simple process can be complicated by necessary post-processing that has to be performed on the skin and

structure in order to ensure that a well-fitted bond is made between the skin halves and internal structure. If the skin halves or the structure do not match each other well, then the bonding process may require more epoxy than necessary or even deform the desired shape of the wing. Post-processing between joining processes can come in the form of sanding the structure to fit into the layup, trimming the excess material of the layup to make the fitting process easier, or other surface preparation techniques.

Force is applied to the structure and skin once they are bonded together in order to ensure that the bond is strong and tight and that the end product matches the desired shape. In this case, that force is applied via a series of weights distributed over the structure itself that presses it down against the inside of the skin it is being bonded to.

Removable Panels and Hatches

Removable panels in wings have, in previous work, been fabricated for the purpose of creating hatches in the skin of a wing in order to access internal components such as servos for control surfaces. These access points are usually reinforced with extra structural components in order to make up for the loss of structural integrity in the wing skin, but they also produce a negative impact in weight due to the otherwise redundant level of structure used in their fabrication.

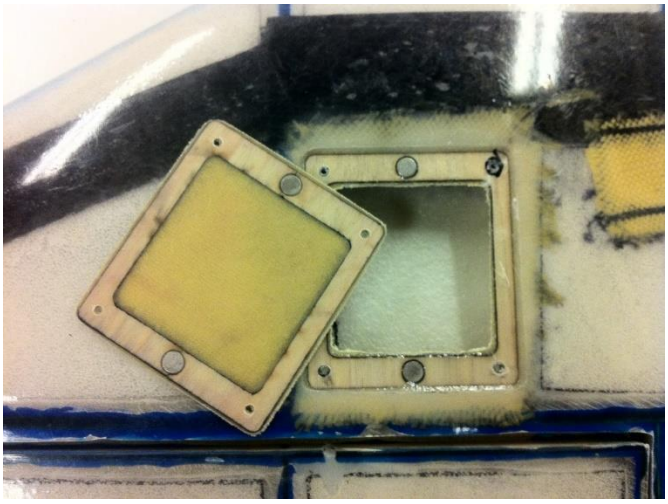

Figure 58: An access point in a wing and its removable panel.

The panels themselves are fabricated in the mold prior to the skin they are meant to fit into. They consist of a thin frame containing magnets with a core panel inside the frame for stiffness. The frame is intended to provide a good border for the hatch from which mounting hardware can be attached. The frame is laminated in the desired materials. Once cured, the excess flashing around the frame is trimmed and the panel itself is adhered to the mold it was first cured in, essentially turning the panel into a part of the parting surface itself before the main skin layup is performed over it with a matching frame and magnets positioned over the panel within the main layup.

The result is a panel that is fitted flush to the skin it is attached to. The panel can be removed freely and the magnets placed into the frames of the panel and skin itself provide a basic level of attachment between the two pieces. Additional hardware such as screws and blind nuts are often attached to the frame of the skin in order to keep the panel attached to its socket.

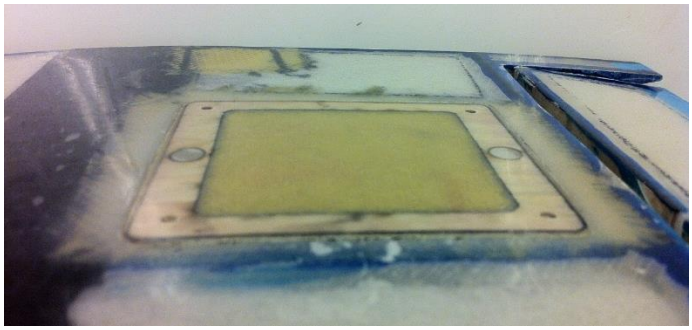

Figure 59: The same access point with its panel in place

This hatch method is the basis for the idea of creating a removable panel containing solar cells. With the additional concept of utilizing the magnets as electrical contacts, additional outside wiring can be minimalized between the removable panel and its socket within the wing skin. The goal of this removable panel is to provide an area of a wing that is susceptible to damage with a replaceable panel that can be swapped out in the event that the panel's cells become damaged. The method for fabricating these panels will be explored and then applied to one of the two complete wings to be produced in this research.

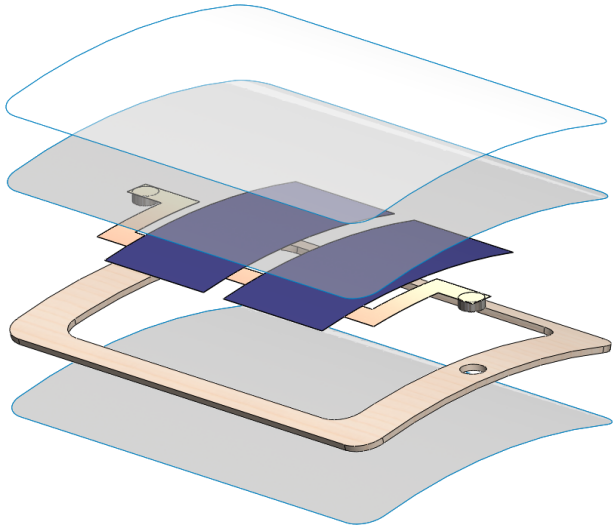

Figure 60: Exploded view of a removable panel concept containing solar cells

Solar Cell Array Integration

The goal of fabricating wings integrated with solar cells in this research is to scale up the embedding processes explored in the single cell testing to that of arrays of solar cells embedded into an actual wing. Two wings will be fabricated with working cell arrays. The same number of actual solar cells will be used in each wing skin while the laminate used for each skin half will be different.

In wings, arrays of solar cells would traditionally be arranged as several strips of solar cells in series that are then wired in parallel. It is desirable that the contribution of voltage to the array's power be greater than that of current in order to keep the guage of wiring low and require a minimal amount of power conditioning once the array is integrated into the power systems of the aircraft. In this case, PowerFilm cells will be arranged into pairs of series-connected cells that are then wired in parallel along the span-wise axis of the wing. The wing used in this case has a span of approximately 24 inches and a chord of 8 inches with a mild taper from root to tip. The arrangement of the cells in this wing is strictly simplistic, since the focus of this research lies more on the process and outcome of integrating the array rather than optimizing the usage of space in the wing. In this configuration, the wing has enough surface area for up to 20 of the PowerFilm cells. Each wing skin half will contain eight working PowerFilm cells while the other 12 cells will be represented by pieces of copper foil. Because of the simple configuration of the array and the general robustness of the PowerFilm cells themselves, no blocking or bypass diodes will be placed within the array circuit. However, if these methods of array encapsulation are to ever be considered for a solar powered or assisted aircraft, it may be necessary to

consider the use of blocking and bypass diodes in order to make the array more reliable in the event of a failure.

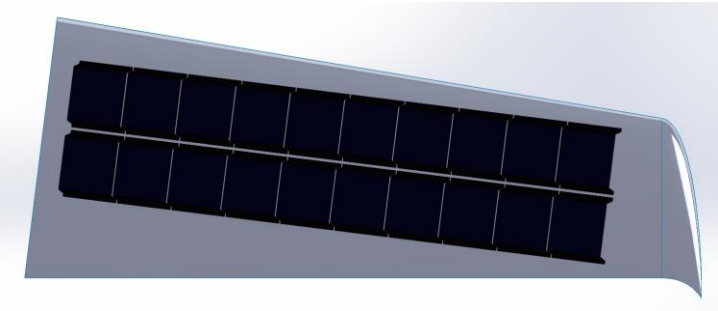

Figure 61: Solar cell configuration over the wing planform

Each laminate type will require one wing skin integrated with cells utilizing the methods developed during the single cell testing period. The three laminate types will produce two complete wings, with one laminate type per wing skin half. The fourth wing skin half will feature a removable panel with an embedded group of solar cells. Wiring for these cells is simplified by the use of flat tabbing and busing wire, which can be integrated directly into the skin and then soldered into an internal connector that is built into the wing structure. Weight of the wing and its components are to be tracked throughout the construction process in order to determine the additional weight penalties of the solar cells, their wiring, and possible encapsulation laminates used. This information, combined with data available from single cell testing will provide a foundation from which a general model of aircraft endurance can be developed for each laminate type.

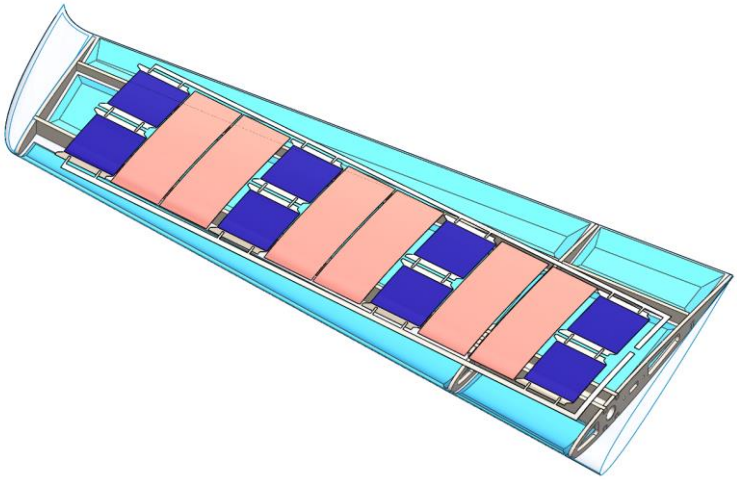

Figure 62: Complete wing model with solar cell array

CHAPTER IV

RESULTS

Single Cell Testing

Weight and cell performance were recorded before and after each prescribed encapsulation process was performed for each sample solar cell. All samples were trimmed to possess 3/8 inches of excess material around the borders of the solar cell, leaving samples approximately 2.75x3.30 inches in size. In both phases of single cell testing, all samples were evaluated by the additional weight their processes and materials add to the solar cell as well as any positive or negative impact on cell performance the encapsulation materials might have once the cells have been integrated into their composites. Using this data, it's possible to develop an endurance model to compare the performance of each laminate material and type based on the impacts that each encapsulation material might have on the endurance parameter of an example aircraft. This model for endurance would exist as a method of applying a figure of merit to each encapsulation material and their respective processes of encapsulation.

Stage One Testing Results

In the first stage of evaluating single cell samples, the parameter varied for experimentation was the actual process of encapsulation while the materials used for each laminate were kept constant. This is indicated in the weight buildup of each encapsulation type in Figure 63, where the only parameter to essential vary for each encapsulation process is going to be epoxy. It is desirable to use a little epoxy as possible while still maintaining an appropriate level of epoxy impregnation in each sample in order to maintain strength and reduce excess weight penalties for each sample.

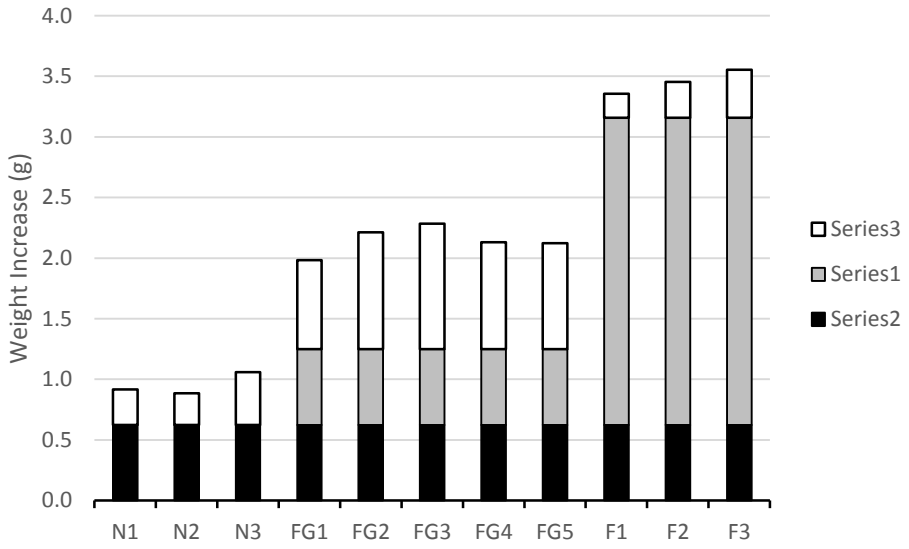

Figure 63: Phase one single cell testing average weight increases for each tested encapsulation process

For samples that contained no laminate, both samples with epoxied edges (N2) and no added epoxy (N1) have a similar amount of excess epoxy weight. The weight of the epoxy in these samples comes from the backing layer of fiberglass, and serves as a benchmark for the amount of epoxy required to impregnate the backing material of each sample. Samples with an epoxy clearcoat (N3) have an expectedly higher added weight

due to the painted layer of epoxy coating each sample. Another useful parameter in weight buildup is the estimation of the weight of a clearcoat of epoxy, which can come from subtracting the weight of N1 and N2 samples from that of N3 samples, since the only real differences between these samples are the additional painted layer of epoxy. A painted layer of epoxy for a 2.75x3.30 inch sample weighs approximately 0.16 grams, or 2.54 grams over an area of a square foot.

Samples with more fiberglass, which in this case are samples with fiberglass laminates, appear to have a much greater potential for retaining excess epoxy. In general it was expected that samples encapsulated in fiberglass would have higher proportions of epoxy weight per layer of fiberglass than samples containing no laminate or film laminates. This effect can be visible when comparing the unmodified or "Normal" encapsulation process for each laminate, which does not include any additional epoxy other than what is required to impregnate their fabric layers.

Laminate Material	Epoxy weight per layer of fiberglass used, including backing layer
None	0.90 g / layer
Fiberglass	0.99 g / layer
Film	0.82 g / layer

This additional epoxy weight per layer of fiberglass is speculated to be due to e tendency for overlapping layers of composite materials to absorb more epoxy than if individual layers. In these individual samples, dry layers of fiberglass were placed into position and then impregnated with epoxy as opposed to being impregnated with epoxy prior to being put into position.

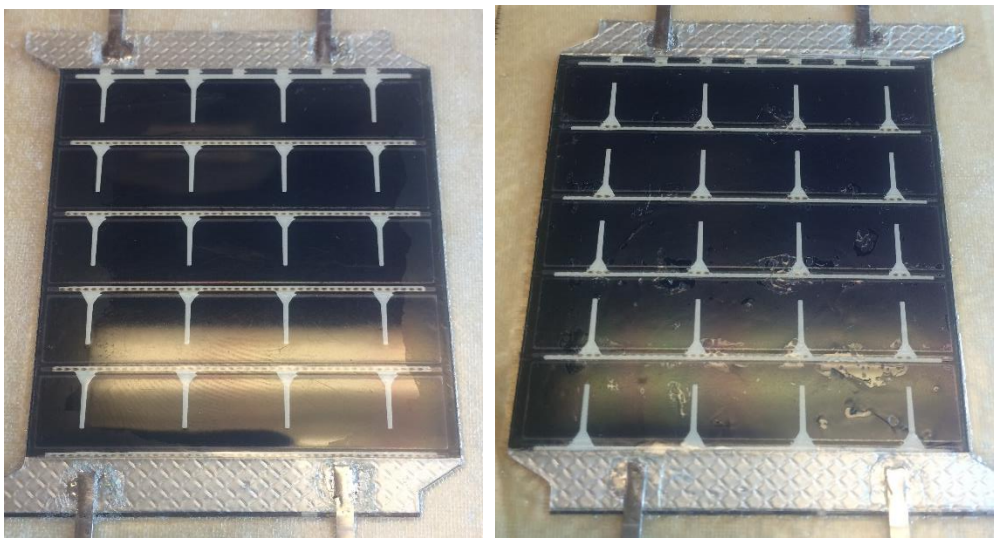

Figure 64: Samples from the group of cells that possessed no laminate material. Right: A cell with the 'normal' embedding process (N1), epoxy bleed at the edges visible; Right: A cell with an epoxy clearcoat (N3), producing a somewhat craggy surface finish

A painted layer of epoxy, not to be mistaken for a clearcoat layer of epoxy, is the epoxy that is smeared onto the surface of cell samples prior to being played into position in the layup. Once these samples are positioned, the excess epoxy between the cell surface and its fiberglass laminate is worked out of the edges of the cell and either wiped away or used in the backing layer of fiberglass. The goal of this process was to eliminate voids between the encapsulating layer of fiberglass and the surface of the cells themselves while at the same time minimizing the amount of excess epoxy added to the layup. Performed effectively, the ‘painted epoxy’ process was intended to produce negligible weight increases while minimizing visual defects in encapsulated cells. This process was not fully refined when it was first used on samples belonging to the FG3 pool, and resulted in a greater yield of excess weight compared to the FG5 pool, which contains a painted layer of epoxy between the cell and fiberglass in addition a clearcoat of epoxy outside the encapsulating layer of fiberglass. Naturally, it is expected that samples in the FG5 pool would be heavier than those in the FG3 sample group, but it is suspected that

excess epoxy smeared onto the surface of cells in the FG3 sample group was not effectively removed prior to the layup being completed, resulting in skewed excess weight results.

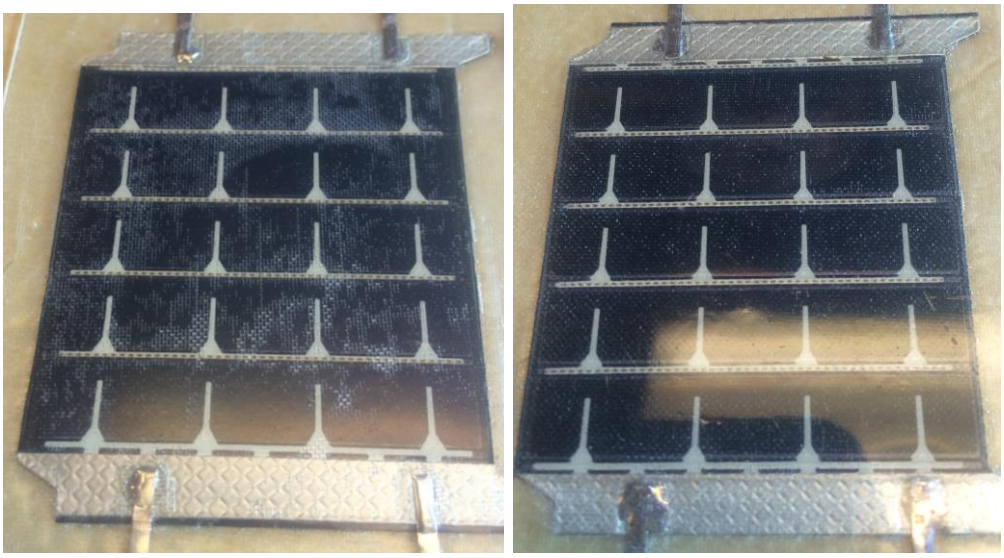

Figure 65: Samples of cells encapsulated in fiberglass. Left: Normal, baseline encapsulating process (FG1); Right: Sample with an epoxy clearcoat and an efficiently applied layer of epoxy between the cell surface and the fiberglass laminate layer (FG5). FG1 samples have matte finish and the fibers are much more visible due to less epoxy being infused into the fabric. FG5 samples have a reflective surface finish and the fibers are less visible.

The initial set of samples, containing no modificaitons and minimal epoxy usage (F1), and the final set of samples, possessing an epoxy clearcoat and painted layer of epoxy on the cell surface prior to encapsulation, have an average weight difference of 0.14 grams per sample, with the latter being the heavier. Assuming that the weight of painted layer of epoxy between the cell surface and encapsulating layer of fiberglass is negligible and done efficiently, the epoxy clearcoat weight is approximately 2.22 grams per square foot surface area. This is unexpectedly less than that of samples that possessed no laminate but also had an epoxy clearcoat layer, but is likely due to some inconsistencies in the distribution of epoxy in the clearcoat layer for either sample group. In the N3 sample

group, the epoxy clearcoat was likely painted slightly thicker over the parting surface than in the FG5 sample group.

The added weight produced in samples using film laminates are expectedly straightforward. The film itself, which is a thicker polyurethane film with a frosted finish, is one of the heavier laminate materials available with an adhesive backing that attaches to the surface of the encapsulated solar cell. Weight differences between film samples that were applied dry (F1) and film samples applied with the help of water (F2) are likely due to the manufacturing variations in the application of epoxy, as opposed to the existence of water contaminants in F2 samples, which is confirmed by visual inspection of F1 and F2 samples, which have indistinguishable appearances from one another. Film laminated samples applied with the assistance of epoxy (F3) possess a higher weight penalty, but are still visually indistinguishable from the other stage one film samples upon visual inspection.

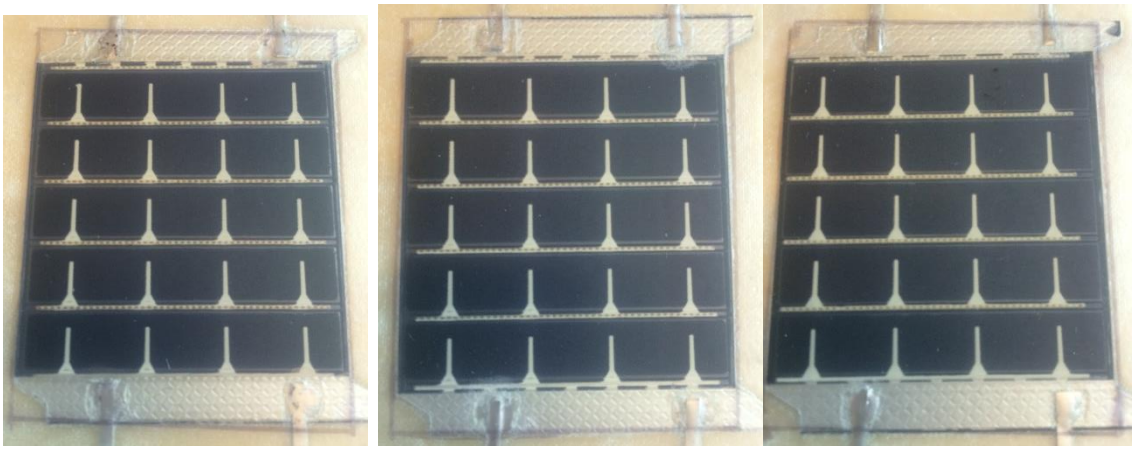

Figure 66: Photos of three different photovoltaic cells that have been encapsulated using the three different processes. Left: Normal (F1); Middle: Assisted with water (F2); Right: Assisted with epoxy (F3). Visual inspection shows no real distinguishing features between each of these samples.

Cell performance between different laminate types varied most for fiberglass samples, primarily due to difficulties developing a process that produced consistently defect-free

samples. Fiberglass laminated samples that had been lightly sanded before encapsulation using a lightly painted layer of epoxy between the cell surface and fiberglass laminate (FG4) show the least amount of degradation in cell performance. However, the proportions of resin and hardener used in the production of these samples were skewed during the preparation stage. While small errors in the mixing stage of epoxy are normally tolerable, errors in mixing proportions can be magnified when mixing smaller amounts of epoxy. Such was the case when FG4 samples were produced. The result was a sticky, textured surface finish, which is suspected to have contributed to FG4's favorable results. Because the textured surface finish of these samples would be difficult to reproduce at a larger scale due to the mixing error, FG4 samples stand as an example of unexpectedly favorable but unreproducible results. With that in mind, FG5 samples, which utilize an epoxy clearcoat and painted layer of epoxy between the cell surface and encapsulating layer of fiberglass, remain as the best performing alternative.

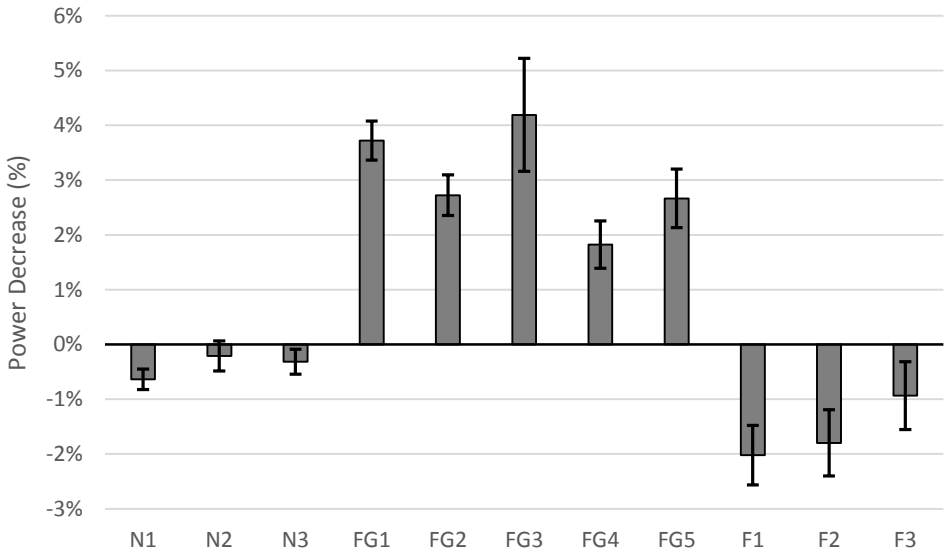

Figure 67: Decreases in maximum power for each tested encapsulation process

Cell samples belonging to the group with no laminate indicate a very slight increase in performance, which can be explained in part by the presence of variations in test results. That said, samples without modification possess the most desired level of performance. Samples encapsulated in film possess a surprising increase in overall performance despite their frosted surface finish, with F3 samples showing the least amount of bonus performance, which is likely due to the additional layer of epoxy between the film and the photovoltaic cells in that sample group.

Table 8: Reference table for and Figure 63 and Figure 67

Ref No.	Laminate	Encapsulation Process	Max Pwr Decrease		Wt Increase (g)	
N1	None	Standard	-0.64%	± 0.19%	0.92	± 0.01
N2	None	Epoxy Edges	-0.21%	± 0.28%	0.88	± 0.01
N3	None	Epoxy Clearcoat	-0.32%	± 0.23%	1.06	± 0.01
FG1	Fiberglass	Fiberglass - Standard	3.72%	± 0.36%	1.98	± 0.01
FG2	Fiberglass	Fiberglass - Epoxy Edges	2.72%	± 0.37%	2.21	± 0.01
FG3	Fiberglass	Fiberglass - Painted Epoxy	4.19%	± 1.03%	2.28	± 0.01
FG4	Fiberglass	Fiberglass - Sanded, Painted Epoxy	1.82%	± 0.43%	2.13	± 0.01
FG5	Fiberglass	Fiberglass - Epoxy Clearcoat, Painted Epoxy	2.66%	± 0.53%	2.12	± 0.01
F1	Film	Film – Standard	-2.02%	± 0.54%	3.36	± 0.01
F2	Film	Film - Water	-1.80%	± 0.60%	3.45	± 0.01
F3	Film	Film - Epoxy	-0.93%	± 0.62%	3.55	± 0.01

Process selection for each laminate type was determined not only based on impacts on maximum power and weight increases, but also on process complexity or difficulty. For instance, while F1 samples showed the greatest performance in their laminate type, the difficulty of attaching an array of cells to the adhesive backing of the polyurethane film without the assistance of water or epoxy makes the F1 process for encapsulating cells in film an undesirable process. For this reason, the best alternative remains the F2 encapsulating process, which utilizes water lightly sprayed onto the adhesive backing to apply the cells similar to window tints, with the water being worked and cleaned away

prior to layup. The relative difficulty of encapsulating samples in fiberglass was similar for all fiberglass samples, allowing them to be evaluated with more emphasis on performance than process difficulty. With that in mind, all samples laminated in fiberglass for stage two of the single cell testing would be lightly sanded prior to layup as well as encapsulated with an epoxy clearcoat and a painted layer of epoxy between the cell surface and encapsulating layer of fiberglass. Effectively, the process chosen for fiberglass encapsulation for future samples was a combination of FG4 and FG5 processes due to their higher performance and lower additional weight when compared to the rest of the tested processes. For samples possessing no laminate, the 'normal' process (N1) would be used for future encapsulation of samples based on its low weight production and favorable results. A close contender was the N2 process, which utilized the use of additional epoxy applied around the edges of samples, but the purpose of this process was to produce a better surface finish on produced parts and was deemed unnecessary since the surface finish between N1 and N2 samples is almost indistinguishable.

Stage Two Testing Results

Stage two samples were produced using the processes decided upon during stage one of testing, with stage two focusing on varying the materials used for each laminate type. This stage of testing primarily focuses on sweeping across a range of different fiberglass materials to record and evaluate their impacts on cell performance and weight increases, with the second of the two film laminate materials also being evaluated on the side.

Weight buildup of the stage two samples follows the same method as the first by isolating the weight of the epoxy used to encapsulate each sample, which includes the backing

layer of fiberglass used for each sample, in order to visualize the relationships between fiberglass weight and the weight of additional epoxy. The weight of the epoxy clearcoat is estimated based on stage one single cell testing results.

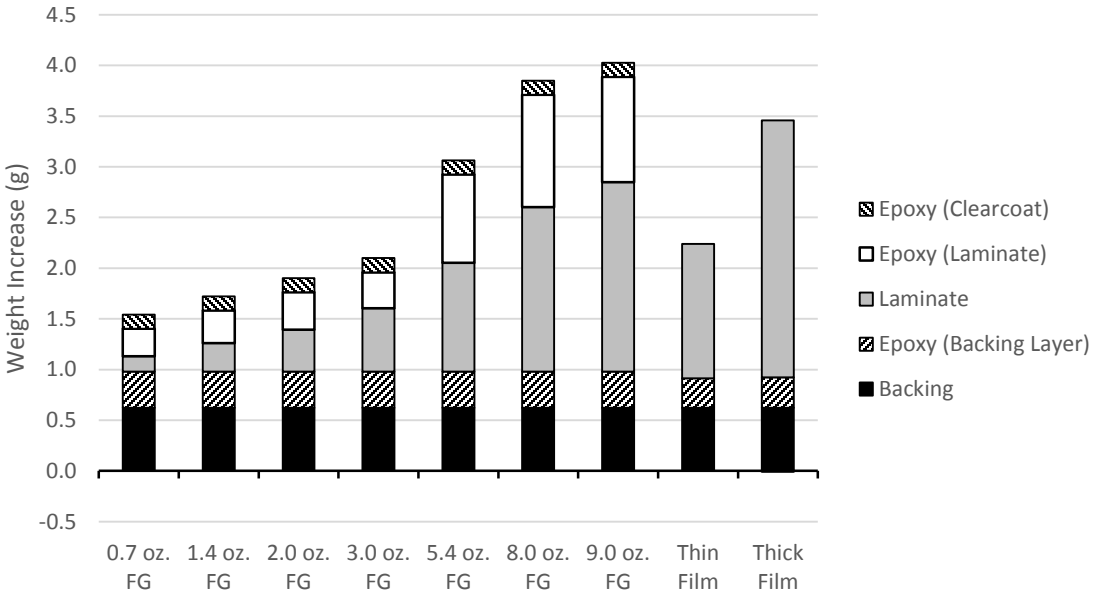

Figure 68: Weight buildup of stage two samples

The amount of epoxy required to completely infuse fiberglass increases with fiberglass weight, most likely due to a combination of fiber count and fiber thickness. A thicker, loose weave of fiberglass fabric is going to require more epoxy in general than a comparatively thinner, tighter weave fiberglass due to the need to fill in gaps between the fibers. Cross-referencing Figure 68 and

Table 9, the weight of epoxy used for increasing weights of fiberglass increases, but the ratio of epoxy weight to laminate weight actually decreases.

Weight of samples laminated in the thin film, when compared to those laminated in the thicker film, is expectedly smaller. Curiously, however, the performance 'boost' from the thinner film, despite having a clear glossy finish compared to its thicker counterpart, is smaller. The matte finish of the thicker film may have a greater tendency to refract or absorb light than the glossy finish of the thinner film, and the performance boost in general may be explained by a higher level of light being absorbed by the polyurethane material than the material coating that is built into the cells themselves.

Performance of the fiberglass laminated single cell stage two samples seems to follow a relationship dictating that increases in fiberglass weight will produce subsequent decreases in cell performance as a result of reduced light transmission through the buildup of fibers in the stronger fiberglass fabrics. However, some fabrics, despite being heavier than others, show significantly better performance. For example, 3.0 oz. fiberglass performs noticeably better than 2.0 oz. fiberglass when used as a laminate material, likewise with the 8.0 oz. fiberglass and the 5.4 oz. fiberglass. The common denominator between these two fabric pairs is that the 3.0 oz. fiberglass and 8.0 oz. fiberglass both possess higher relative fiber counts compared to other fabrics near their weight. Despite the higher amount of epoxy used in either fabric compared to its lighter weight partner, which has been proven to have a negative impact on cell performance based on comparing N1 and N3 lamination processes in the first stage of testing, the performance of a cell encapsulated in fiberglass is more dependent on the fibers of the of the fabric than the amount of epoxy used in infusing it.

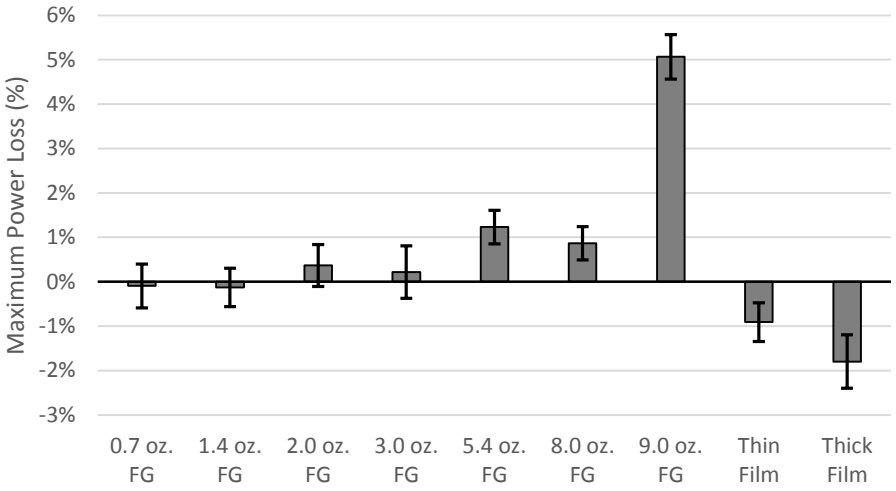

Figure 69: Maximum power loss for tested stage two samples

The weight of the fiberglass, which is the parameter from which the fabric is usually referred to by (apart from its weave), is actually consequential to both its fiber count and fiber thickness. While the thickness of the individual fibers is not available, the fiber count of the fabric is available from the manufacturer as well as the fabric thickness. Based on Figure 70, there may be a loose correlation between epoxy ratio and maximum power loss in the samples tested, but a much stronger correlation between fabric thickness and maximum power loss, with some overlap between points.

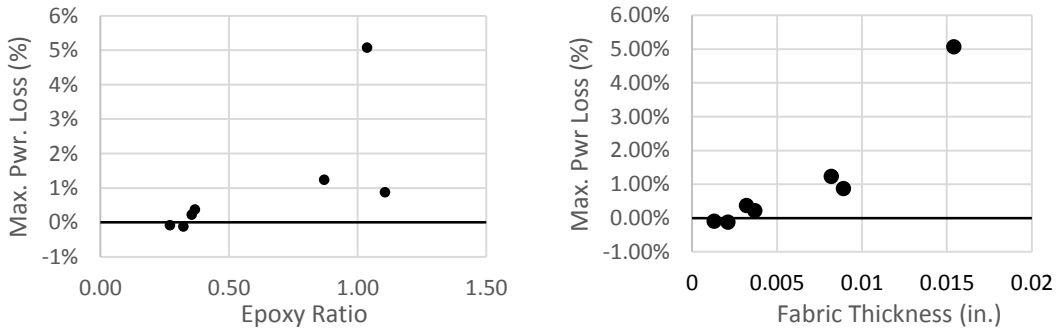

Figure 70: Plots of laminate epoxy ratio versus max power loss (Left) and fabric thicknes versus max power loss (Right)

However, it was found that the strongest correlation between maximum power and the properties of the fabrics used as laminates was the ratio of fabric weight, which may be

more representative of fiber thickness than fabric thickness considering fabric thickness can vary depending on the tightness of the fabric weave, over the average thread count of the fabric itself. The correlation between this ratio and the maximum power loss experienced by tested samples is easier to visualize over a logarithmic scale of the fabric weight and fiber count ratio, available in Figure 71.

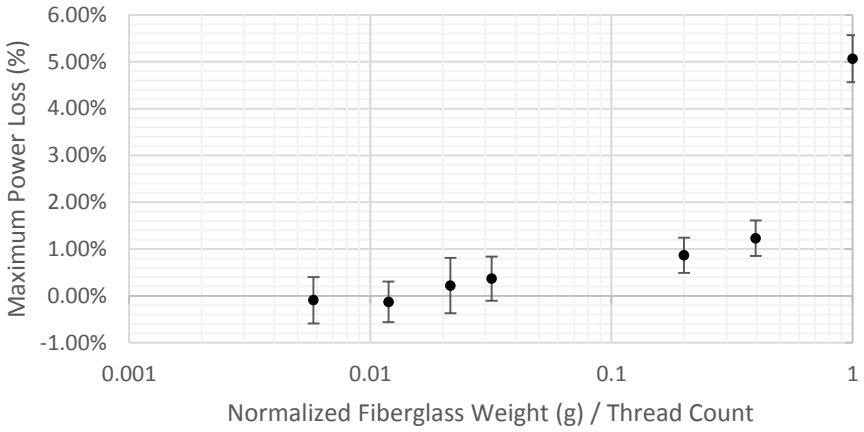

Figure 71: The ratio of fiberglass weight over threat count on a logarithmic scale plotted against the maximum power loss experienced byt te tested stage two samples

Figure 71 confirms that there is a potentially strong correlation between the fabric fiber count and thickness, here represented by fabric weight, and light effective light transmission. Fabrics like 2.0 and 5.4 oz fabric may have lower weights than 3.0 and 8.0 oz. fabric respectively, but their low number of thicker threads results in lower light transmission when acting as a laminate for a solar cell.

Table 9: Data table for stage two single cell test results, including the epoxy ratio, which is the ratio of weight of epoxy infused within a respective laminate to the weight of that laminate

Laminate Material	Laminate Type	Max. Pwr. Decrease	Wt. Increase (g)	Epoxy Ratio
0.7 oz. FG	Fiberglass	-0.09% ± 0.49%	1.54 ± 0.01	1.78 ± 0.19
1.4 oz. FG	Fiberglass	-0.13% ± 0.43%	1.72 ± 0.01	1.16 ± 0.10
2.0 oz. FG	Fiberglass	0.37% ± 0.47%	1.90 ± 0.01	0.89 ± 0.07
3.0 oz. FG	Fiberglass	0.22% ± 0.59%	2.10 ± 0.01	0.57 ± 0.05
5.4 oz. FG	Fiberglass	1.23% ± 0.38%	3.06 ± 0.01	0.81 ± 0.03
8.0 oz. FG	Fiberglass	0.87% ± 0.38%	3.85 ± 0.01	0.68 ± 0.02
9.0 oz. FG	Fiberglass	5.07% ± 0.50%	4.03 ± 0.01	0.55 ± 0.02
Thin Film	Film	-0.91% ± 0.44%	2.23 ± 0.01	---
Thick Film	Film	-1.80% ± 0.60%	3.45 ± 0.01	---

Figure of Merit: Endurance

The figure of merit to provide a final level of evaluation of single cell samples in relation to their effect on aircraft performance needed to effectively include both weight increases when scaled up to an array and measured impacts on performance. This can be accomplished by joining measured weight values and cell performance from single cell tests with the existing endurance model discussed in the background section in order to estimate the increase or decrease in overall endurance that each laminate material might have on the example aircraft's endurance when scaled up to a 40 cell array. It was important to keep in mind that cells operating at 5% efficiency such as the ones used in this research are operating near the minimum efficiency that might produce a net increase in endurance, so it was expected that some of the laminates used in this research might produce a net decrease in aircraft endurance for the 5ft wingspan, 5lb aircraft model.

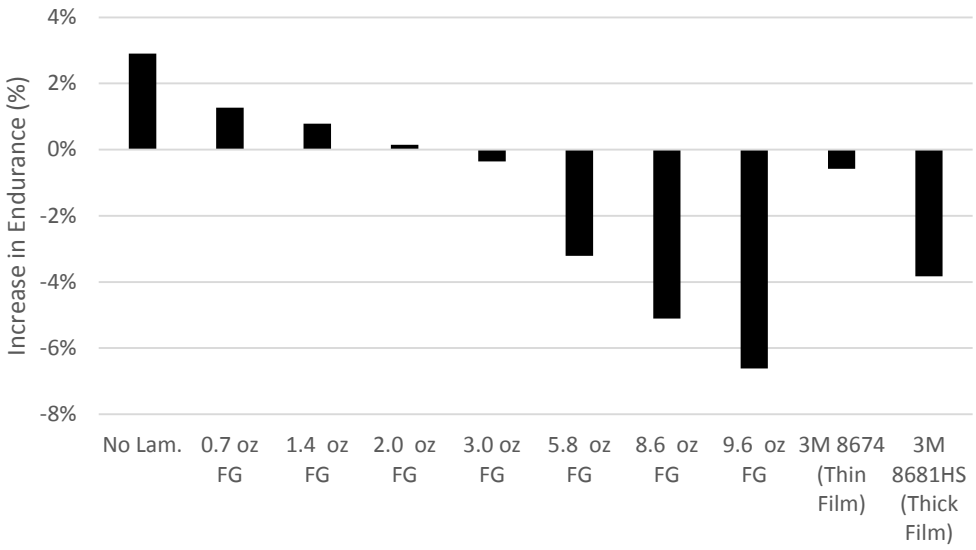

Figure 72: Scaled up increases or decreases in endurance for each laminate material and laminate type

Single cell sample test results were scaled up by putting weight increases (laminates and wiring) into terms of grams per cell, which was then multiplied by the number of cells used in covering the wing. Endurance is, as expected, highest for cells utilizing no additional laminate material. Increasing the fiberglass weight for fiberglass laminates provides a gradual decrease in endurance. The two films tested, despite having positive cell performance bonuses in individual cell testing, see a net decrease in aircraft endurance, albeit not as severe as some of the heaviest fiberglass materials. This is believed to be due to the severe weight penalties applied to the use of the film laminates, which are significantly greater than most of the lighter fiberglass laminate materials.

Static Load Testing

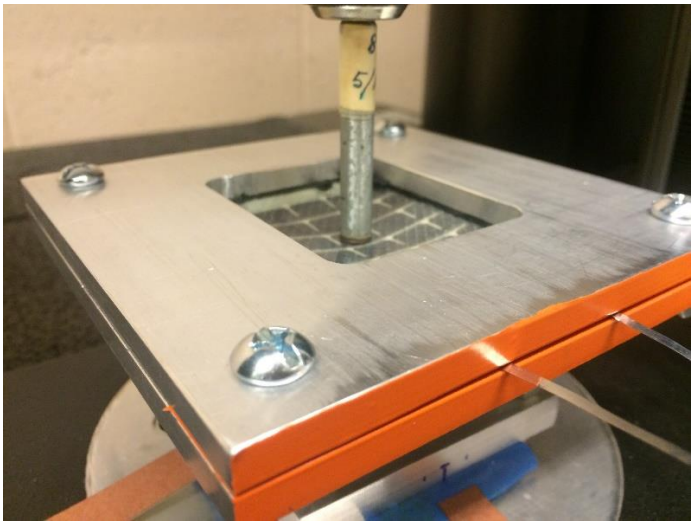

Figure 73: A fiberglass laminated specimen under out-of-plane deflection loading

Five separate specimens, each with different laminate materials, were loaded out of plane to a specified depth of approximately 8mm, which is where it was expected that the desired partial failure of specimens might occur according to results from the tested aluminum dummy sample. Samples were clamped together between two layers of rubber tape between aluminum plates with the intention of holding specimens in place during the testing period. However, this tape proved not to be as strong as was hoped, and was observed flexing and slipping during the testing of specimens. This behavior is visualized in gathered data as curved areas, where the specimen is being loaded but the rubber material is also flexing, and flat spots, where the rubber material is actually slipping along the surface of the loaded specimen, with increases in the compressive rod of the Instron 6599.

Figure 74: A specimen laminated in 3.0 oz. fiberglass after it has been tested, with outer edge wrinkling (Left) and a photo of a 0.7 oz fiberglass specimen being placed within the holding apparatus with rubber capturing material adhering to its edges (Right)

Solar cell specimens were observed wrinkling at their outer edges at higher deflections as stresses became concentrated at the midpoint of the longer edge of the specimens. In all samples tested, the composite sandwich of each specimen either failed or outright ruptured at higher deflections, usually coinciding with a rapid unloading of the specimen. Two samples that displayed this behavior most prominently were the 9.0 oz. and 3.0 oz. fiberglass laminated samples, which unloaded once these cracks had formed. It is suspected that, had the cells not been present in the composite sandwich itself, these cracks would have propagated further toward the compressive tool's loading point until ultimate failure.

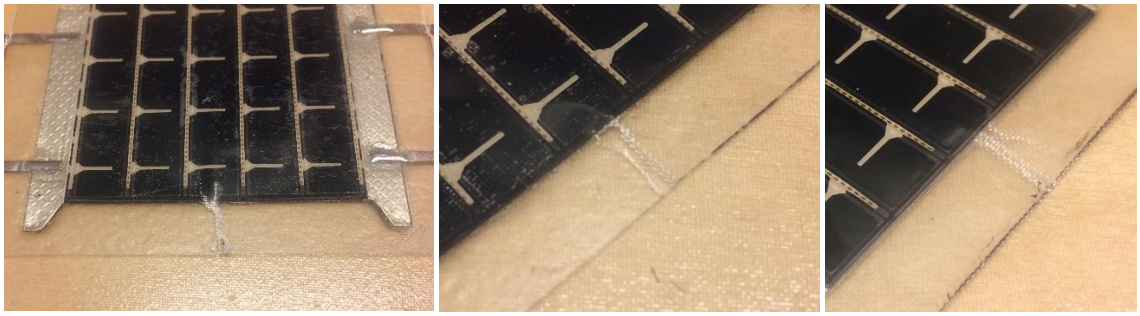

Figure 75: Cracks formed in the middle of the longer sides of each test specimen.

The out of plane loading tests indicate that heavier fiberglass laminates require higher levels of loading to achieve the same level of deflection, while lighter fiberglass, film or un-laminated specimens require lower loads to achieve the same amount of deflection by a significant factor. The lightest fiberglass, the thin polyurethane film, and the un-laminated specimens all seem to have similar resistance to out of plane deflection, suggesting that the backing material of each of those samples, which was made out of 3.0 oz. fiberglass, was taking the majority of the loading in each case, with the 0.7 oz. laminated specimen showing marginally better resistance to loading than the other two. The polyurethane laminated sample was expected to behave similarly to the un-laminated specimen when loaded due to the ease with which the polyurethane coating could be stretched by hand.

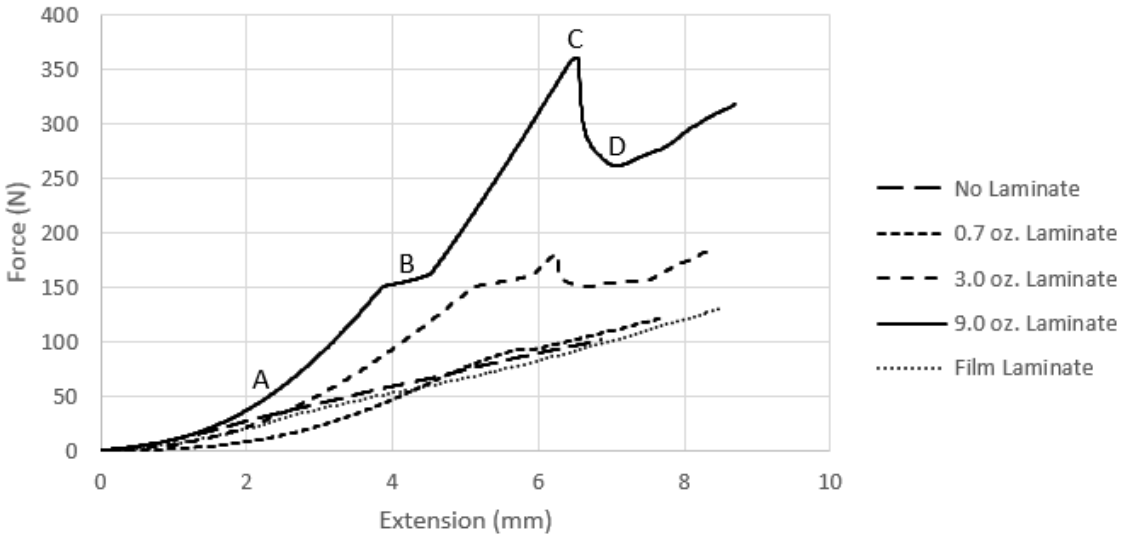

Figure 76: Out-of-plane loading test specimen results in force versus deflection

Results from the out-of-plane loading tests indicate that each sample underwent a number of phases as deflection was increased. These phases are more visible in samples containing fiberglass laminates, and are annotated on Figure 76 as follows. Lighter

samples, those with light fiberglass, film and no laminate at all, do not appear to explicitly experience all of these loading behaviors; however, evidence of crack formation in all tested samples suggests that all samples experience these loading behaviors to a certain degree, with heavier fiberglass laminated samples experiencing them to a more exaggerated degree.

Region A: The specimen becomes loaded while the rubber material used to hold the specimen in place also flexes, resulting in a curve.

Region B: The rubber material slips along the surface of the specimen as the shear forces between the specimen and the rubber material exceeds what the rubber material is capable. Deflection occurs without much increase in loading until the specimen appears to have deflected enough for the loading of the specimen to be transferred into the fibers of the test specimen itself as opposed to the rubber capturing material.

Region C: The specimen, which has begun to buckle at the edges, reaches a maximum point at which the fibers of the specimen can withstand the concentration of forces at its edges, and experiences a rapid unloading as the fibers at the edges of the specimen fail in the form of a crack that propagates toward the center of the specimen.

Region D: The crack has reached the edge of the solar cell, and can no longer propagate without further loading of the sample, which results in the sample beginning to resist further deflections.

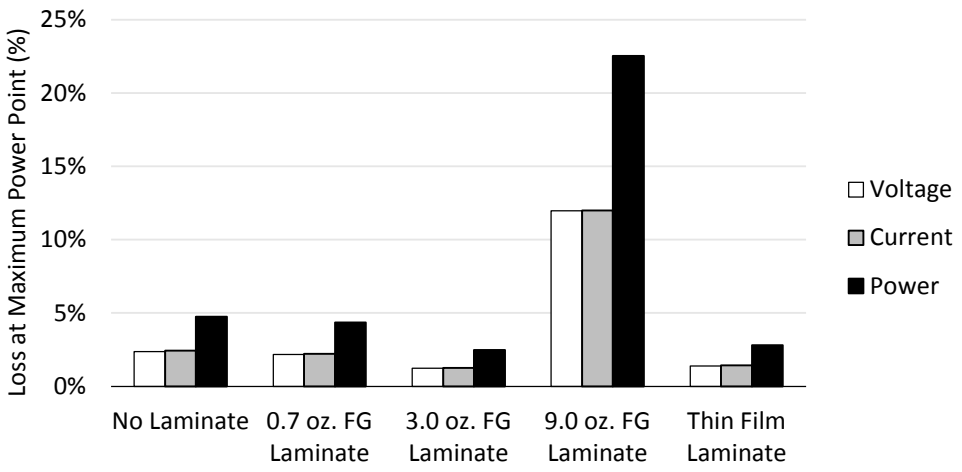

Figure 77: Losses experienced by each specimen after being tested at their maximum power points.

Partial failure of the tested cell specimens was achieved both structurally and in cell performance tests. Each sample experienced a degree of partial failure after being loaded, with the un-laminated specimen showing the greatest indications of a loading-induced performance failure while the power losses experienced by the 9.0 oz fiberglass laminated sample are believed to come from light transmission obstructions as opposed to loading-induced failure.

Cell performance results after loading tests have been performed confirm that fiberglass and film laminates do provide redundant protection to cell performance. The specimen containing no laminate experienced a higher drop in performance than the majority of the tested samples. The specimen that was encapsulated in 9.0 oz. fiberglass, however, experienced a high spike in power loss when compared to the other tested specimens. It is expected that this is due to the fact that this specimen, when compared to the other fiberglass specimens, was the only one to experience delamination from the surface of the solar cell at the Region C failure point. This delamination and the visual defects that it forms, are expected to be the primary cause of this higher loss in power. The failure of

the 9.0 oz fiberglass specimen suggests that, at some point, heavier fiberglass laminates may delaminate from their encapsulated cell samples under load and result in greater power losses due to a loss in light transmission. However, it should be kept in mind that the load required to produce this failure in the 9.0 oz. fiberglass laminated specimen was significantly greater than the next-strongest 3.0 oz fiberglass laminated specimen.

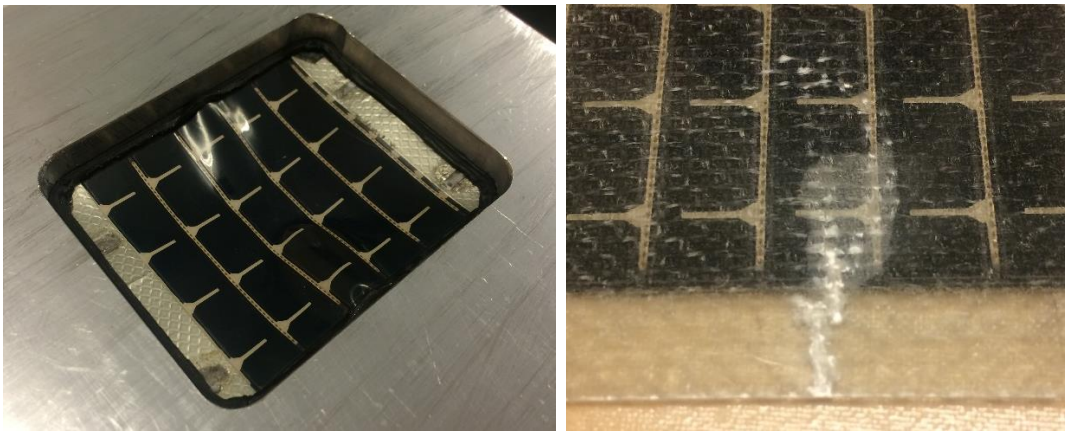

Figure 78: Left: The specimen with no laminated was observed to experience a significant level of delamination from its fiberglass backing. Right: The delamination experienced in the 9.0 oz laminated sample produced a noticeable defect in the specimen in the form of a void, which is believed to have reduced cell performance significantly by reducing light transmission

Wing Construction

Two complete wings were constructed with the intention of containing fully functional cell arrays on each of the four wing skins. These arrays would be wired individually to a connector mounted to the root of the wing to which a male connector could be joined for monitoring voltage and current output of the full array. Both of the two wings were built in the same fashion that a flight-ready wing would have been, with the exception of lacking control surfaces, in order to accurately model the marrying of skins integrated with cell arrays, traditional small-scale structure and required internal wiring.

Three of the four wing skins would be fabricated using a different laminate type for its integrated solar cell array, while the fourth wing skin would implement a prototype removable and replaceable solar panel that was intended to mount flush to the skin and with the same contours as the outer skin surface it is built upon. This removable panel was the result of several iterations of development, with complexities stemming from the dual use of magnets as both electrical contacts and attachment points.

Weight for each skin, and internal structure was tracked throughout the construction process of each wing in order to develop a more accurate weight model for the implementation of solar cell arrays into the skin of a wing for each laminate type. By comparing and estimating weight increases between the four different wing skins, it was possible to develop a revised endurance model for each laminate type combined with performance results from single cell testing. Performance of each array was evaluated before and after wing skin integration for the sake of confirming functionality, but only for open circuit and closed circuit conditions for the entire array because individual cells could not actually be evaluated once they had been integrated into the wing skin due to their respective coatings obstructing access to wiring between individual solar cell terminals.

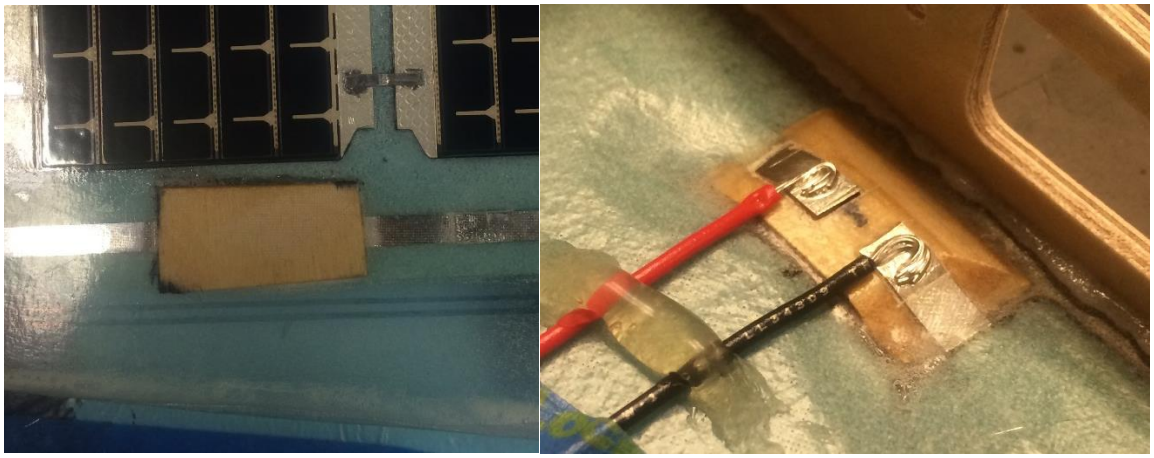

Figure 79: Left: The plywood shim as viewed from the outer surface of the wing,w ith bus wires tucking beneath it. Right: The plywood shim as viewed from inside the wing, with internal wiring soldered to the exposed bus wire terminals

The endpoints of each busing wire terminal would meet close to the root of the wing, guided beneath the rest of the layup by a small chamfered piece of plywood that had been fitted into the root core panel of the wing skin. These wires would be tucked beneath the plywood piece and brought into the inner surface of the layup to act as a transition point between the wiring of the solar cell array itself to the internal wiring of the wing leading into the connector at the wing root. Fiberglass around each bus tab would be cut away to expose the bare bus wire, to which the internal wiring would be soldered. The plywood was intended to both act as a strong anchor to make up for the increase in stress concentrations of the wing itself as well as a thermal sink for the two terminal tabs once they were soldered to the internal wiring. The vinyl core material of the wing skin would have been unsuitable if used in place of the plywood piece due to its tendency to blacken and melt at higher temperatures, and soldering to tabs directly against fiberglass might have resulted in disruption of the layup fibers.

Both wings were also built with the intention of being resistant to damage due to handling while maintaining a level of realistic construction detail. With this in mind,

strips of additional fiberglass were applied at the leading and trailing edges of each wing as well as the areas between core panels where ribs would be joined to the skin. These strips were intended to reinforce areas where the wing would be most susceptible to handling damage and deformation.

Un-Laminated Array Skin

The layup process for the un-laminated cell array skin did not involve the use of an epoxy clearcoat. Instead, fiberglass strips were placed over the busing wire that joined the positive and negative terminals of each solar cell pair that had been wired in series in order to prevent the wiring from potentially delaminating from the surface of the wing skin, as smooth metal materials are notorious for doing so. The cells themselves as well as the tabbing wire joining each solar cell pair, were left exposed, directly adhered to the outer skin via epoxy.

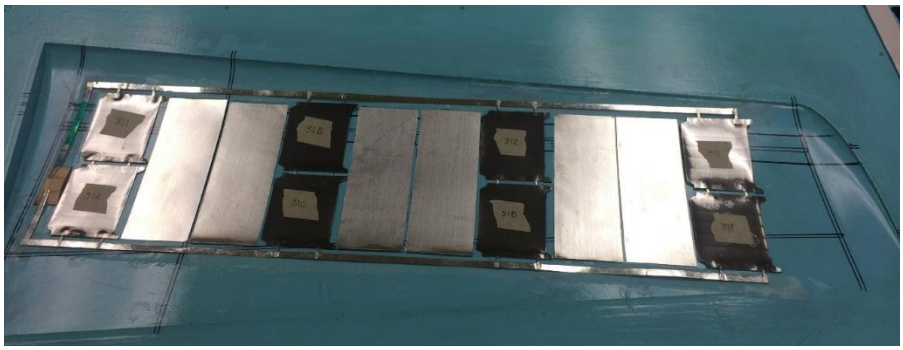

Figure 80: The cell array for the no-laminate skin, positioned within its mold prior to layup for test fitting

Layup Process for the Un-Laminated Skin

1. Application of epoxy-impregnated fiberglass strips positioned where the bus wires of the array will be
2. Solar cell array and plywood shim positioned on the currently dry parting surface with bus wire positioned over the fiberglass strips.

3. Taking care to avoid shifting the array on the smooth, dry surface of the released parting surface, the 3.0 oz. outer fiberglass layer, infused with fiberglass, is positioned over the parting surface and array before being worked smooth against the array and parting surface.
4. Wetted reinforcing fiberglass strips are added to the leading and trailing edges of the wing skin mold
5. Epoxy wetted carbon fiber tow is positioned along the quarter chord of the wing
6. Pre-prepared vinyl core panels are positioned in their prescribed places
7. Wetted rib cap fiberglass strips are positioned over each rib plane in the skin
8. The inner fiberglass layer, wetted with epoxy, is placed carefully over the layup and gingerly worked smooth
9. The layup is bagged and placed under vacuum

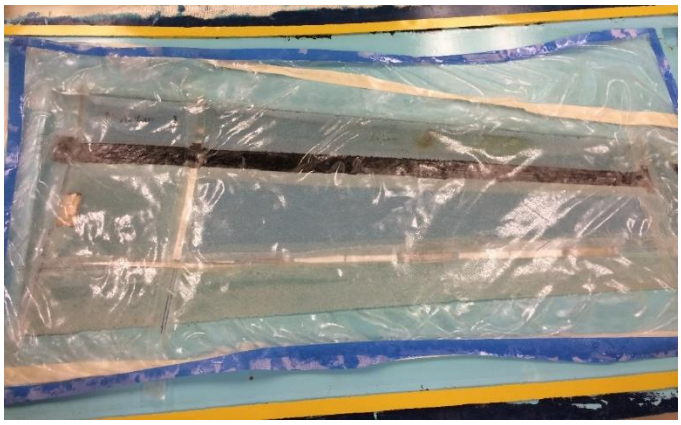

Figure 81: The wing skin containing the un-laminated array at the end of the layup process prior to being bagged and vacuumed

Keeping the cell array in position proved difficult with no available means of affixing the array to the parting surface available that would not have damaged the release film applied to the parting surface, so care had to be taken to avoid shifting the array and copper foil dummy cells during application of the outer fiberglass layer. Because this layup contained no epoxy clearcoat, unlike the rest of the skins produced, this skin was

expected to be measurably lighter than the rest of the skins produced. This can be accounted for utilizing estimates for clearcoat layer weight developed in the single cell testing phase of this research in order to effectively compare this wing skin to the others if necessary.

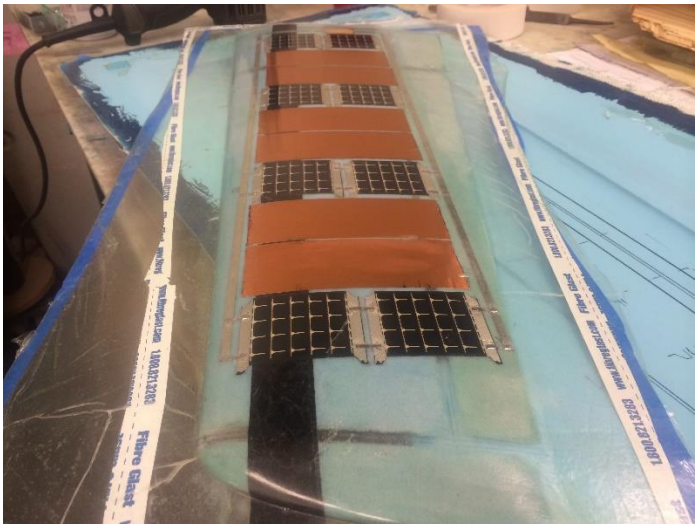

Figure 82: The wing skin containing the un-laminated cell array as it was just after being removed from its mold. All skins skins were weighed just after being removed from their molds after curing

Fiberglass Laminated Array Skin

The fiberglass laminated skin, compared to the un-laminated skin, was easier to integrate cells into due to the viscosity of the epoxy used to adhere the array and dummy cells to the parting surface of the mold, but at the same time more difficult due to the additional time required to prepare the array for integration with the fiberglass laminate. This skin was fabricated with an epoxy clearcoat, which is applied approximately 45 minutes to an hour before the rest of the layup takes place and consists of a layer of epoxy mixed with a small amount of epoxy thickening colloidal silica that is painted as thin as possible over the prepared parting surface. This layer, in normal use, is intended to be sanded in preparation for painting of the finished part. If the part did not have an epoxy clearcoat

prior to sanding, then the act of sanding the skin in preparation for painting might damage the outer skin fabric of the wing and compromise its strength. The epoxy clearcoat as an added effect of putting a clear finish on the wing surface if left un-sanded, which was taken advantage of in the single cell testing phase of this research.

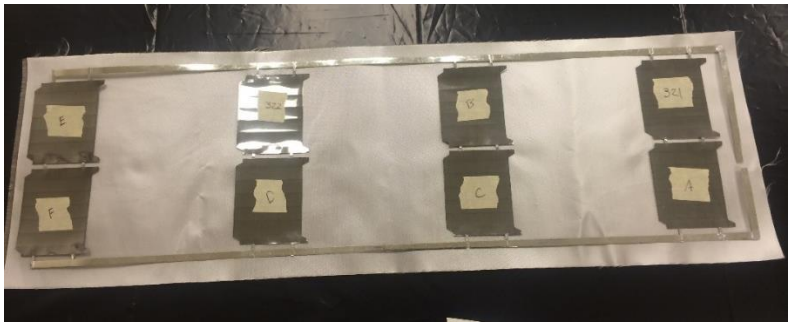

Figure 83: The cell array for the fiberglass laminated skin with prepared fiberglass laminating sheet

Abridged Layup Process for Fiberglass Laminated Skin

1. Application of the epoxy clearcoat, which is allowed to set for 45 minutes to an hour after application
2. Wetted fiberglass laminate layer is positioned over the area where the array will be placed and carefully set onto the sticky surface of the partially cured epoxy clearcoat
3. The array is smeared with the prescribed "painted" layer of epoxy and then placed onto its fiberglass laminate layer
4. The excess epoxy of the painted epoxy layer is worked gently out from the edges of each solar cell in the array to be used in the outer skin layer
5. The outer skin layer, is placed over the array, and excess epoxy from the "painted" layer of epoxy used on the cells is worked into the fabric
6. The rest of the layup continues as normal

The fiberglass laminate used to coat the cell array was trimmed to the dimensions of the array itself and placed over a pre-marked position of the solar cell array. While the array and its copper film dummy cells stayed in position easier than in the un-laminated skin,

the array and its dummy cells were still capable of being shifted and moved, so care still needed to be made to prevent the components of the array from shifting. Placement of the skin components that contact the epoxy clearcoat is made difficult due to the fact that the epoxy clearcoat becomes quite sticky once it is partially cured during the layup process. If care is not taken when applying fiberglass to the sticky surface of the parting surface, then it is possible to pull up the release film on the parting surface when attempted to adjust the fiberglass on the epoxy clearcoat.

Film Laminated Array Skin

The array for the film-laminated skin was prepared well in advance to the actual layup itself. The thin film used to encapsulate this particular array has a tendency to stick to non-porous, smooth surfaces it is applied to on the side without adhesive. This was first observed in previous work in layups utilizing this film. This meant that the array using this film could be adhered to a released parting surface securely enough for a layup to be performed over it without the use of any complex processing techniques. Ideally, this process of pre-attaching the film laminated array to the parting surface of the mold would be performed by vacuum bagging the array to the mold surface. In order to facilitate adhering the film-laminated array to the parting surface of the mold using this technique, a thin tedlar film was applied to the adhesive backing of the film after it was attached to the solar cell array in order to prevent the bagging materials from getting stuck to what would have otherwise been the exposed adhesive backing of the film-laminated cells.

The cells themselves were vacuumed in the mold for approximately an hour before the layup was performed, which left the film-laminated array essentially adhered to the

parting surface of the mold. At this point, the epoxy clearcoat was applied over the parting surface and the tedlar backing of the array before the rest of the layup was performed as normal. The layup was simplified due to the process of vacuuming the pre-prepared film-laminated array to the surface of the mold in order to temporarily bond it to the mold surface.

Removable Panel Development and Wing Skin Integration

The removable panel would be fabricated as two different components: The panel itself, and the wing skin which it is fitted into. Magnets would be used in both the panel and the "socket" for the panel in order to both establish electrical contact between the panel's solar cells and the internal wiring of the wing as well as provide a level of attachment between the two parts without the use of additional hardware. This was to be achieved through the use of neodymium disc magnets approximately 3/16 inches thick and ¼ inches in diameter. The resistance between two sides of these magnets was measured at approximately 1Ω.

The complication with using magnets as electrical contacts between molded parts stems directly from the fact that the "socket" piece is molded from the panel itself. The removeable solar panel was the easier of the two pieces to fabricate, since fiberglass covering the magnets after layup would be trimmed away to expose the bare metal of magnets. Normally, the magnets that are used in removable panels intended for use as access hatches are placed beneath a layer of fiberglass, which helps to hold the magnets in place since the smooth surface of neodymium magnets makes them difficult to bond to wood and composites using epoxy. In order to use the magnets in the removable solar

panel as electrical contacts, these magnets would have to be exposed and in-contact with each other when the socket portion of the removable panel is being manufactured. Any obstructions between the two magnets, such as fiberglass, epoxy or release films, might prevent electrical contact from being established, so it was believed that care would need to be taken to integrate the magnets into the layup process of the socket portion of the removable panel in such a way that contact would be established between the magnets within both the panel and the socket once the part was fully cured.

The initial iteration of the removable panel prototype involved the simplest form of integrating the magnets as electrical contacts. A simple panel containing a pair of solar cells was fabricated with wiring and two magnets representing the positive and negative terminals of the solar cell pair. These magnets were physically soldered to the tabbing wires linking to either terminal of the solar cell pair. The fiberglass covering the magnets was cut away to leave the metal, conductive surface of the magnets exposed. The panel was trimmed and adhered to a glass plate to be used as a parting surface, and after being prepared with wax and liquid release film, the socket of the panel was molded over the hatch, with the socket magnets encapsulated behind a layer of fiberglass. The panel fit well within its socket, but electrical contact between the two pieces could not be established due to two major problems:

1. The soldering method used to conductively bond the tabs of the solar cell to the magnet essentially demagnetized the rare earth magnets at the terminals, reducing the magnetic attractive force between the socket and removable panel

2. The fiberglass, and possibly the release layer as well, between the socket magnets and the panel magnets prevented the magnets from touching each other to form electrical contact.

Unable to solder the magnets to the tabs due to the consequence of losing the magnetic force of attraction between the two contact surfaces, a conductive epoxy was explored as an alternative in the second iteration of the panel and socket. A new panel was fabricated, this time simplified by the use of a pair of magnets wired in contact with each other using conductive epoxy to bond the tabbing wire and magnets together. Copper foil dummy cells were also soldered to the tabbing wire linking the "terminals" of the test panel together in order to simulate solar cells. This time, in order to ensure that the magnets were in contact with each other throughout the manufacturing process of the socket, release was removed from the surface of the magnets prior to layup, and holes were created in the outer fabric of the socket where the socket's magnets were positioned in order to allow the two magnets to remain in direct contact while the socket was left to cure. It was believed at the time that the attraction force between the magnets would prevent any problems with the magnets being bonded together, which was only partially correct. While the magnets only became loosely bonded together due to the epoxy that had seeped around their joining point, the bond strength between either pair of magnets was far greater than the bond strength between the tabbing wires in the socket and the brittle conductive epoxy bonding the magnets to the tabbing wire. The result was that the magnets in the socket pulled the magnets out from the panel when the panel was first removed from its socket, and electrical contact between the panel and the socket could not be established once the detached magnets were adhered back into their sockets with a combination of conductive and normal epoxy.

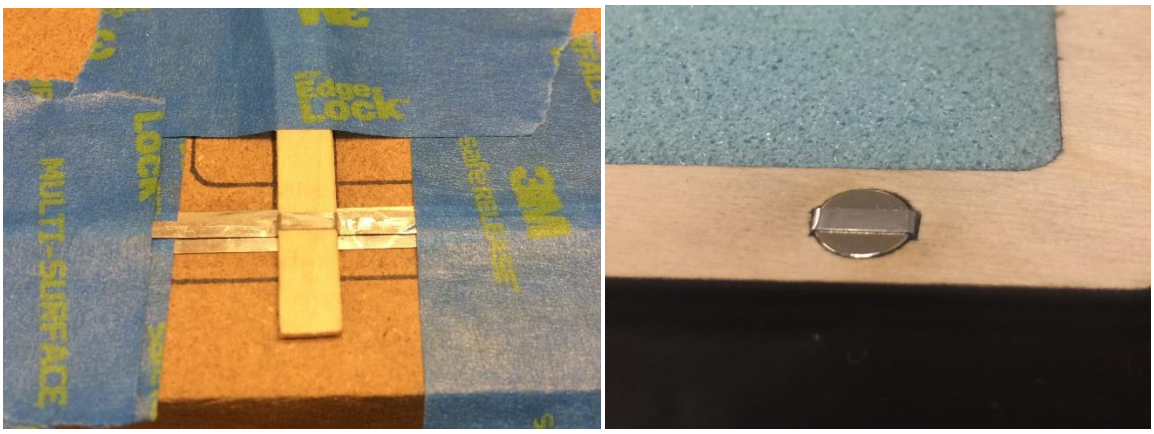

Figure 84: Left: Tabbing wire restraints were soldered to the busing wire using a piece of of crafting stick with dimensions matching those of the neodymium magnets, since applying solder to the magnets would demagnetize them. Right: Each magnet is held in place by the tabbing wire restraining it and the plywood frame that it fits into

The third iteration of the panel required that measures be taken to ensure that the magnets are not able to be removed from their contact points within the layup of either the panel or socket. While previous iterations of the removable panel prototype had tackled the integration of the magnets during the layup process itself, the third iteration of the prototype shifted the integration of the socket's magnets into the post-processing stage of the manufacturing process after the socket had been cured. The socket piece itself would be manufactured without the magnets initially, and then holes would be drilled into the socket piece after it had been cured so that magnets could be placed directly over the panel's magnets, therefore establishing electrical contact, before the sockets magnets would be epoxied carefully in place.

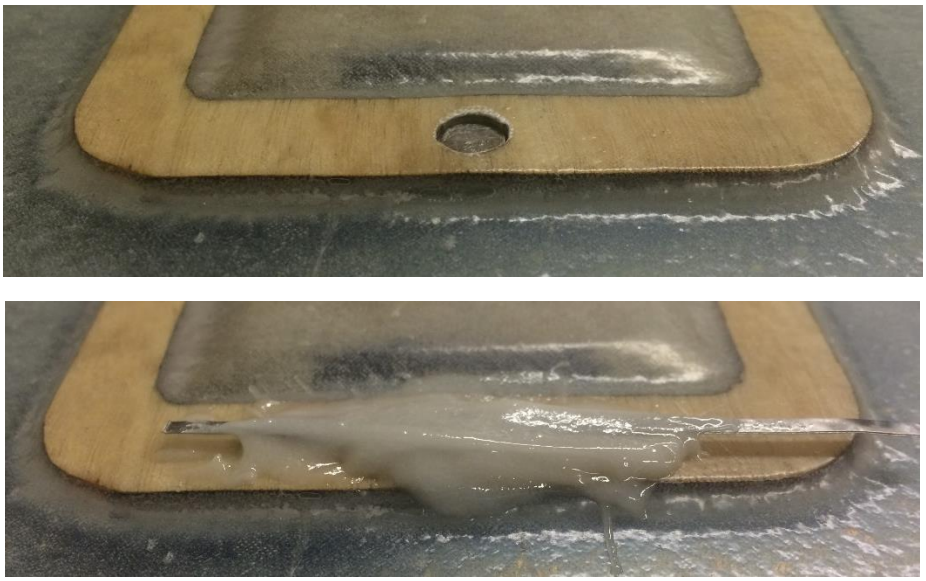

Figure 85: An external view of the socket after holes for the socket's magnets have been drilled with the corresponding magnet of the panel visible through the hole (Top) and the magnet, with its tabs exposed, after it has been epoxied into place with electrical contact between the socket and the panel established (Bottom)

Magnets in the third iteration of the removable panel would be restrained in place using an extra piece of tabbing wire that would wrap around the magnet, attached to main tab of the solar cell wiring on both sides of the magnet. Combining this restraint with the plywood frame to which the magnets were fitted into, it was believed that it would take significantly higher forces to coax the magnet to break its tabbing wire restraint and debond from its point on either the panel or the socket. This method of integrating restrained magnets into the panel and socket via post-processing of the socket allowed for a much more hassle-free manufacturing process for the removable panel at the cost of an extra day waiting for the epoxy used to bond the magnets to the socket to cure. Electrical contact was established and this third iteration of the removable panel prototype was copied over to the larger, working prototype of the fourth wing skin, which contained a functioning removable solar panel.

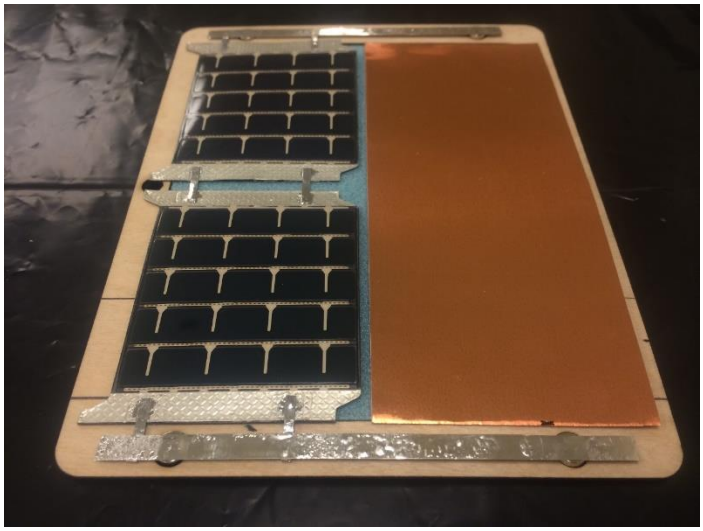

Figure 86: The materials of the prototype removable solar panel with working cells, test fitted prior to layup

The removable panel itself was prepared first, containing an array of 2 functioning cells and two dummy copper foil cells. The layup for the panel was similar to the skin layup for the fiberglass-laminated array skin and contained core, an outer skin and an inner skin in addition to a thin plywood frame to act as a stiff border for the removable panel and a point for the restrained magnets connected to the terminals of the array to be fixed to. This panel was fabricated, trimmed and then affixed to the surface of the mold in the same spot from which it was manufactured to act as part of the parting surface for the layup of the rest of the wing. The corresponding socket of the removable panel contained its own thin plywood frame, with prepared holes that would be drilled out after the skin was cured. Magnets with the same tabbing-wire restraining mechanism were placed in direct contact with the magnets of the removable panel through the holes drilled into the skin, and were epoxied into place after test fitting confirmed that electrical contact between the magnets of the panel and the magnets of the socket had been established.

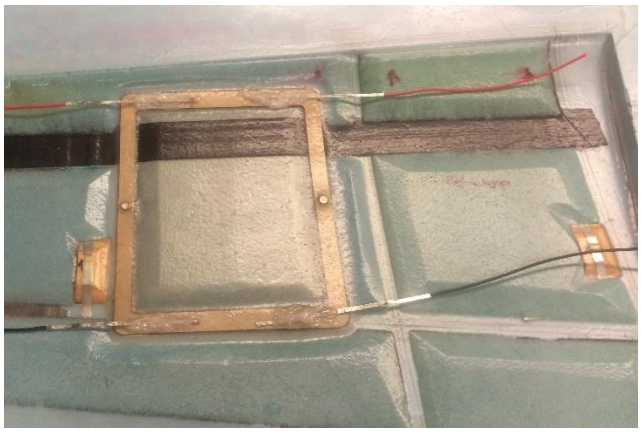

Figure 87: The inside of the wing skin containing the removable panel, after magnets have been epoxied into place with internal wires

Implementation of the large removable panel resulted in a significant increase in thickness in the layup as it was performed around the removable panel. The size of the panel itself required it to be placed toward the root of the wing, and it was inevitable that it would disrupt some of the internal structure of the wing as well as the structural members of the wing skin itself. Modifying the internal structure to accommodate the contours of the thicker parts within the skin required that the original structure be trimmed and sanded where the removable panel was positioned. Space on the skin of the wing that would have otherwise been utilized for additional solar cells had to be sacrificed in order to make room for the removable panel, and four of the 20 simulated cells within the array of the wing had to be removed. The array was constructed in order to still contain 8 functioning cells, with two sheets of the copper film representing two solar cells each being removed.

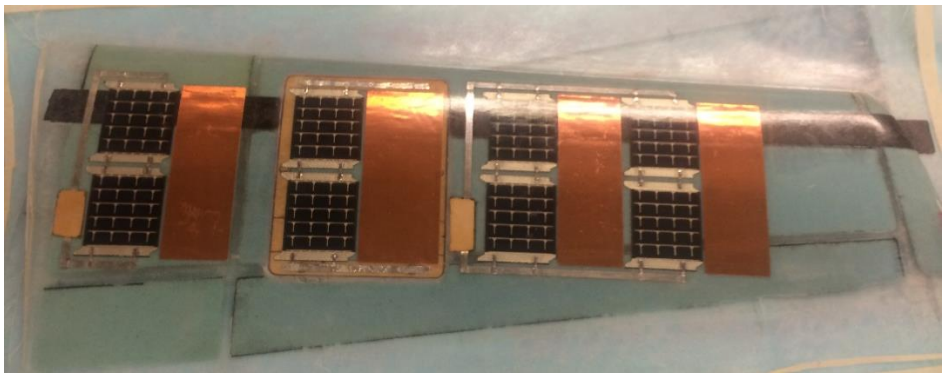

Figure 88: Completed wing skin with removable panel attached

The integration of the removable panel in the fourth wing skin created an interruption in the bus wire of the full wing array, which required it to be divided into two smaller arrays and then wired together internally after being cured. Each layup utilized a similar plywood shim to feed the terminal tabs from the outer surface to the inner surface of the layup for soldering to the internal wiring.

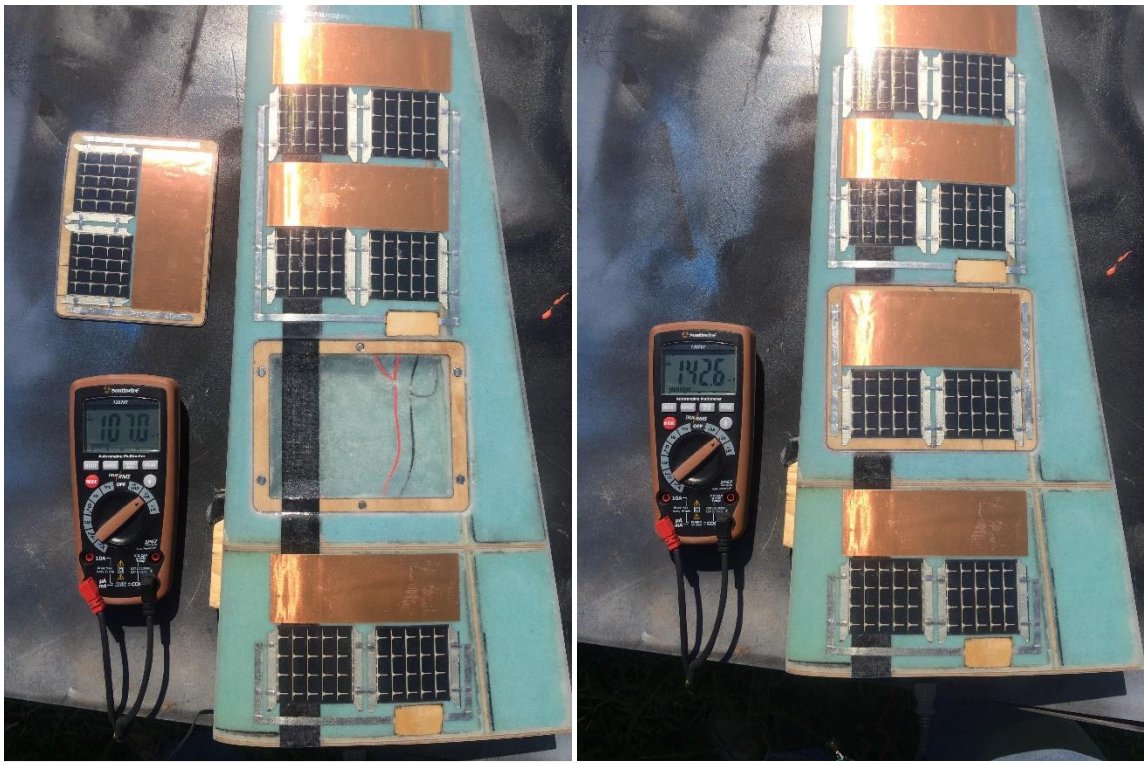

Figure 89: Outdoor testing of the wing, confirming function of the removable panel by measuring short circuit current with the panel removed (left) and the panel in position (right). The increase in short circuit current between the panel being removed and replaced indicates that the panel is adding power to the array.

Internal Wiring

The internal wiring of the wings consisted of 22 gauge wire soldered to the terminal contacts of each wing skin half. The wiring was soldered to these terminals before the wing was completely bonded together, and each skin half was wired independently from the other into a female USB connector that was then mounted to the root rib of the wing. The output of each skin-integrated array could then be measured simply by plugging a male USB connector into the female with its wires connected to a multimeter.

Figure 90: The female USB connector, as it was mounted in the root rib of the wing near the main spar

Array Performance Testing Before and After Skin Integration

Two of the eight functioning cells within each wing skin array were fully tested before construction of the full array for batch testing purposes while the other six were only tested for basic functionality under indoor lighting. Each full array, once soldered together, underwent an outdoor test under daylight in open circuit and closed circuit conditions to establish that all cells in the array were functioning. This test was performed again after each array was integrated into its respective wing skin. By comparing voltage and short circuit current between tests, the functionality of each array

confirmed that none of the cells in any of the four produced skins experienced a failure during construction of either wing. Variations in voltage and current are due to differences in daylight conditions between pre-integration and post-integration measurements, and each skin produced approximately the same open circuit voltage and short circuit current when tested after wing construction.

Table 10: Array short circuit current and open circuit voltage before and after wing integration

	Before Integration		After Integration	
	Array V_{OC} (V)	Array I_{SC} (mA)	Array V_{OC} (V)	Array I_{SC} (mA)
Skin 1: No Laminate	8.12	174	9.08	165.7
Skin 2: Fiberglass Laminate	8.02	151.4	9.15	166
Skin 3: Film Laminate	7.84	142.5	8.74	163
Skin 4: Skin Array	8.255	63.35	8.98	123.1
Skin 4: Panel	7.55	23.8	8.94	38.4

Measurements taken from arrays within Skin 4 before integration were taken during cloudy conditions while all other array tests were performed during clear weather. Each wing contains a total of 8 functioning cells, and each wing produced approximately 165 mA under short circuit conditions after completion. The lack of significant variation between each short circuit current test for the four wing skins as well as the overall similarity to pre-integration measurements suggests that all functionality of all cells before and after integration is the same.

Detailed Weight Buildup and Revised Endurance Calculation

The component weights of each skin are divided amongst the materials the skin is composed of, and the epoxy used to produce each wing skin is calculated by subtracting

the weight of the dry materials from the total weight of the cured, untrimmed skin. The skin containing the removable panel carries the highest weight of each of the four skins while the skin containing the photovoltaic cell array with no encapsulating laminate is the lightest of the four skins. The skin containing the fiberglass laminated array is, surprisingly, heavier than the skin containing the thin polyurethane film, which was expected to be the heaviest of the three laminate-testing skins produced. The epoxy ratio used to produce each skin is calculated by dividing the epoxy weight in each wing by total weight of all the structural composite materials to which epoxy was intentionally applied to during the layup, excluding any fiberglass laminates.

$$\text{Epoxy Ratio} = \frac{W_{\text{Epoxy}}}{W_{\text{Structural Fiberglass}} + W_{\text{Carbon Fiber Tow}}}$$

	Epoxy Ratio
Skin 1: No Laminate	1.12 ± 0.06
Skin 2: Fiberglass Laminate	1.30 ± 0.06
Skin 3: Film Laminate	0.80 ± 0.06
Skin 4: Fiberglass Laminate w/ Panel	1.51 ± 0.06

For Skin 4, which contained the removable panel, the weight of the panel and its components were excluded from the calculation of the skin's epoxy ratio. Skin 3 possesses the lowest epoxy ratio, likely because Skin 3 required no additional epoxy during the layup process in order to integrate the film-laminated array into the wing skin, while all other skins required excess epoxy applied as a direct result of attempting to achieve desired surface finish or for the reduction of visual defects in the integration of the cell arrays of each other skin. In the case of Skin one, extra epoxy had to be applied at the edges of each cell after application of the outer structural fiberglass layer in order to

ensure that there were no voids between the edges of the cell and the structural fiberglass layer. In single cell testing, this extra epoxy could be scraped away due to the simplistic nature of the layup of the single cell samples. When applied to a wing, the excess epoxy could not be scraped away easily without rising disturbing the positioning of the cell array.

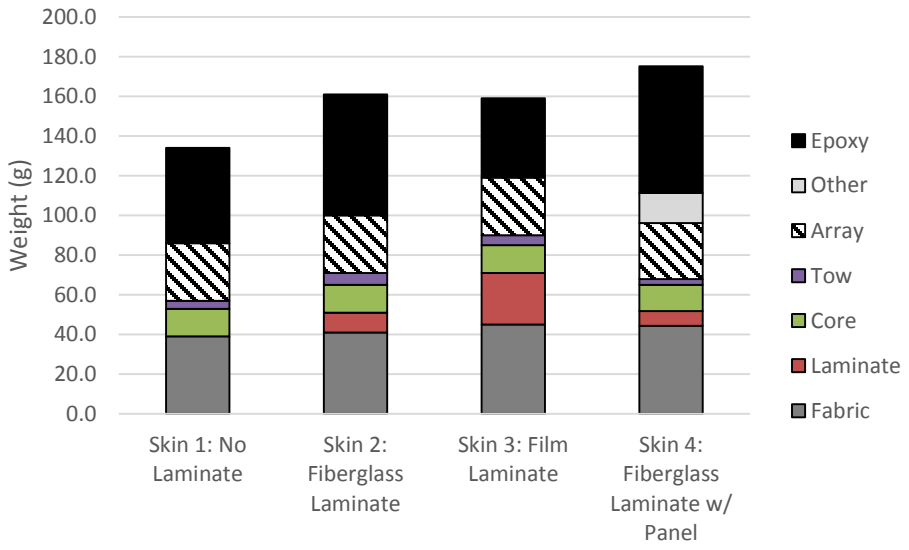

Figure 91: Component total weight breakdown for each wing skin, untrimmed

Extra epoxy in Skin 2, which contained the cell array laminated in fiberglass, likely comes from multiple sources. The clearcoat layer of skin 2 was mistakenly painted on too thick. This was noticed during layup when the 'painted layer' of epoxy between the cell surface and fiberglass laminate was being applied. A gentle pressure on the cells as they were being positioned resulted in a noticeable compression felt between the cells and the mold surface, which is normally does not happen if the epoxy clearcoat layer is painted thin. Visual evidence of this thicker epoxy clearcoat is visible as an irregular, wavy, reflection that is cast by the copper film dummy cells, which is due to irregularities in the thickness of the epoxy clearcoat layer. In addition to the thicker epoxy clearcoat, the

painted epoxy between the cell surface and laminating fiberglass was not efficiently used in the layup process. This painted epoxy layer is usually worked out of the edges of each cell during the layup process in order to be used in the backing or outer structural layer of fiberglass. While this method worked during single cell testing, the differences between layup styles for the single cell samples and the wing resulted in the excess epoxy worked from the edges of each cell not being utilized efficiently in infusing the outer structural layer of fiberglass with epoxy. In single cell testing, the fiberglass was placed dry over the wet layup, allowing the excess epoxy to be soaked into the backing layer of fiberglass before more epoxy was added to efficiently infuse the backing layer of fiberglass with epoxy without adding excess epoxy to the layup. However, in production of the wing, fiberglass layers are added to the layup once they have already been infused with epoxy, thus resulting in the excess epoxy worked out of the edges of each cells simply being added to the weight of the wing as excess. The outer structural layer of fiberglass could have possibly been added to the wing layup while it was dry as opposed to being infused with epoxy beforehand, but the process of infusing it with epoxy over the cell array came at the risk of moving the array out of position and pre-impregnating the fabric with epoxy before integrating it into the layup was ultimately favored.

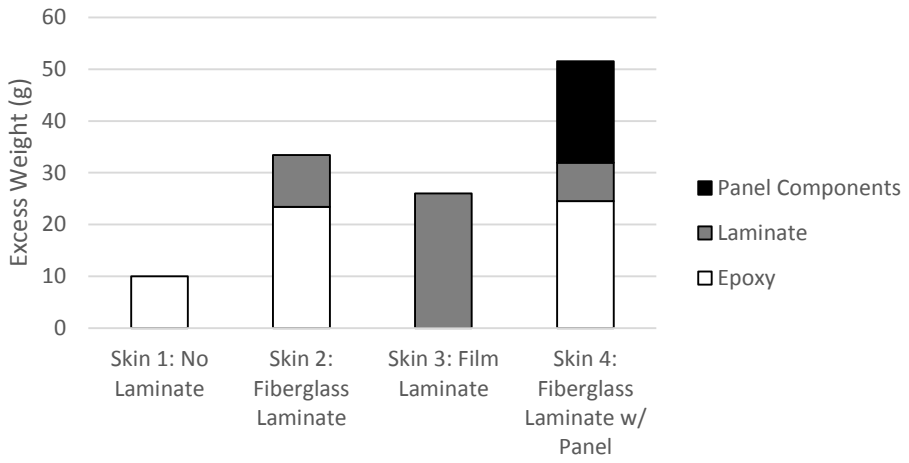

Figure 92: Excess weight by components (epoxy, encapsulation material and panel components)

The excess weight of the epoxy used to produce each wing skin was estimated by calculating a reference epoxy weight for each wing skin utilizing the epoxy ratio for Skin 3, scaled based on the weight of the materials for each respective wing. This reference value for epoxy weight represented the amount of epoxy the skin should have required to be produced based on the weight of its structural composite materials. By subtracting this reference value from the actual epoxy weight, the estimated excess epoxy weight was obtained.

$$W_{\text{Epoxy Adjusted}} = ER_{\text{Skin 3}}\left(W_{\text{Structual Fiberglass}} + W_{\text{Tow}}\right)$$

$$W_{\text{Epoxy Excess}} = W_{\text{Epoxy Actual}} - W_{\text{Epoxy Adjusted}}$$

Another source of excess weight came from the laminate materials themselves, while the excess epoxy weight would include any epoxy used in infusing fiberglass laminates with epoxy. A third category of excess skin weight was unique to Skin 4, which contained the removable panel, which was made up of the weight of the magnets and the weight of the

two thin plywood frames used in the panel and its socket; both of which were components exclusive to the fabrication of Skin 4 and its removable panel.

Table 11: Detailed excess weight breakdown

	Excess Weight (g)				Excess Wt Per Cell (g)	
	Epoxy	Laminate	Panel Components	Total	New	Old
Skin 1: No Laminate	10.00 ± 2.83	0.00	0.00	10.00 ± 2.83	0.50 ± 0.14	0.00
Skin 2: Fiberglass Laminate	23.4 ± 4.42	10.00 ± 1.00	0.00	33.40 ± 4.54	1.67 ± 0.23	1.12 ± 0.02
Skin 3: Film Laminate	0.00	26.00 ± 1.00	0.00	26.00 ± 1.00	1.30 ± 0.05	1.33 ± 0.02
Skin 4: Fiberglass w/ Panel	24.53 ± 4.63	7.41 ± 1.00	19.55 ± 1.98	51.49 ± 5.14	3.22 ± 0.32	1.12 ± 0.02

The greatest amount of excess weight was present in Skin 4, which held a significant weight increase due to the integration of its removable panel both coming from excess epoxy and panel components. While the layup of Skin 4 itself was not significantly inefficient compared to Skin 2, the epoxy required to fabricate a wing with a removable panel increases the amount of excess epoxy it uses. Excess epoxy, in this case, is defined as the amount of epoxy used to produce the wing skin in excess of the amount of epoxy needed to produce a wing skin that does not have solar cells.

Total excess weight, when divided by the number of cells simulated on the wing (20) provides the weight increase, per solar cell, in a wing utilizing that particular laminate. Compared to the old values for weight increases developed from single cell testing for cells without a laminate, cells laminated and 3.0 oz. fiberglass and cells laminated in the thin polyurethane film, all encapsulation methods indicate a significant increase in weight per cell when scaled up to arrays of cells except for the wing skin with cells encapsulated in film, which is very similar to its original estimated value of 1.33 grams increase in weight per cell due to the fact that the skin containing the array encapsulated in Film did

not require any excess epoxy in order to be scaled up to an array of multiple cells compared to a single cell test sample.

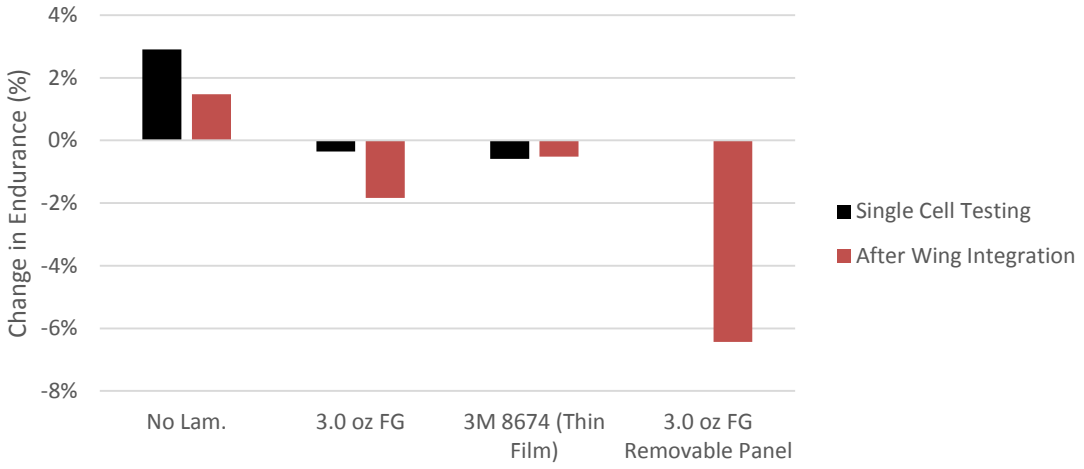

Figure 93: Endurance comparison between single cell testing and array integration

These updated values for weight per cell within a wing allowed the endurance model that was last investigated from single cell testing to be updated for the values acquired from wing construction. The updated values for weight increase per cell allowed for a visualization of the differences in endurance seen by the simulated aircraft between single cell testing results and the detailed weight breakdown conducted after wing construction. Due to the amount of excess epoxy present in the wings constructed, cells with no laminating material as well as cells encapsulated in fiberglass see approximately a 1.5% decrease in endurance, which is proportional to the difference in increase weight per cell of either encapsulation method while the estimated endurance of the aircraft with solar cells encapsulated in film stays relatively the same.

Based on wing construction data, the aircraft would see almost a 4.5% decrease in endurance with the integration of one removable panel containing four cells. This endurance calculation takes into account the removal of two of the 40 solar cells in order

to accommodate the panel. The implementation of a removable panel containing solar cells has a significant impact on endurance of the aircraft.

CHAPTER V

CONCLUSIONS

The encapsulation methods and materials experimented with in this research yielded mixed results with a small level of uncertainty—particularly related to cell performance results before and after encapsulation and weight related estimates for array integration into full wing skins. However, these results have allowed for some conclusions to be made for different relationships between encapsulation materials, cell performance, aircraft performance and array integration.

Encapsulation Processes

The encapsulation processes experimented with for each encapsulation material were conducted under fairly optimal conditions due to the fact that these processes were tested on single cell test specimens as opposed to arrays of cells with the assumption that testing an array of cells would have yielded more realistic results for expected increases in weight before and after composites integration. However, single was necessary in order to fully evaluate individual cells due to the difficulty of evaluating an array of cells individually when they are fully encapsulated using the cell testing apparatus that had been developed and constructed.

Based on results from stage one of single cell testing and the pictured evidence provided from encapsulated specimens, it is likely that the elimination of visual defects in samples such as voids and epoxy starved or visible fibers in fiberglass encapsulation materials contributed to decreasing the negative impacts that those encapsulation materials had on cell performance. The surface finish of different specimens likely also has influence on cell performance, as is visible in particular for the FG4 (Figure 67) specimen group, which had an odd, textured surface finish due to an error in the mixing ratio of epoxy for that specimen's encapsulating layer of fiberglass. If fiberglass materials are to receive more attention as potential candidates for encapsulation materials of cells, then it may be beneficial to investigate methods of manipulating the surface finish of cured fiberglass materials in order to determine if there is indeed a relationship between surface finish of encapsulating fiberglass materials and their effects on embedded solar cell performance.

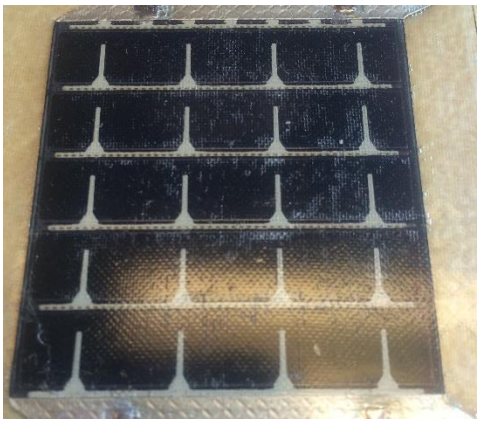

Figure 94: A specimen from the FG4 single cell test sample group with its odd texture visible when reflected into light

Encapsulation Materials

Each encapsulation material as well as any available gradient of material options provided varying results regarding cell performance, possible increases in durability and aircraft performance.

No Encapsulation Material

Both single-cell specimen and full array results indicate that cells integrated into a wing without any additional encapsulation material have not only the most favorable cell performance after integration, but also the highest bonus increase to endurance, making this method of photovoltaic cell wing integration most attractive for cases where added levels of cell durability are considered unnecessary. For example, the Powerfilm cells used in this research would be considered fairly robust compared to other more fragile thin film photovoltaic options available. They are also pre-laminated, making any additional protection in the form of an encapsulating layer of fiberglass or polyurethane 3M film potentially redundant. In this case, where Powerfilm cells are to be integrated into an aircraft wing skin with the goal of maximizing bonuses to aircraft endurance, it would likely be preferable to integrate those cells without additional encapsulating materials.

Fiberglass Encapsulation Material

Fiberglass fabric is available in various fabric weights, strengths and weaves. When used as an encapsulation material for cells embedded within a composite wing skin, it was shown to offer an additional level of resistance to out of plane loading, which can be increased by using heavier weaves of fiberglass fabric. The additional durability of fiberglass as well as the relatively cost effective price associated with fiberglass fabrics makes them an appealing encapsulation material for photovoltaic cells embedded into composite wing skins. However, these benefits may be potentially offset by the negative impacts in cell performance and aircraft performance.

While increasing the weight of fiberglass fabric as an encapsulation material may provide better benefits to durability, doing so also decreases light transmission to the cells and can significantly increase the weight penalty associated with the integration of cells into a wing, which leads to decreases in overall aircraft performance. It is at this point that the use of fiberglass as an encapsulation material becomes a tradeoff between higher durability and lower performance; a decision they may be influenced by mission parameters or flight conditions of the aircraft.

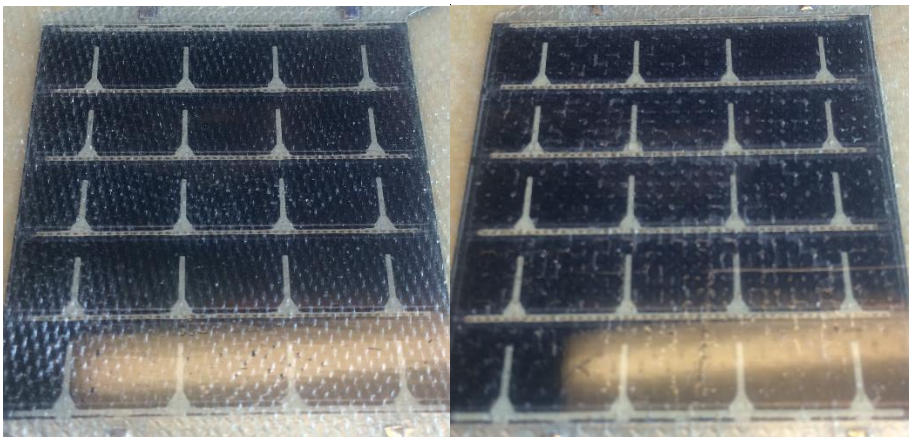

Figure 95: Left: 8.0 oz. fiberglass encapsulated sample Right: 5.4 oz. encapsulated sample

While heavier fiberglass fabric weights carry penalties to aircraft and cell performance when used as an encapsulation material, these penalties can be partially mitigated by choosing fabrics with higher fiber counts over fabrics with lower fiber counts. For instance the 8 oz. fiberglass fabric evaluated in this research possessed a significantly lower cell performance penalty than the 5.4 oz. fiberglass (Figure 69), which possessed a much lower fiber count—thus implying that the individual fibers of that fabric were arranged in a thicker, looser weave than the 8.0 fiberglass.

Film Encapsulation Material

The 3M polyurethane film encapsulation materials, as an alternative to fiberglass fabric, have some significant differences from fiberglass that give them their own appeal. The 3M film provided better cell performance than fiberglass encapsulation materials, which aided in offsetting weight penalties on aircraft performance. The thin film tested in this research possessed similar endurance performance to some of the lighter fiberglass

fabrics evaluated in this research despite its relatively high weight. Due to the nature of the film and its adhesive backing, this encapsulation material is also the easiest to combine with a solar cell or array of solar cells with the aid of water. Arrays can be integrated into their film encapsulation materials prior to wing integration; making manufacturing much less complicated compared to fiberglass encapsulation materials, which have to be integrated into the array during the time-sensitive layup process.

The film encapsulation materials, however, do not offer much in the way of resistance to out of plane forces, suggesting they would do little to protect cells in the event of an impact. However, the film materials did show some resistance to abrasion, and they do not suffer from the same issues of delamination that fiberglass encapsulation materials have with the surface of the solar cell.

Wing Integration

Due to differences in encapsulation processes between single cell testing and wing integration, weight breakdown data from wing integration suggested that excess weight would more likely be introduced into the manufacturing process of a wing skin embedded with solar cells due to some of the added complications of embedding an array of cells into a wing versus a single cell into a composite backing. The excess weight was highest for the wing containing fiberglass encapsulation material for its cell array, which came as a result of the inefficient use of epoxy during the layup process of that wing skin.

Future work with array integration into wing skins would be advised to seek out methods of streamlining the integration processes for arrays of cells into a wing skin in order to minimize increases in weight to keep them more in-line with the values produced during single cell testing.

The method of wiring the wings, which used a plywood shim to transfer the wiring of the arrays from the outer surface of the layup to the inner surface of the layup, proved to be an easy, effective method of handling the skin-embedded wiring and minimized the amount of internal wiring in each wing skin. It was also relatively easy to adapt the plywood shim method to multiple separate arrays for the case of the skin containing the removable panel.

The removable solar panel was proven functional, however, the early prototype developed in this research is not quite the full realization of a removable, replaceable solar panel on a wing. The method of manufacturing the removable panel is such that the wing is manufactured using its original panel. If a new panel were fabricated using similar methods as the original panel, it would likely not fit into the wing quite as well as the original panel and would potentially require modification of the wing or the panel itself to achieve a desired quality of fit. However, it is potentially possible to create a consistent fit between removable panels using a “master” removable panel, which the wing could be cast on, which would designed with slightly looser tolerances that might

allow small variations in manufacture of separate removable solar panels easier to deal with when fitting those panels to the wing skin.

While the removable panel could potentially provide interchangeability in the event of damage with other new panels, the process of building that panel into a wing comes with several complications and penalties. The integration of a large removable panel into a wing skin has the potential to adversely affect the structural performance of the skin as well as the structure of the wing itself, which has to be modified to accommodate the removable panel. This negative impact on the structural integrity of the wing has the potential to warrant reinforcement of the skin and its structure, which would ultimately increase the already inflated weight penalty of the integration of the panel itself into the wing. These weight penalties on aircraft endurance are inflamed by the possibility that solar cells may have to be removed from the wing in order to accommodate the removable panel, further reducing aircraft performance.

Extrapolation of Results

The PowerFilm cells used in this research, while potentially unrealistic in their application as cells used to assist an aircraft with the intention of increasing endurance as an alternative to more battery capacity, were a cost effective analogue for determining the potential performance impacts of composites integration processes on cell and aircraft performance.

The results from single cell testing cell performance and the weight increases developed from wing integration were applied to more efficient thin film cells (~16%) developed by MicroLink Devices and applied to the simulated endurance model using the three different encapsulation material conditions covered in wing integration:

1. No encapsulation material
2. 3.0 oz. Fiberglass
3. Thin Film

These results were then compared to endurance increases provided by PowerFilm cells as well as the endurance bonus provided by the addition of a second 1350mAh battery to the aircraft. Cell counts were also adjusted to utilize the full available planform of the wing for both the PowerFilm cell and MicroLink cells, bringing the cell count for the PowerFilm cells up to 66 from 40 and the MicroLink cell count up to 72. The results of this endurance comparison are provided in Figure 96, and indicate that the impacts of solar cell performance and weight increases for each integration process has a magnified effect on relative increases or decreases in endurance when applied to cells of a higher efficiency. However, the justification for the use of solar cells as an alternative for increasing aircraft endurance over simply adding another battery to the airframe is indicated by the higher relative endurance bonus provided by the higher efficiency solar cells compared to that of adding a second battery.

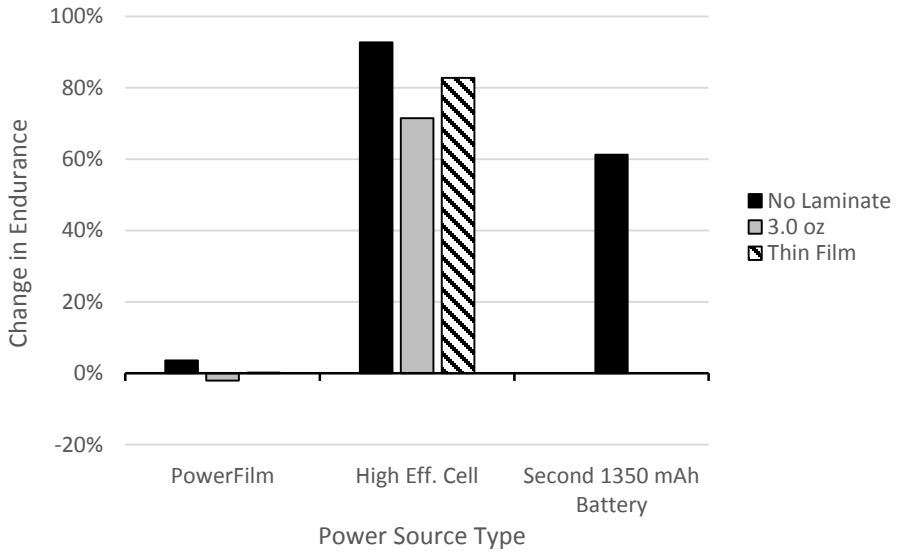

Figure 96: Simulated impacts of encapsulation processes on aircraft endurance using high efficiency cells compared to PowerFilm cells and additional battery.

Future Work

The next phase for this research would most likely be the design and fabrication of a solar powered or solar power-assisted electric UAV utilizing some of the techniques explored in this research for the integration of an array of higher efficiency cells into a wing skin. This further research would be expected to explore the optimization of array placement and efficient use of wing surface for an array of cells with the goal of maximizing increases in endurance.

The designer would also likely need to investigate methods of integrating cells into composite skins with the addition of blocking and bypass diodes in order to ensure that damaged cells are properly handled by the power system, which would also require the integration of a maximum power point tracker (MPPT) and voltage regulator in order to

condition the power from the solar cell array for the power system of the aircraft, adding some further complexity to the considerations that need to be made for the number of cells to be placed in series and parallel in the array in order to optimize the array for power conditioning.

While the removable panel prototype did come with significant foreseeable negative impacts on performance, the concept still remains in its infancy. The prototype developed in this research exists as a proof of concept. That is, it's possible to make the removable panel function utilizing current existing techniques for casting wing skins on their removable components with the addition of using fastening magnets as electrical contacts. Further research into the development of this removable panel is likely to glean more efficient process of integration as well as achieving the desired effect of interchangeability between removable panels and wings. Weight reduction as well as further optimization of space usage should yield more favorable results for the implementation of an interchangeable removable solar panel into a composite wing.

REFERENCES

[1] Boucher R. J., 1984, "History of Solar Flight," AIAA/SAE/ASME 20th Joint Propulsion Conference, 1984, Cincinnati, Ohio.

[2] Noth, A., 2008, "History of Solar Flight," Autonomous Systems Lab, Swiss Federal Institute of Technology, Zurich.

[3] Hurd, W. R., 2009, "Application of Copper Indium Gallium Diselenide Photovoltaic Cells to Extend the Endurance and Capabilities of Unmanned Aerial Vehicles," Naval Postgraduate Schoool, Monterey, California.

[4] Coba, J. V., 2010, "Application of Copper Indium Gallium Diselenide Photovoltaic Cells to Extend the Endurance and Capabilities of the Raven RQ-11B Unmanned Areial Vehicle", Naval Postgraduate Schoool, Monterey, California.

[5] Green, M. A., Emery, K., Hishikawa, Y., Warta, W., Dunlop, W., "Progress in Photovoltaics: Research and Applications," Wiley Online Library, 827-837, 2013.

[6] ASTM Standard E-927-10, "Standard Specification for Solar Simulation and Photovoltaic Testing," ASTM International, West Conshohocken, PA, 2013, www.astm.org. .

[7] Gleskova, H., Cheng, I., Wagner, S., Sturm, J. and Suo, Z., 2005, "Mechanics of Thin-Film Transistors and Solar Cells on Flexible Substrates," Solar Energy, 80, pp. 687-693.

[8] Maung, K., Hahn, H. and Ju, Y.S., 2010, "Multifunctional Integration of Thin-Film Solar Cells on Carbon-Fiber-Reinforced Epoxy Composites", Solar Energy, 84(12), pp. 450-458.

[9] Okeson, M., Kellogg, K. and Kallmeyer, A., "Impact Damage Growth in Fiberglass/Epoxy Laminates Subjected to Moisture and Low Temperature Thermal Cycling," Department of Mechanical Engineering, North Dakota University, Fargo, North Dakota.

[10] Noth A., Siegwart R, 2006, "Design of Solar Powered Airplanes for Continuous Flight," Swiss Federal Institute of Technology, Zurich.

[11] Bisaillon, J.C., Cummings, J.R., Culik, J.S., Lesko, J.D., Sims, P.E., Rand, J.A., "Non-Traditional Light Sources for Solar Cell and Module Testing," AstroPower, Inc., Neward, DE.

APPENDICES

Encapsulation Material Data

Laminate Weight Data

Laminate	Material	Dry Weight (oz./yd^2)	Wetted Weight (oz./yd^2)	Epoxy Ratio
Fiberglass	0.7 oz./yd^2	0.78	2.40	2.08
Fiberglass	1.4 oz./yd^2	1.43	3.57	1.50
Fiberglass	2.0 oz./yd^2	2.12	4.09	0.93
Fiberglass	3.0 oz./yd^2	3.19	5.37	0.68
Fiberglass	5.8 oz./yd^2	5.49	9.03	0.65
Fiberglass	8.6 oz./yd^2	8.30	15.06	0.81
Fiberglass	9.6 oz./yd^2	9.56	16.37	0.71
Film	3M 8681HS	12.96	---	---
Film	3M 8674 (Thin Film)	6.78	---	---

Fiberglass Fabric Material Data

	Threads		
Fiberglass	X	Y	Fabric Thickness (in)
0.7 oz./yd^2	56	56	0.0013
1.4 oz./yd^2	60	47	0.0021
2.0 oz./yd^2	40	39	0.0032
3.0 oz./yd^2	60	58	0.0037
5.8 oz./yd^2	18	18	0.0082
8.6 oz./yd^2	54	18	0.0089
9.6 oz./yd^2	16	14	0.0154

Single Cell Testing

Stage One Single Cell Testing

Sample Listing

Laminate Type	Sample Range	Process Used	Reference
None	001 - 003	Standard	N1
None	004 - 006	Epoxy Edges	N2
None	007 - 009	Epoxy Clearcoat	N3
Fiberglass	010 - 012	Standard	FG1
Fiberglass	013 - 015	Painted Epoxy	FG2
Fiberglass	016 - 018	Epoxy Edges	FG3
Fiberglass	019 - 021	Sanded, Painted Epoxy	FG4
Fiberglass	022 - 024	Epoxy Clearcoat, Painted Epoxy	FG5
Film	025 - 027	Standard	F1
Film	028 - 030	Water	F2
Film	031 - 033	Epoxy	F3

Individual Specimen Data

Sample	Avg V_{loss}	Avg A_{loss}	Avg P_{loss}	Wt_{inc} (g)	$I_{SC,loss}$	$V_{OC,loss}$	$P_{peak,loss}$	$I_{M,loss}$	$V_{M,loss}$	FF_{loss}
001	-0.13%	0.03%	0.07%	0.94	-2.83%	-0.23%	0.47%	0.45%	0.02%	3.44%
002	-0.49%	-0.45%	-0.90%	0.91	-0.59%	0.12%	-1.46%	-0.61%	-0.85%	-0.99%
003	-0.51%	0.90%	0.45%	0.90	-0.49%	0.31%	-0.92%	-0.25%	-0.66%	-0.73%
004	-0.19%	0.09%	-0.07%	0.86	-0.61%	0.47%	0.05%	0.16%	-0.11%	0.19%
005	-0.37%	-0.08%	-0.43%	0.85	-0.31%	0.15%	-0.82%	-0.21%	-0.61%	-0.67%
006	-0.21%	0.07%	-0.12%	0.94	-0.44%	0.46%	0.14%	0.30%	-0.12%	0.12%
007	0.17%	0.48%	0.63%	1.02	0.19%	0.47%	0.74%	0.54%	0.20%	0.08%
008	-0.68%	0.14%	-0.52%	1.05	-0.14%	0.16%	-1.84%	-0.72%	-1.13%	-1.85%
009	-0.38%	0.24%	-0.14%	1.11	-0.08%	-0.56%	0.15%	0.44%	0.11%	0.79%
010	1.61%	2.16%	3.57%	2.04	2.89%	1.33%	3.41%	2.13%	1.57%	-0.81%
011	1.74%	2.08%	3.60%	1.92	2.94%	1.31%	3.41%	2.09%	1.53%	-0.84%
012	1.62%	2.01%	3.43%	1.99	2.71%	1.30%	4.34%	2.29%	2.09%	0.38%
013	0.73%	0.88%	1.56%	2.16	0.63%	0.85%	2.31%	1.40%	0.93%	0.85%
014	1.02%	1.15%	2.10%	2.25	1.08%	0.62%	2.45%	1.35%	1.11%	0.77%
015	1.32%	1.47%	2.64%	2.23	2.24%	1.00%	3.41%	1.74%	2.22%	0.19%
016	1.25%	1.66%	2.74%	2.23	2.51%	0.70%	3.13%	1.83%	1.32%	-0.06%

Sample	Avg V_{loss}	Avg A_{loss}	Avg P_{loss}	Wt_{inc} (g)	$I_{SC,loss}$	$V_{OC,loss}$	$P_{peak,loss}$	$I_{M,loss}$	$V_{M,loss}$	FF_{loss}
017	1.83%	2.12%	3.72%	2.42	3.04%	0.77%	4.74%	2.67%	2.13%	0.99%
018	1.43%	1.65%	2.88%	2.20	2.80%	0.23%	4.70%	2.36%	2.40%	1.73%
019	0.37%	0.38%	0.68%	2.26	1.00%	-0.47%	1.51%	0.75%	0.77%	0.97%
020	0.49%	0.66%	1.08%	2.11	1.12%	-0.47%	1.94%	1.01%	0.94%	1.29%
021	0.45%	0.60%	0.99%	2.02	0.97%	-0.39%	2.02%	1.01%	1.02%	1.44%
022	0.60%	0.91%	1.43%	2.10	1.33%	-0.31%	2.43%	1.26%	1.18%	1.42%
023	0.89%	0.93%	1.69%	2.16	1.94%	-0.16%	2.28%	1.17%	1.19%	0.50%
024	1.18%	1.32%	2.32%	2.11	2.46%	-0.23%	3.29%	1.64%	1.67%	1.08%
025	-1.68%	-1.83%	-3.29%	3.30	-4.59%	-1.17%	-1.15%	-0.54%	-0.60%	4.41%
026	-2.19%	-2.63%	-4.63%	3.34	-4.44%	-1.10%	-3.95%	-1.95%	-1.96%	1.55%
027	-1.50%	-1.53%	-2.86%	3.43	-3.40%	-1.40%	-0.96%	-0.45%	-0.51%	3.70%
028	-0.90%	-0.91%	-1.66%	3.48	-2.90%	-1.32%	0.73%	0.38%	0.36%	4.78%
029	-1.57%	-1.80%	-3.19%	3.44	-3.83%	-0.85%	-1.67%	-0.83%	-0.83%	2.91%
030	-2.07%	-2.34%	-4.25%	3.44	-3.86%	-0.70%	-4.45%	-2.21%	-2.20%	0.13%
031	-1.69%	-1.82%	-3.34%	3.38	-3.53%	-0.77%	-2.31%	-1.56%	-1.56%	1.93%
032	-0.97%	-1.15%	-1.96%	3.63	-3.11%	-0.86%	-0.85%	-0.43%	-0.41%	3.03%
033	-1.28%	-1.45%	-2.54%	3.65	-4.23%	-0.54%	0.35%	0.20%	0.16%	4.91%

Specimen Sample Group Performance Data

Ref No.	Avg V_{loss}	Avg A_{loss}	Avg P_{loss}	Wt_{inc} (g)	$I_{SC,loss}$	$V_{OC,loss}$	$P_{peak,loss}$	$I_{M,loss}$	$V_{M,loss}$	FF_{loss}
N1	-0.37%	0.16%	-0.13%	0.92	-1.30%	0.06%	-0.64%	-0.14%	-0.50%	0.57%
N2	-0.26%	0.03%	-0.21%	0.88	-0.45%	0.36%	-0.21%	0.08%	-0.28%	-0.12%
N3	-0.30%	0.28%	-0.01%	1.06	-0.01%	0.02%	-0.32%	0.09%	-0.27%	-0.33%
FG1	1.66%	2.08%	3.53%	1.98	2.85%	1.31%	3.72%	2.17%	1.73%	-0.42%
FG2	1.03%	1.16%	2.10%	2.21	1.32%	0.82%	2.72%	1.50%	1.42%	0.60%
FG3	1.50%	1.81%	3.11%	2.28	2.78%	0.57%	4.19%	2.29%	1.95%	0.89%
FG4	0.44%	0.54%	0.91%	2.13	1.03%	-0.44%	1.82%	0.92%	0.91%	1.23%
FG5	0.89%	1.05%	1.81%	2.12	1.91%	-0.23%	2.66%	1.36%	1.35%	1.00%
F1	-1.79%	-2.00%	-3.60%	3.36	-4.14%	-1.22%	-2.02%	-0.98%	-1.02%	3.22%
F2	-1.51%	-1.69%	-3.03%	3.45	-3.53%	-0.96%	-1.80%	-0.89%	-0.89%	2.61%
F3	-1.31%	-1.48%	-2.61%	3.55	-3.62%	-0.72%	-0.93%	-0.60%	-0.60%	3.29%

Specimen Sample Group Weight Data

Ref No.	Wt_{inc} (g)	Dry Backing Wt (g)	Dry Laminate Wt (g)	Epoxy Wt (g)
N1	0.92	0.62	---	0.29
N2	0.88	0.62	---	0.26
N3	1.06	0.62	0.00	0.44
FG1	1.98	0.62	0.62	0.73
FG2	2.21	0.62	0.62	0.96
FG3	2.28	0.62	0.62	1.03
FG4	2.13	0.62	0.62	0.88
FG5	2.12	0.62	0.62	0.87
F1	3.36	0.62	2.53	0.20
F2	3.45	0.62	2.53	0.30
F3	3.55	0.62	2.53	0.40

Stage Two Single Cell Testing

Sample Listing

Laminate Type	Sample Range	Laminate Material
Fiberglass	101 - 103	0.7 oz / yd^2
Fiberglass	104 -106	1.4 oz / yd^2
Fiberglass	107 - 109	2.0 oz / yd^2
Fiberglass	110 - 112	3.0 oz / yd^2
Fiberglass	113 - 115	5.8 oz / yd^2
Fiberglass	116 - 118	8.6 oz / yd^2
Fiberglass	119 - 121	9.6 oz / yd^2
Film	122 - 124	3M 8674 (Thin Film)

Individual Specimen Data

Sample	Avg V_{loss}	Avg A_{loss}	Avg P_{loss}	Wt_{inc} (g)	$I_{SC,loss}$	$V_{OC,loss}$	$P_{peak,loss}$	$I_{M,loss}$	$V_{M,loss}$	FF_{loss}
101	-0.21%	-0.22%	-0.38%	1.59	-0.08%	-0.66%	-0.07%	-0.04%	-0.11%	0.62%
102	-0.60%	-0.47%	-1.02%	1.56	-0.08%	-0.98%	-0.30%	-0.32%	-0.62%	0.43%
103	0.07%	0.26%	0.35%	1.48	0.39%	-0.22%	0.09%	0.08%	0.17%	0.00%
104	-0.30%	-0.36%	-0.63%	1.67	0.16%	-0.71%	-0.26%	-0.28%	-0.53%	0.02%
105	-0.16%	-0.23%	-0.35%	1.77	0.23%	-0.73%	-0.22%	-0.21%	-0.43%	0.07%

Sample	Avg V_{loss}	Avg A_{loss}	Avg P_{loss}	Wt_{inc} (g)	$I_{SC,loss}$	$V_{OC,loss}$	$P_{peak,loss}$	$I_{M,loss}$	$V_{M,loss}$	FF_{loss}
106	-0.14%	-0.11%	-0.20%	1.73	0.23%	-0.77%	0.09%	0.10%	0.18%	0.72%
107	0.35%	0.45%	0.77%	1.95	0.39%	0.49%	0.46%	0.42%	0.88%	0.01%
108	0.54%	0.52%	1.02%	1.92	0.23%	0.46%	0.95%	0.89%	1.83%	1.14%
109	-0.21%	-0.33%	-0.53%	1.84	0.00%	-0.37%	-0.30%	-0.37%	-0.67%	-0.30%
110	-0.18%	-0.11%	-0.32%	2.08	-0.46%	0.50%	-0.25%	-0.24%	-0.48%	-0.51%
111	0.44%	0.35%	0.74%	2.09	-0.08%	0.87%	0.45%	0.43%	0.88%	0.09%
112	0.33%	0.31%	0.60%	2.13	-0.08%	0.63%	0.45%	0.43%	0.88%	0.33%
113	1.33%	1.57%	2.68%	3.07	-0.08%	3.10%	1.74%	1.72%	3.43%	0.42%
114	1.00%	1.11%	1.95%	3.02	0.16%	2.43%	0.96%	1.03%	1.98%	-0.62%
115	0.96%	1.10%	1.86%	3.10	-0.47%	3.21%	0.99%	1.00%	1.98%	-0.80%
116	1.25%	1.42%	2.40%	3.86	-0.31%	3.89%	0.75%	0.74%	1.49%	-2.18%
117	0.98%	2.55%	3.39%	3.85	-0.54%	2.04%	1.41%	1.45%	2.84%	1.36%
118	0.47%	0.63%	0.96%	3.84	-0.62%	2.05%	0.43%	0.45%	0.87%	-0.57%
119	4.34%	4.88%	8.32%	4.00	0.15%	9.56%	4.99%	5.02%	9.76%	0.06%
120	4.62%	5.20%	8.87%	4.03	0.08%	9.90%	5.45%	5.49%	10.65%	0.75%
121	4.04%	4.62%	7.84%	4.05	0.00%	8.86%	4.76%	4.78%	9.32%	0.50%
122	-1.14%	-1.31%	-2.22%	2.26	-0.08%	-4.56%	-0.06%	-0.01%	-0.08%	4.36%
123	-1.43%	-1.47%	-2.78%	2.23	-0.31%	-2.53%	-1.42%	-1.37%	-2.81%	0.04%
124	-1.27%	-1.34%	-2.50%	2.21	-0.31%	-2.29%	-1.24%	-1.19%	-2.45%	0.16%

Specimen Sample Group Performance Data

Material	Avg V_{loss}	Avg A_{loss}	Avg P_{loss}	Wt_{inc} (g)	$I_{SC,loss}$	$V_{OC,loss}$	$P_{peak,loss}$	$I_{M,loss}$	$V_{M,loss}$	FF_{loss}
0.7 oz. FG	-0.24%	-0.14%	-0.35%	1.54	0.08%	-0.62%	-0.09%	-0.09%	-0.19%	0.35%
1.4 oz. FG	-0.20%	-0.23%	-0.39%	1.72	0.21%	-0.74%	-0.13%	-0.13%	-0.26%	0.27%
2.0 oz. FG	0.23%	0.21%	0.42%	1.90	0.21%	0.19%	0.37%	0.31%	0.68%	0.28%
3.0 oz. FG	0.20%	0.18%	0.34%	2.10	-0.21%	0.67%	0.22%	0.21%	0.43%	-0.03%
5.4 oz. FG	1.10%	1.26%	2.16%	3.06	-0.13%	2.91%	1.23%	1.25%	2.46%	-0.33%
8.0 oz. FG	0.90%	1.53%	2.25%	3.85	-0.49%	2.66%	0.87%	0.88%	1.74%	-0.47%
9.0 oz. FG	4.33%	4.90%	8.34%	4.03	0.08%	9.44%	5.07%	5.10%	9.91%	0.43%
Thin Film	-1.28%	-1.37%	-2.50%	2.23	-0.23%	-3.13%	-0.91%	-0.86%	-1.78%	1.52%
Thick Film	-1.51%	-1.69%	-3.03%	3.45	-3.53%	-0.96%	-1.80%	-0.89%	-0.89%	2.61%

Specimen Sample Group Weight Data

Laminate Material	Wt_{inc} (g)	Backing Layer Dry Wt (g)	Laminate Dry Wt (g)	Epoxy Clearcoat Wt (g)	Backing Layer Epoxy Wt (g)	Laminate Epoxy Wt (g)	Laminate Wet Wt (g)	Laminate Epoxy Ratio
0.7 oz. FG	1.54	0.62	0.15	0.14	0.36	0.27	0.56	1.78
1.4 oz. FG	1.72	0.62	0.28	0.14	0.36	0.32	0.74	1.16
2.0 oz. FG	1.90	0.62	0.41	0.14	0.36	0.37	0.92	0.89
3.0 oz. FG	2.10	0.62	0.62	0.14	0.36	0.36	1.12	0.57
5.4 oz. FG	3.06	0.62	1.07	0.14	0.36	0.87	2.08	0.81
8.0 oz. FG	3.85	0.62	1.62	0.14	0.36	1.11	2.87	0.68
9.0 oz. FG	4.03	0.62	1.87	0.14	0.36	1.04	3.05	0.55
Thin Film	2.23	0.62	1.33	---	0.29	---	---	---
Thick Film	3.45	0.62	2.53	---	0.30	---	---	---

Endurance Estimaion

Aircraft and Solar Cell Parameters

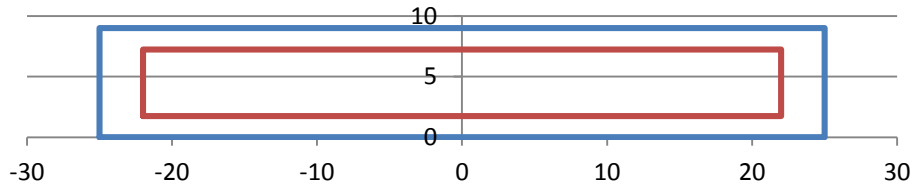

Aircraft			Propulsion			Solar		
ρ =	0.002377		V_{bat} =	11.1	V	n_{series} =	2	
C_{Do} =	0.035		Cap_{bat} =	1350	mAh	$n_{parallel}$ =	20	
$W_{airframe}$ =	5	lb	η_p =	0.7		n_{cell} =	40	
S =	450	in^2				l_{cell} =	2.2	in
b =	50	in				w_{cell} =	2.75	in
AR =	5.56					A_{cell} =	6.05	in^2
c =	9	in				V_M =	3	V
K =	0.08					I_M =	28	mA
V_{end} =	45.37	ft/s				P_{cell} =	0.084	W
						W_{cell} =	1.02	g
						W_{wire} =	1.1	g
						W_{elec} =	26.02	g

Endurance Calculations

Laminate	$W_{lam/cell}$ (g)	$I_{M,loss}$	$V_{M,loss}$	W_{solar} (g)	W_{total} (lb)	Vend (ft/s)	P_{req} (W)	P_{solar} (W)	End. (hr)	E_{inc}
No cells	0	0	0	0	5.00	45.37	33.03	0.00	0.32	0.00%
No Lam.	0	-0.14%	-0.50%	110.82	5.24	46.47	35.48	3.38	0.33	2.90%
0.7 oz FG	0.56	-0.09%	-0.19%	133.35	5.29	46.69	35.98	3.37	0.32	1.27%
1.4 oz FG	0.74	-0.13%	-0.26%	140.55	5.31	46.76	36.15	3.37	0.32	0.78%
2.0 oz FG	0.92	0.31%	0.68%	147.75	5.33	46.83	36.31	3.33	0.32	0.14%
3.0 oz FG	1.12	0.21%	0.43%	155.62	5.34	46.90	36.49	3.34	0.32	-0.36%
5.8 oz FG	2.08	1.25%	2.46%	194.15	5.43	47.28	37.36	3.24	0.31	-3.21%
8.6 oz FG	2.87	0.88%	1.74%	225.62	5.50	47.58	38.08	3.27	0.30	-5.10%
9.6 oz FG	3.05	5.10%	9.91%	232.69	5.51	47.64	38.24	2.87	0.30	-6.61%
3M 8674	1.33	-0.86%	-1.78%	163.85	5.36	46.98	36.67	3.45	0.32	-0.58%
3M 8681HS	2.53	-0.89%	-0.89%	211.97	5.47	47.45	37.77	3.42	0.31	-3.83%

Wing Integration Weight Buildup

Wing 1

Skin 1: No Laminate
Skin 2: Fiberglass

Weight

Skin 1				Skin 2			
Outer Fabric	25	± 1	g	Outer Fabric	26	± 1	g
Inner Fabric	8	± 1	g	Inner Fabric	9	± 1	g
Laminate	0	± 0	g	Laminate	10	± 1	g
Core	14	± 1	g	Core	14	± 1	g
Tow	4	± 1	g	Tow	6	± 1	g
Extras	6	± 1	g	Extras	6	± 1	g
Cells and Wiring	19	± 1	g	Cells and Wiring	19	± 1	g
Dummy Cells	10	± 1	g	Dummy Cells	10	± 1	g
Total	134	± 1	g	Total	161	± 1	g
Epoxy	48	± 3	g	Epoxy	61	± 3	g
Epoxy Ratio	1.12	± 0.06		Epoxy Ratio	1.30	± 0.06	

Comparison

Skin 1			
Extra Epoxy	10.00	± 2.83	g
Add. Wt. Per Cell	0.50	± 0.14	g

Skin 2			
Adj. Epoxy	37.60	± 3.25	g
Extra Epoxy	23.40	± 4.42	g
Laminate Wt	10	± 1	g
Extra Wt	33.40	± 4.54	g
Add. Wt. Per Cell	1.67	± 0.23	g

Wing 2

Skin 3 Film Laminate
Skin 4 Fiberglass Laminate With Panel

Weight

Skin 3			
Outer Fabric	28	± 1	g
Inner Fabric	10	± 1	g
Laminate	26	± 1	g
Core	14	± 1	g
Tow	5	± 1	g
Extras	7	± 1	g
Cells and Wiring	19	± 1	g
Dummy Cells	10	± 1	g
Total	159	± 1	g
Epoxy	40	± 3	g
Epoxy Ratio	0.80	± 0.06	

Skin 4			
Outer Fabric	28	± 1	g
Inner Fabric	6	± 1	g
Laminate	5	± 1	g
Core	11	± 1	g
Tow	3	± 1	g
Extras	6	± 1	g
Cells and Wiring	12	± 1	g
Dummy Cells	8	± 1	g
Frame	3.07	± 0.01	g
Frame Fiberglass	2	± 1	g
Total	140	± 1	g
Epoxy	55.93	± 3	g
Epoxy Ratio	1.12	± 0.06	

Comparison

Skin 3			
Adj. Epoxy	40	± 3	g
Extra Epoxy	0		g
Laminate Wt	26	± 1	g
Extra Wt	26.00	± 1	g
Add. Wt. Per Cell	1.30	± 0.05	g

Skin 4			
Adj. Epoxy	36	± 3	g
Extra Epoxy	19.93	± 5	g
Laminate Wt	7.41	± 1.00	g
Panel Add. Wt	19.55	± 1.98	g
Extra Wt	51.49	± 5.14	g
Add. Wt. Per Cell	3.22	± 0.32	g

Panel			
Outer	2.41	± 0.01	g
Inner	2.41	± 0.01	g
Frame	3.07	± 0.01	g
Cells+W+M	6.16	± 0.01	g
Copper	2.04	± 0.01	g
Core	2.18	± 0.01	g
Total	18.27	± 0.96	g
Epoxy	7.88	± 0.96	g
Excess Epoxy	4.60	± 0.96	g

Adjusted Endurance Calculations

Laminate	$W_{lam/cell}$ (g)	$I_{M,loss}$	$V_{M,loss}$	W_{solar} (g)	W_{total} (lb)	Vend (ft/s)	P_{req} (W)	P_{solar} (W)	End. (hr)	E_{inc}
No Lam.	0.50	-0.14%	-0.50%	130.86	5.29	46.66	35.93	3.38	0.64	1.48%
3.0 oz FG	1.67	0.21%	0.43%	177.62	5.39	47.12	36.98	3.34	0.62	-1.83%
3M 8674 (Thin)	1.30	-0.86%	-1.78%	162.82	5.36	46.97	36.65	3.45	0.63	-0.51%
FG & Rem. Panel	3.22	0.21%	0.43%	235.47	5.52	47.67	38.30	3.00	0.59	-6.43%

VITA

James Leonard

Candidate for the Degree of Master of Science

Thesis: INTEGRATION OF PHOTOVOLTAIC CELLS INTO COMPOSITE WING SKINS

Major Field: Aerospace Engineering

Biographical:

Education:

Completed the requirements for the Master of Science in aerospace engineering at Oklahoma State University, Stillwater, Oklahoma in December 2014.

Completed the requirements for the Bachelor of Science in aerospace engineering at Oklahoma State University, Stillwater, OK in May 2010.

Experience:

Professional Memberships: